Synthesis of 2,2-dipyridylamine organometallic complexes for antiplasmodial application

By

Remofilwe Manye

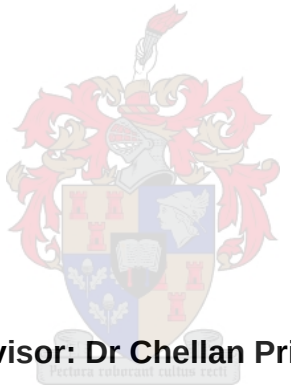

Supervisor: Dr Chellan Prinessa

Faculty of Science

Department of Chemistry and Polymer Science

March 2021

DECLARATION

By submitting this thesis electronically, I declare that the entirety of the work contained therein is my own, original work, that I am the sole author thereof (save to the extent explicitly otherwise stated), that reproduction and publication thereof by Stellenbosch University will not infringe any third party rights and that I have not previously in its entirety or in part submitted it for obtaining any qualification.

Abstract

Six iridium, rhodium and ruthenium half-sandwich organometallic complexes (**C1**-**C6**) of the ligand 2,2-dipyridilamine with either a chlorido and iodido ancillary ligand were synthesized using a reported method and their biological activity was investigated. **C1**-**C6**, complexes bearing a PF_6^- counterion, have been reported in literature. Single crystal structures of iridium (**C1**) and rhodium (**C2**) chlorido complexes were solved and both were found to have crystallised in the orthorhombic $P2_12_12_1$ space group. The aqueous solubility of **C1**-**C6** ranged from poor (<10 µg/mL) to good solubility (> 60 µg/mL). The ruthenium-iodido complex **C6** was the least soluble up to 7 µg/mL. Hydrolysis studies were conducted, and it was found that chlorido complexes **C1**, **C5** and **C6** did not undergo hydrolysis. The chlorido complexes **C2** and **C3** did undergo hydrolysis, however, complete displacement of the chlorido with deuterium oxide did not occur.

Novel complexes **C7**-**C12**, analogues of **C1**-**C6** bearing a NO_3^- counterion were also synthesized using an adapted method of the PF_6^- complexes. The crystal structures of complexes **C7** and **C9** were solved. Iridium chlorido complex **C7** was found to crystallise in the monoclinic $P2_{1/c}$ space group and ruthenium chlorido complex **C9** was found to crystallise in the triclinic *P*-1 space group. Complexes **C7**, **C8**, **C9**, **C11** and **C12** were found to have good solubility to a maximum concentration of 200 µM. Iridium iodido complex **C8** was moderately soluble >41 µg/ml. Hydrolysis studies of complexes **C7**-**C12** showed that chlorido complexes **C8** and **C9** and iodido complex **C12** were hydrolysable. Generally, chlorido complexes for both PF_6^- and NO_3^- counterions were relatively easily hydrolysable compared to iodido complexes with the exception of chlorido complex **C7** and iodido complex **C12**.

The *in vitro* biological antiplasmodial activity of the ligand, 2,2-dipyridilamine, and complexes **C1**-**C6** was evaluated against two *Plasmodium falciparum* strains, complexes **C7**-**C12** were not evaluated due to time constraints. The ligand was found to be inactive up to a concentration of 5mM against 3D7 strain, a chloroquine sensitive strain of *Plasmodium falciparum* parasite. The complexes showed activity against the 3D7 strain, however, the complexes were not as active as currently used antimalarial drugs. Rhodium complexes **C2** (IC_{50} = 4.72 µM) and **C5** (IC_{50} = 5.76 µM) were the most active and iridium chlorido complex **C1** (IC_{50} = 8.93 µM) was the least active amongst complexes **C1**-**C6**. Activity of the chlorido versus iodido complexes of iridium and rhodium were presumed to be associated with their relative solubility in aqueous based medium, the more soluble complexes were more active. This argument was not applicable for the ruthenium complexes, the less soluble complex **C12** (IC_{50} = 7.91 µM) showed better activity than the more soluble complex **C6** (IC_{50} = 7.57 µM). The ligand and complexes showed no activity against chloroquine sensitive NF54 strain in a two- and three-day assay. The inactivity may be related to the use of hypoxanthine in the growth media which could be countering the compounds' mode of action resulting in a delayed response time.

Acknowledgements

It has been a great privilege for me to have the following people contribute towards my research. My supervisor, Dr Prinessa Chellan, for her unwavering support both academically and financially. I would also like to thank her for the encouragement throughout this project.

Stellenbosch university for funding. Central Analytical Facility (CAF) for training and use of the NMR facilities for characterization, most especially Elsa Malherbe and Dr Jaco Brand for their willingness to help. Dr Marietjie Stander for mass spectrometry data. Dr Leigh Loots for solving my crystal structures. Prof. Lubbe Wiesner at the University of Cape Town and Prof. Vicky Avery Griffith University for the antiplasmodial testing.

The technical and support staff of De Beers and Inorganic building.

Dr Chellan's research group, Lydia, Christoff and Chandre for their kindness, advice and assistance when necessary. The organometallics research group for their advice, support and encouragement.

My friends, Chandrē, Chelsea, Emile, Lauren, Megan and Stacey for their moral support and making Stellenbosch my second home.

Special appreciation for my mother, Matshidiso Manye, for her prayers, guidance, encouragement, love and for always being there for me through all the good and bad times. To my late father who wanted nothing but the best for me, I would not be where I am today if it weren't for his motivation.

List of abbreviations:

2,2-Dipyridylamine	Dpa
3D7	Chloroquine sensitive *Plasmodium falciparum* strain
μM	Micromolar
A2780	Cancer cell line
ACT	Artemisinin-based combination therapy
CHO	Chinese Hamster Ovarian cancer cells
CQ	Chloroquine
CQR	Chloroquine resistant
CQS	Chloroquine sensitive
DCM	Dichloromethane
Dd2	Chloroquine resistant Plasmodium falciparum strain
DHA	Dihydroartemisinin
DHFR	Dihydrofolate reductase
DHPS	Dihydropteroate synthase
DMSO	Dimethyl sulfoxide
DNA	Deoxyribonucleic acid
FQ	Ferroquine
IC_{50}	Half maximal inhibitory concentration
IPC5202	Artemisinin-resistant Plasmodium falciparum strains
K1	Multi-resistant Plasmodium falciparum strain
LSG	Late stage gametocyte
MLEM	Model List of Essential Medicines
MOA	Mechanism of action
NAI	Naturally Acquired Immunity
NF54	Chloroquine sensitive Plasmodium falciparum strain
nm	Nano molar
P. berghei	Plasmodium berghei

P. falciparum	Plasmodium falciparum
P. knowlesi	Plasmodium knowlesi
P. malariae	Plasmodium malariae
P. ovale	Plasmodium ovale
P. vivax	Plasmodium vivax
p-cym	Para-Cymene
PGM	Platinum group metal
ppm	Parts per million
RBCs	Red blood cells
RI	resistance indices
SCE	Saturated calomel electrode
Sep	Septet
WHO	World Health Organization

Table of Contents

Chapter 1

Organometallic complexes as antimalarials: A review

1.1. Introduction

Research into the use of metal complexes in the medicinal field has been growing. Since researchers have found that incorporating metal ions into organic pharmacophores can improve their therapeutic efficacy.[1,2] The successful application of cisplatin as an anticancer agent has brought attention to the potential application of metal complexes as therapeutics.[3] This investigation into metallo-drugs is far advanced with some new metal containing drugs already in use and others in clinical trials.[4] There are several properties offered by metals that can be taken advantage of in order to design better therapeutic agents.[4] Different metals possess a wide range of coordination numbers, geometries, thermodynamic and kinetic properties as well as accessible redox states.[4] With the study of metal complexes as viable new medicines gaining momentum, it is important for us to better understand their interactions in a biological environment and how it could affect their therapeutic efficacy.

Several metal complexes with proven efficacy against *P. falciparum,* one of the causative agents of malaria, have been reported.[1] Malaria is one of the deadliest diseases in the world, threatening more than one third of its population. It is caused by parasites of the *Plasmodium* genus which are transmitted into the blood stream through the bites of female Anopheles mosquitoes.[5] Malaria is mostly prevalent in tropical regions thriving in large areas of Africa and South-East Asia, some parts of South and Central America, as well as the Eastern Mediterranean and Western Pacific. It thrives in these countries due to their tropical or subtropical climates which are favourable for mosquitoes to proliferate, i.e. survive and be able to reproduce[6]. In high risk areas, the most susceptible people are pregnant women and infants owing to the fact that they have compromised or no naturally acquired immunity (NAI) to the disease.[7] A greater risk is observed for underprivileged people who have little to no access to health care.[8]

According to the World Health Organization (WHO), in 2019, an estimated 229 million cases of malaria were reported worldwide, an increase of 1 million cases since 2018.[9] This resulted in about 409 000 deaths. Africa accounts for 93% of reported malaria cases and 89% of deaths.[9] The *P. vivax* parasite is mostly widespread in the WHO region of America where it accounts for about 72.3% of all its reported malaria cases.[6] There have been inconsistencies in reported cases for individual countries with some countries having more cases while others have a reduced number of cases over the course of the years. The mortality rate on the other hand displays a decrease since 2010. From the estimated total of 409 000 deaths reported, about 67% of these were the deaths of children under the age of 5 years. Although with reduction in malaria cases and reported deaths, the statistics are still significantly high and alarming. Nonetheless, according to the WHO there were 10 countries that successfully eliminated malaria during the period 2010-2019 with some countries expected to have eradicated the *P. falciparum* malaria by 2025.[6]

Malaria places the biggest toll on the African continent.[6] The social and economic toll on individuals, families, communities as well as governments can be high.[10] It has been estimated that at least US$ 12 billion per year is used for all necessary costs which include, purchase of drugs and supplies for

treatment; and public health interventions against malaria.[10] Consequently, considerable economic growth is lost.[8]

Access to treatment of malaria is often problematic in areas of low-income. This is worsened by the escalation of drug resistance with one of the first line antimalarial drugs, chloroquine (CQ), becoming increasingly ineffective in nearly all parts of the world where malaria caused by P. falciparum is found.[11] Today, CQ is only used for the treatment of P. vivax infections in regions where resistance hasn't been developed.[11] As of 2016, Artemisinin-based combination therapies (ACTs) have been declared as the first and second lines (most effective) of treatment for uncomplicated cases of malaria as well as CQ resistant (CQR) malaria caused by the *P. vivax* parasite.[11] The use of ACTs has significantly decreased the global malaria burden.[12] In the past, access to ACTs has been reported to be limited but, an increase in procurement of ACTs treatment courses has been observed in recent years.[11] However, for some of these antimalarial drugs, reports of their resistance are beginning to rise.

To overcome the spread of drug resistant parasites of malaria, new drugs incorporating metal derivatives of current antimalarial drugs are being investigated.[13] Drugs of this nature are of great value as they include both an organic pharmacophore, i.e., a compound's substructure responsible for a particular pharmacological interaction with its intended target, as well as a metal. This rapid advancement of the study of organometallic complexes as antiplasmodials could potentially find candidates that are more efficacious against resistant and sensitive strains than pre-existing drugs. This review focuses on the use of organometallic complexes in the treatment of malaria.

1.2. What is malaria: Causes of malaria, Life cycle of the parasite.

Malaria is caused by the protozoan Plasmodium parasites. It is a febrile disease, i.e. has fever-like symptoms such as headache, muscle aching, dizziness, chills, diarrhoea, etc. Due to the nature of its symptoms, diagnosis can be difficult. If not treated in its early stages, malaria can become severe and may have lethal complications such as anaemia, renal failure, and convulsions.

There are several types of Plasmodium parasite that cause malaria. Five of these species that are known to cause human malaria are *P. falciparum, P. vivax, P. malariae, P. ovale and P. knowlesi* (zoonotic). By zoonotic, this implies that *P. knowlesi* normally infects animals but may be transmitted to humans on rare occasions.[14] *P. falciparum* and *P. vivax* are the most prevalent and dangerous, with *P. falciparum* being the most severe, resulting in higher mortality rate, and *P. vivax* often causing notable morbidity. The *P. falciparum* parasite is the most prevalent, especially in the WHO region of Africa.[14]

Antimalarials are developed on the basis of the parasite's biological profile as well as what stage of the parasite life cycle the antimalarial could target.[2] The life cycle of plasmodium parasite comprises two different stages with each occurring in different hosts, the human which is the intermediate host (I-IV, *Figure 1*) where the asexual phase occurs, and the female Anopheles mosquito, the definitive host (V and VI, *Figure 1*) where the sexual phase of parasite occurs.[15] In the asexual phase, asexual reproduction takes place. This process entails splitting and forming generations (known as schizogony), resulting in the formation of merozoites which then develop into male and female gametocytes in the intermediate host.[15] In the sexual phase, sexual reproduction takes place, fertilisation of gametes occurs in a process known as sporogony to produce sporozoites.[15]

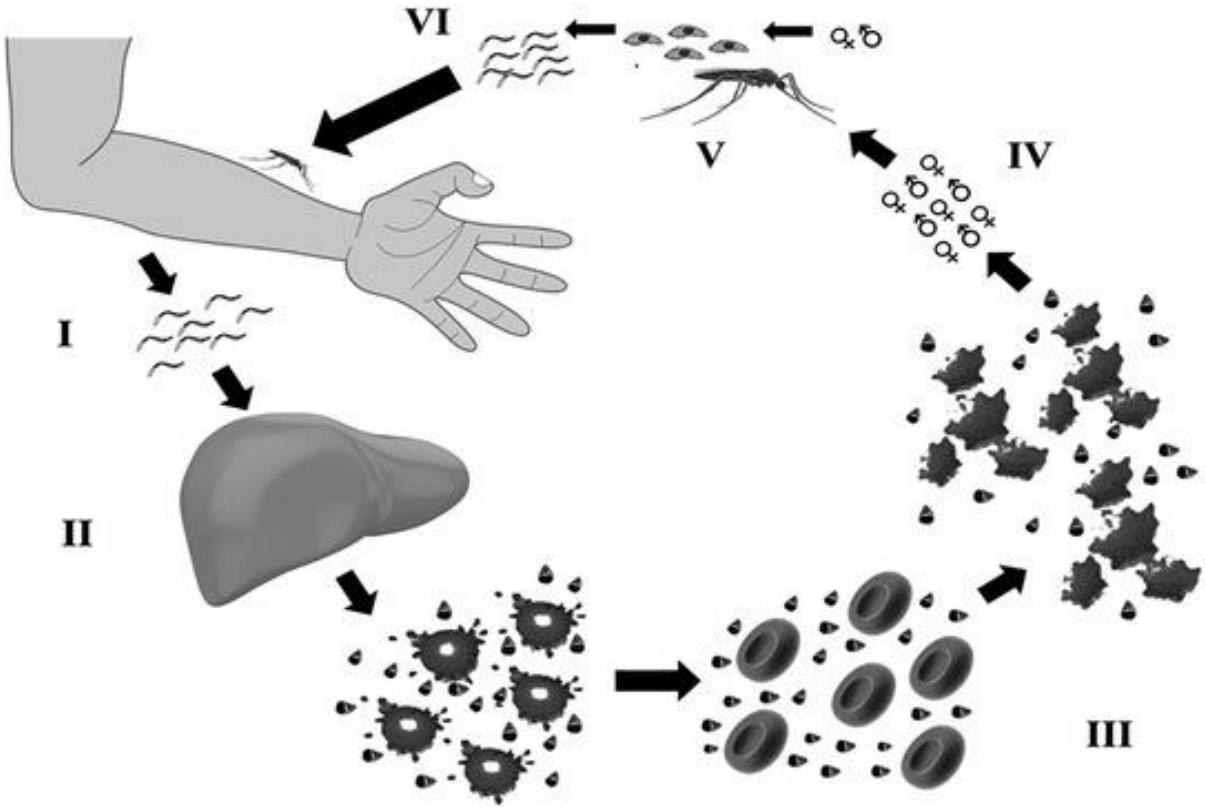

Figure 1: Life cycle of plasmodium malaria parasite. Taken from Epidemiology of Infectious Diseases.[2]

When a parasite carrying female Anopheles mosquito bites a human, it injects sporozoites (step I, *Figure 1*) into the human body. The sporozoites travel through the bloodstream to the liver (step II, *Figure 1*) and starts infecting the hepatocytes (*Figure 1*).[16] Once it has infected the liver cells, it pushes its nucleus to the periphery. The nucleus of the sporozoites multiply and eventually develop into schizonts which contain merozoites.[15]

When mature, the schizont bursts and merozoites are released into the bloodstream. Once in the bloodstream, they start to invade red blood cells (RBCs) (step III, *Figure 1*).[16] Once inside the RBC, merozoites situate themselves in the intraerythrocytic parasitophorous vacuole. There it develops into a ring-like structure appearing as a round body within a vacuole in its centre which is referred to as a young trophozoite.[15]

The trophozoite feeds on the haemoglobin proteins of the erythrocyte leaving behind a hematin globin pigment side product called malarial pigment or hemozoin pigment[17], as biocrystals[18], so as to prevent free heme since it is toxic to the parasite.[17] This pigment is different for every malaria species and it can therefore be used as an identification tool to determine which type of plasmodium parasite caused an infection. As the ring form or trophozoite develops, it enlarges in size and becomes irregular in shape and is termed the amoeboid form or late trophozoite form. As the amoeboid form develops further, its nucleus starts dividing by mitosis, then the cytoplasm also starts to divide into “mechoschizonts”. The mechoschizonts eventually bursts releasing merozoites, hemozoin and pyrogens into the bloodstream. Once pyrogens are released, the host begins to experience fever-like symptoms. This incubation period takes about 7-18 days. How long the infection takes before showing symptoms after infection depends on which parasite caused infection.[15]

The merozoites then begin to invade “healthy” or uninfected erythrocytes. This provide evidence as to why malaria causes anaemia since RBCs are being damaged. Once the erythrocyte cycle has occurred a number of times, the merozoite no longer forms the trophozoite or schizont, instead they form male and female gametocytes (step IV, *Figure 1*).[19] These gametocytes are then taken up by a mosquito when it feeds on the blood of this infected human[16].

A female Anopheles mosquito feeds on the blood of a host containing RBCs with male and female gametocytes (step V, *Figure 1*). The mosquito then digests the gametocytes which are then released into the gut of the mosquito. The female gametocytes undergo a process called maturation to form female gametes/ macrogametes. Male gametocytes on the other hand divide to form male gametes/ microgametes. Nuclear material and cytoplasm of male gametocyte divides to form 8 microgametes with long actively motile whip-like filaments. Male and female gametes undergo fertilization to form a zygote. The zygote develops into the ookinete, which further develops into the oocyst, i.e., a multiplicatory phase within which numerous sporozoites are seen. Sporozoites begin to develop in here and then multiply causing rupture. Sporozoites are then released and reach the salivary glands of the mosquito. Once in the salivary gland, the mosquito can then bite another human and the cycle repeats itself (step VI, *Figure 1*).[15]

Different antimalarials target different stages of the life cycle of the malaria parasite in the intermediate host, i.e., human. Various sites at which the parasite life cycle occurs allow for different mechanisms of action (MOA) to be possible. The most productive method is by inhibiting the formation of hematin.[20]

1.3. History of organic antimalarials

Traditional herbal remedies were initially used for the treatment of malaria for many centuries.[12] The isolation and development of chemicals effective in the treatment of malaria began in the 1800’s. Despite some of these therapeutics being very effective, there were limitations. These include side effects as well as malaria strains becoming resistant to the antimalarial drugs as time progressed.[21] Listed below are some examples of the earliest antimalarial drugs to be isolated and developed.

The first successful treatment of malaria was by quinine (*Figure 2*), a chemical found in the bark of the cinchona tree in 1820.[12] To this day, quinine is known to be one of the greatest drugs for treatment of this disease.[21] Since 2006, quinine is no longer regarded as a front-line defence drug for treatment seeing that the Plasmodium parasite has developed resistance against the drug, with the first report of resistance in the 1980’s.[21] However, it is still used in cases where artemisinins are unavailable.[21]

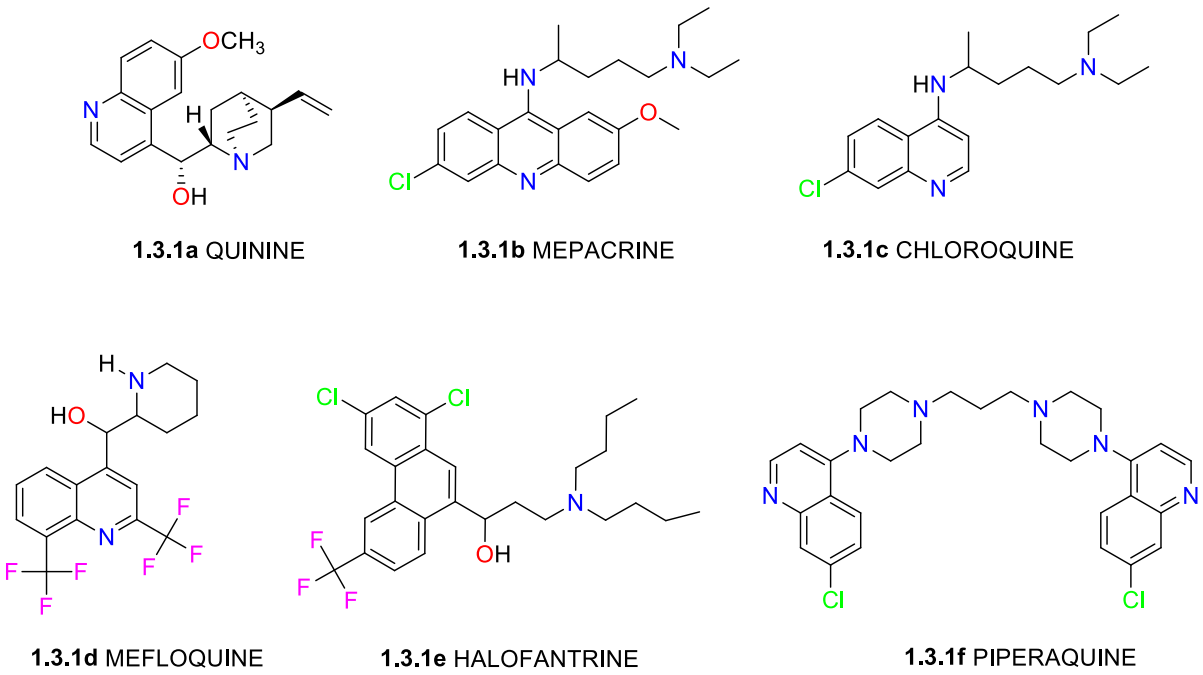

1.3.1a QUININE **1.3.1b** MEPACRINE **1.3.1c** CHLOROQUINE

1.3.1d MEFLOQUINE **1.3.1e** HALOFANTRINE **1.3.1f** PIPERAQUINE

Figure 2: Structures of antimalarials that have been used in the past.

Mepacrine (*Figure 2*) is another antimalarial drug that was developed in the 1920's[22] that was mainly used as a prophylactic as well as for the cure thereof.[21] However, the use of this drug has declined due to its undesirable side effects[21] linked to the liver such as acute liver injury which can lead to death.[22] CQ (*Figure 2*) was used in the treatment of all types of malaria with very little side effects.[21] Its MOA involves inhibiting hemozoin biocrystallization (prevention of crystallisation of heme produced by malaria parasite in RBCs), a well-known method of detoxifying in mammals.[12] Although a good antimalarial drug, several malaria strains began to show resistance to CQ. The first report of resistance was in the 1950's, and now CQ is mainly used to treat non-resistant strains caused by *P. vivax*. [21] Mefloquine (*Figure 2*), a drug which was used both as a prophylactic and treatment,[21] was developed with the aim of treating CQR strains of malaria. It was later, reported to have resistant strains.[21] Due to its undesirable side effects linked to central nervous system toxicity, mefloquine is not used extensively anymore.[21] Halofantrine (*Figure 2*), initially intended for treatment of all kinds of malaria including multidrug resistant strains of *P. falciparum*, has a similar mode of action to quinine as well as mefloquine. Its use declined after it was reported to have been associated with the death of a patient due to cardiotoxicity.[23] The use of piperaquine, (*Figure 2*) a synthetic drug believed to be as efficacious as chloroquine and more tolerable in the treatment of *P. falciparum* and *P. vivax* malaria plunged as a result of growing drug resistance of *P. falciparum* malaria strains.[24] Similar to chloroquine, piperaquine treats malaria by inhibiting the formation of hemozoin. However, piperaquine gained back its reputability when it was established that combining it with an artemisinin derivative produces a highly efficacious, affordable, short course treatment with not many side effects.[24] This combination is now recommended by WHO Model List of Essential Medicines (MLEM) whereby piperaquine needs to be used in combination with dihydroartemisinin.[24]

The global increase in the occurrence and transmission of malaria as well as resistance to known antimalarials emphasizes the need for more effective therapeutic agents. Emergence of resistant strains can be attributed to (i) expeditious reproduction period of the parasite leading to large populations of the mosquito and (ii) the miscellaneous use and misuse of antimalarials.[25] Presently,

there are fourteen antimalarial drugs for curative treatment and six for prophylaxis on the current WHO MLEM .[26] It is recommended that a combination of the drugs be taken in order to treat malaria caused by the *P. falciparum* parasite instead of monotherapy.[26]

One popular drug in the treatment of malaria today is artemisinin (*Figure 3*) isolated by a from a plant called *Artemisia annua.*[21] It is a sesquiterpene lactone which consists of a peroxide group that is believed to be an integral part of the drug's mode of action. This drug was first identified with the aim of treating CQR strains of malaria. However, it has been proven that artemisinin has been the most successful in treating multi-drug resistant strains of *P. falciparum* malaria.[12]

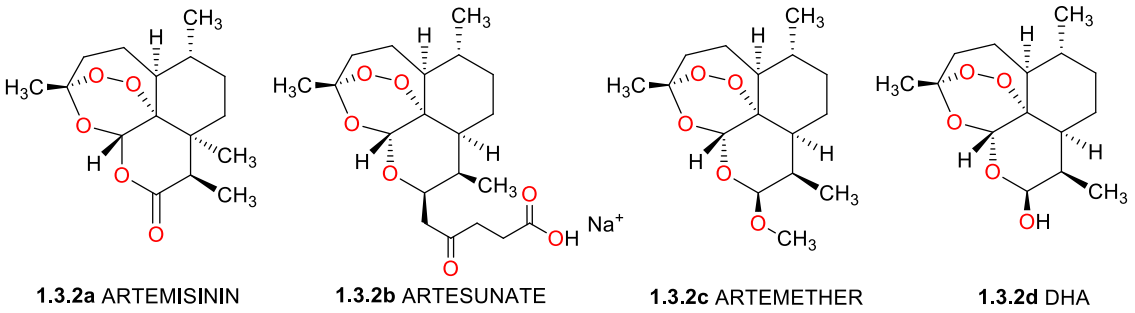

Figure 3: Structures (from left to right) of artemisinin, artesunate, artemether and dihydroartemisinin (DHA).

There are currently two derivatives of artemisinin that are included in the WHO MLEM, specifically artesunate and artemether (*Figure 3*). These two, together with dihydroartemisinin (DHA) (*Figure 3*) are some of the most effective antimalaria drugs today.[27] However, artesunate and artemether are prodrugs. This means that they are metabolized after administration, into the active DHA metabolite.[21] What sets artemisinin apart from other antimalarial drugs is the fact that it does not only target the late stages of the parasite's erythrocytic stage but also targets the early stages making it more efficacious.[27] It works by significantly reducing the number of *Plasmodium* parasites in the infected patient's bloodstream[11] by killing the ring stage forms of the parasite in the intermediate host (human) during the early stages of infection.[27]

As of 2016, artemisinin-based combination therapies (ACTs) have been declared as the first and second line (most effective) of treatment for uncomplicated cases of malaria as well as CQR malaria caused by *P. vivax* parasite.[11] The WHO recommends the use of artemisinin-based combination therapy, i.e. by combining two drugs which have different MOA, in order to be more efficacious and less prone to resistance development.[28] ACTs actually combine artemisinins (or one of its derivatives) with a partner drug.[11] Determining which partner drug to pair with artemisinins depends on its pharmacokinetic properties.[27] The artemisinin is employed to promptly decrease the number of parasites within three days of its course. Subsequently, the partner drug is responsible for clearing out the residual parasite in the bloodstream since it has a longer half-life.[11] For this reason, the partner drug usually has a longer half-life, i.e. must be able to remove remaining parasites once artemisinins are expelled from the body.[27]

The use of ACTs has significantly decreased the global malaria burden.[12] Like many other antimalarial drugs, its limitation is onset of resistance. Resistance to ACTs is slow to develop but, it has been reported at the Thailand-Cambodia border in 2008.[27] It is believed that this is not the first actual emergence of resistance. The first emergence may have been in 2001 prior to distribution of these drugs in Cambodia.[27]

Amodiaquine (*Figure 4*) is a drug usually used in combination with artesunate to make ACTs as recommended by WHO MLEM. Is it said that its MOA as well as side effects are similar to those of CQ.[29] However, amodiaquine also modifies the DNA of the host. Even with their similarities, amodiaquine is actually a better therapeutic for uncomplicated cases of *P. falciparum* malaria compared to CQ in some parts where resistance has not developed, such as Africa, some parts of South America as well as Oceania.[30] It has also been reported to be effective on some CQR strains. Notable side effects of amodiaquine have been reported such as leukopenia, hepatitis and agranulocytosis typically in cases where it was applied as prophylaxis.[30] Due to its side effects, the use of amodiaquine as a prophylactic may be complicated particularly in pregnant women thus it is used for treatment only.

Sulfadoxine (*Figure 4*) is a sulfonamide that was used for prophylaxis of malaria but was discontinued due to growing resistance. Sulfadoxine and pyrimethamine (*Figure 4*) have been used together since 1981[21] for treatment of CQR malaria caused by plasmodium parasite.[31] In combination, these drugs inhibit plasmodial forms of dihydrofolate reductase (DHFR) as well as dihydropteroate synthetase (DHPS) which are two of the most fundamental enzymes in the folate biosynthetic pathway of the parasite.[32] Due to their synergistic effect, sulfadoxine and pyrimethamine are better when used in combination as opposed to single compounds.[31] However, resistance started emerging following point mutations in the genes of these enzymes.[32] In order to avoid treatment failure attributed to resistance, sulfadoxine and pyrimethamine is now used in combination with artesunate. Incorporating artesunate into this combination has a number of benefits including; helping reduce spread of resistance, prevent recurrence of malaria infection and hindering with transmittance of *P. falciparum* parasite to name a few.[33] This combination is listed both for treatment and chemoprevention on WHO MLEM whereby: for treatment, it is recommended to be taken in combination with artesunate whereas for prophylaxis, amodiaquine is the preferred combination drug.[26]

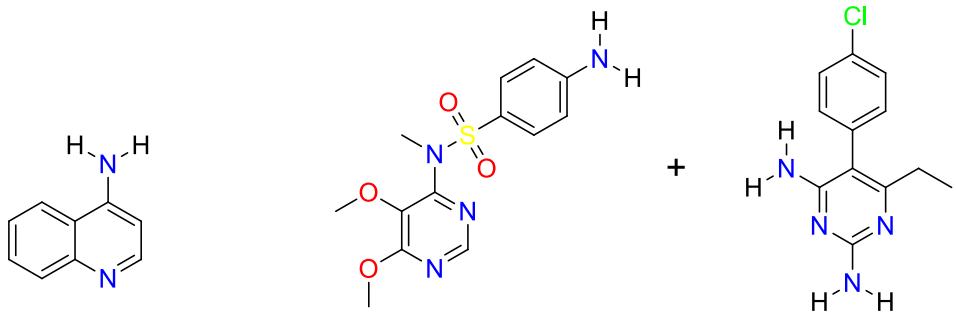

1.3.3a 4-AMINOQUINOLINE SULFADOXINE (**1.3.3b**) + PYRIMETHAMINE (**1.3.3c**)

Figure 4: Structures (from left to right) of 4-amodiaquinoline, sulfadoxine and pyrimethamine.

One evident factor to take note of is that none of the therapeutics mentioned above, or on the WHO MLEM, 2019, have metals incorporated into them.

1.4. Metal complexes as antiplasmodials

Metals play a fundamental role in our everyday lives. With regards to human health, several metals are essential to vital biological processes. The periodic table contains a variety of metals thus it may have been intriguing for researchers to explore the applicability of other metals to living organisms.[34] To this day, cisplatin (*Figure 5*) is still a leading drug for treatment of different types of cancer. Metals

with similar chemical and physical properties to platinum, i.e. iridium, rhodium, ruthenium, osmium and palladium, termed platinum group metals (PGMs) are also of interest to researchers.[35] It has been reported that complexes of these metals have shown great activity as anticancer, antibacterial, antiplasmodial and antivirals agents.[1,36, 37,38,39]

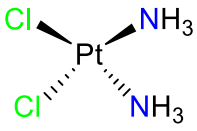

1.4.1a CISPLATIN

Figure 5: Structure of cisplatin.

The first class of metal-based antimalarial drugs were developed by incorporating metals into the already existing drug CQ, i.e. ruthenium (Ru(II))-CQ binuclear complex (see **1.4.2a** on *Figure 6*).[2,40] Ruthenium (Ru) was the metal chosen due to the extensive research that has been done on its application in various fields of medicine.[2] Upon comparison to CQ, it was found that the Ru(II) complex was five times more potent against strains of *P. falciparum* and *P. berghei* (causative agent of malaria in rodents). Additionally, this drug showed excellent antiplasmodial activity against CQR strains.[40] Arene-Ru(II)-CQ complexes (see **1.4.2b** on *Figure 6*) were also synthesized and these were found to have substantial activity against malaria.

A ferrocene complex, ferroquine (FQ) however, demonstrated the greatest efficacy against CQ sensitive (CQS) and CQR strains of *P. falciparum* (*Figure 6*) *in vitro* and *in vivo*.[2,41] The synthesis of this complex involves the insertion of a ferrocene moiety into the lateral chain of the known antimalarial, CQ.[41] This great efficacy observed for FQ can be attributed to the fact that ferrocene is a very stable, highly lipophilic metal that has accessible redox states and low toxicity. To this day, ferroquine (FQ) is the most effective potential organometallic antimalarial currently in development. It is twenty times more potent than CQ with a similar MOA.[2] For this reason, FQ is undergoing phase II clinical trials as an antimalarial drug.[2] This guided research to the development of ruthenocene analogues of FQ. These complexes showed a similar MOA to that of FQ with good activities.[2]

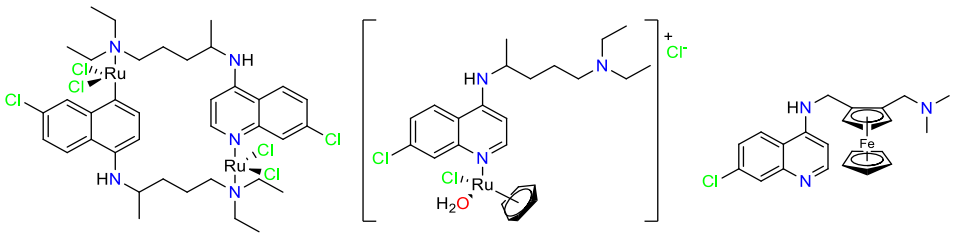

1.4.2a **1.4.2b** **1.4.2c** FERROQUINE

*Figure 6: Structures of Ru binuclear complex (**1.4.2a**), arene-Ru(II)-CQ(**1.4.2b**) and ferroquine (FQ)(**1.4.2c**).*

The second metal to be considered for integration into CQ was gold (Au) (see **1.4.3a** on *Figure 7*). These complexes displayed great potential as therapeutics for not only malaria, but other diseases as well.[2] Following these results, Navarro, *et al*, developed new similar complexes with a PGM, iridium (Ir).[42] The three compounds (*Figure 7*) were synthesized, characterized and their *in vitro* activity against the *Plasmodium berghei* strain of malaria was tested. Upon investigation by comparison of the complexes IC_{50} values, it was found that complex **1.4.3c** showed the highest activity whereas

complexes **1.4.3b** and **1.4.3d** showed lower activity. With an IC_{50} value of 59 nM, complex **1.4.3c** showed a slight increase in activity in comparison to CQ.[42] In contrast, complex **1.4.3b** (72 nM) and **1.4.3d** (126 nM), were not as active. These results further validates that introducing a metal into an inorganic scaffold has the potential to increase its activity.[1,2,42]

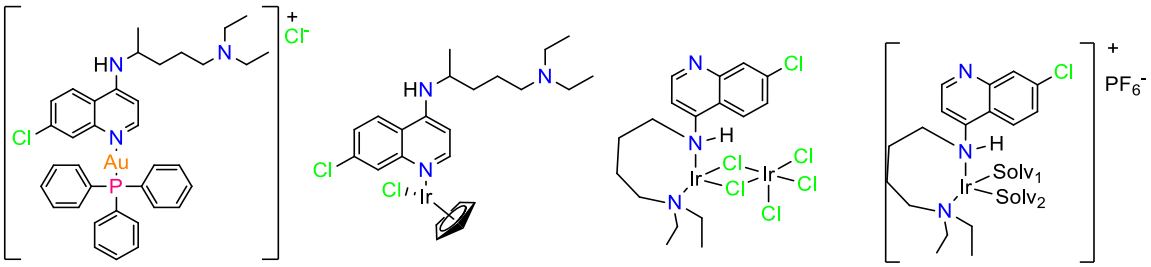

1.4.3a **1.4.3b** **1.4.3c** **1.4.3d**

*Figure 7: Structures of gold complex (**1.4.3a**) and CQ derivatised complexes (**1.4.3b-d**).*[42]

Rhodium (Rh) has not always been the metal of choice in the field of medicine, it is only recently that researchers have developed an interest in it. One of the reasons for this sudden interest in Rh is due to the variety of biological and chemical properties that are adjustable. Developing Rh complexes as antimalarials also offers varying MOAs and diversifies the range of said drugs.[43] The earliest example of an antimalarial Rh complex was also reported by Navarro *et al* in 1996 where they synthesized Rh and Ru complexes of CQ and tested their activity against *Plasmodium berghei* (*Figure 8*).[44]

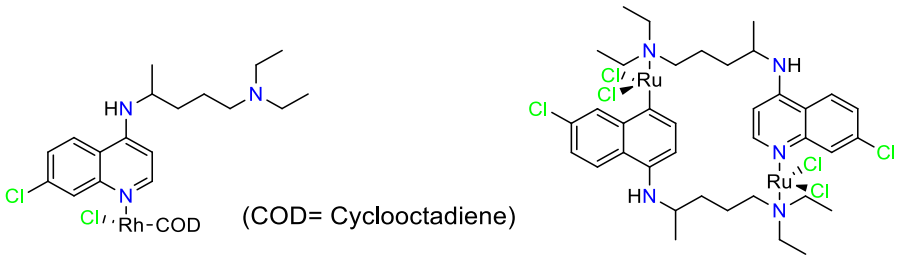

1.4.3e **1.4.3f**

*Figure 8: Structure of RhCl(COD)(CQ) (**1.4.3e**) and $[RuCl_2(CQ)]_2$ (**1.4.3f**).*[44]

From this study, it appeared that both complexes had inhibitory action with complex **1.4.3f** having similar activity to CQ diphosphate and complex **1.4.3e** being five times more active. Since complex **1.4.3e** showed better activity, further investigations were done against CQ resistant strains of *Plasmodium falciparum*. Reportedly, this incorporation of Ru also led to a 2-5 fold increase in activity without acute toxicity.[44]

Ekengard *et al.* reports the synthesis of *N,N* and *N,O* chelating chloroquine derivatives of iridium and rhodium complexes.[45] Electronic variation of the salicylaldimine (*N,O*) ligands in the *para* position of the salicyl moiety was also explored. This was done by introducing H, F, Cl, Br, I, NO_2, OMe and *t*-Bu to study the effect on the antimalarial activity of the resulting ligands and complexes. The *in vitro* biological activity of the ligands and complexes were tested against two strains of the *P. falciparum* parasite, i.e., CQS strain, NF54, and the CQR strain, Dd2, with CQ and artesunate as references. Ruthenium analogues of these ligands that had been previously reported showed that incorporating the ruthenium para-cymene moiety showed poor activity against the malaria strains.[46] Iridium analogues of these complexes on the other hand showed moderate activities whereas the *N,N*

derivatives showed inactivity. It was found that the salicylaldimine rhodium complexes with electron withdrawing groups on the para position of the salicyl moiety exhibited the best activities against both strains. Additionally, complexes **1.4.4.3e (Rh)** (IC_{50} = 0.016 ± 0.002 μM), **1.4.4.3f (Rh)** (IC_{50} = 0.020 ± 0.006 μM) and **1.4.4.3g (Rh)** IC_{50} = 0.018 ± 0.006 M (*Figure 9*) showed better activity than CQ (IC_{50} = 0.027 ± 0.011 μM) against the CQS NF54 strain, however, not as active as artesunate (IC_{50} = <0.005 μM). The exceptional activity of complex **1.4.4.3e (Rh)** was reported to have the best antiplasmodial activity of complexes without a ferrocene moiety.[45]

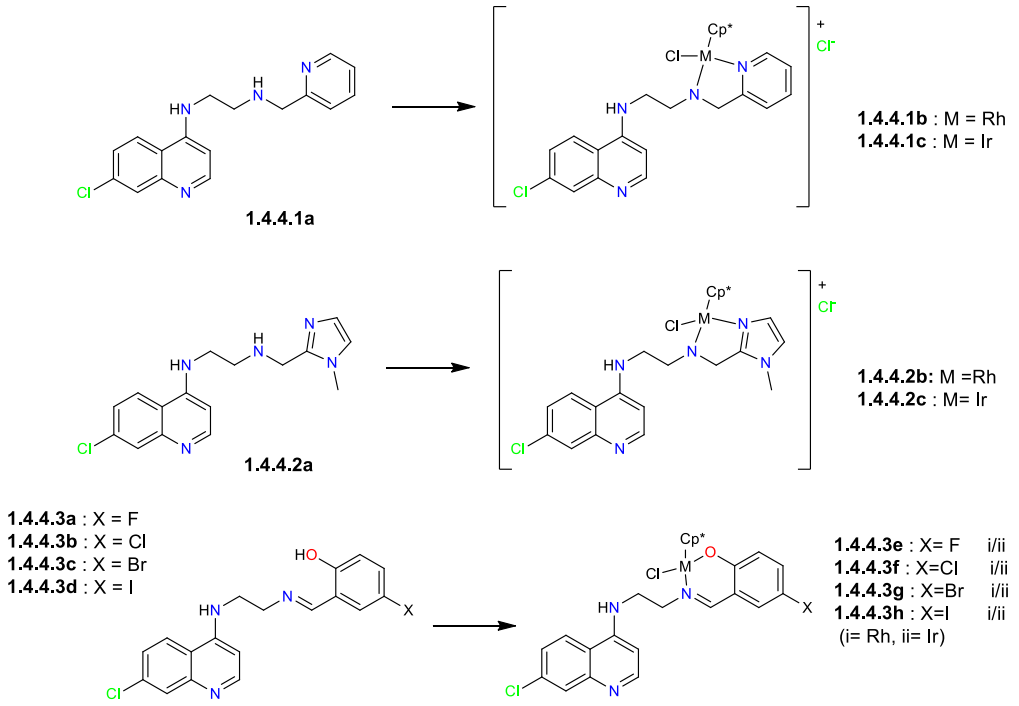

Figure 9: Structure of ligands and complexes reported by Ekengard.[45]

Seven iridium complexes of 7-chloroquinoline-1,2,3-triazole hybrid ligands were synthesized, the ligands' and complexes' *in vitro* biological activity against CQS NF54 *P. falciparum* strain(*Figure 10*).[47] The *in vitro* assays showed that all the ligands were not highly potent against the NF54 *P. falciparum* strain (IC_{50} = 9.97 – 28.02 μM). Incorporation of the iridium metal shows significant improvement in activity where complex **1.4.5.2** was over a 100-fold more active than its parent ligand **1.4.5.1f**. Complexes showed activity in the order **1.4.5.2** > **1.4.5.3a** > **1.4.5.3e** > **1.4.5.3b** > **1.4.5.3d** > **1.4.5.3c** > **1.4.5.4**. This trend in activity showed that the introduction of the hydrophobic R groups does not have a significant role in the resulting potency against the NF54 *P. falciparum* parasite strains. The monodentate coordinated complex **1.4.5.4** showed the least activity (IC_{50} = 48.45 $\pm$ 1.73 μM) suggesting that stability provided by the coordination of the metal in a bidentate fashion as seen for complexes **1.4.5.3a**-**1.4.5.3f** plays an important role in the efficacy of the complex against NF54 malarial strains. Complexes that showed higher activity against NF54 were also tested against CQR K1 strain, activity was found to be in the IC_{50} range of 0.13 – 3.06 μM. Analysis of the resistant indices of the complexes indicated trace existence of resistance. The *in vitro* cytotoxicity of the complexes against Chinese Hamster ovarian cancer cell line was also evaluated using emetine as a positive control. No cytotoxicity was displayed by the complexes. β-Haematin inhibition studies were conducted to investigate the potential MOA of this class of complexes using **1.4.5.1g**, **1.4.5.3d** and **1.4.5.3f** with antimalarial drug CQ as a control. The complexes did show β-haematin inhibition, however, not to the same degree CQ.[47]

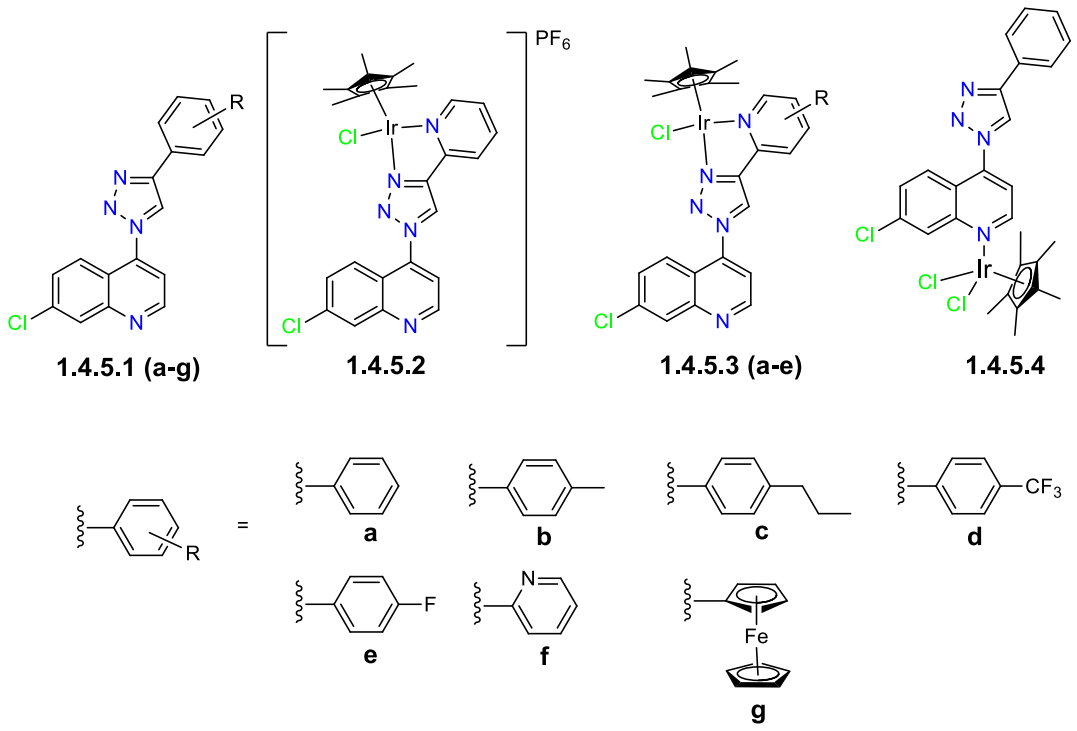

Figure 10: Structure of 7-chloroquinoline-1,2,3-triazole hybrid ligands and ruthenium complexes reported by Melis et al.[47]

Metal complexes of other existing clinical drugs for potential malaria treatment have also been synthesized, these include quinoline derivatives, i.e., mefloquine, amodiaquine and primaquine. Moreover, several metals were investigated in conjunction with Rh, Cu, Fe, Au, Ni, Pt, etc. It was discovered that these modified drugs could potentially be the next generation of therapeutics.[2]

Iridium, rhodium and ruthenium pyridyl- and quinolyl imino half sandwich organometallic complexes containing the drug sulfadoxine were synthesized and their antiparasitic activity evaluated by Chellan *et al.*[48] (*Figure 9*). The *in vitro* antiplasmodial activity against various parasite strains and *Mycobacterium tuberculosis* bacteria were evaluated. The parasite strains included three *P. falciparum* strains, i.e., 3D7 CQ sensitive strain, CQR strain, Dd2, as well as NF54 (sexual late stage gametocyte (LSG)), and, *Trichomonas vaginalis*. It was reported that several complexes exhibited efficacy in the sexual LSG assay against *P. falciparum* strains. However, upon investigation of sulfadoxine and other known antimalarial drugs (pyrimethamine and CQ) in the same assays, no evidence of any inhibitory action was found, they were all inactive.

Researchers have shown interest in benzimidazole and its derivatives due to its antiplasmodial activity against antimalarials[49] as well as antitumor[50] and antiretroviral activity[51]. For this reason, it is recognized as a promising organic scaffold in medicine. A study on the synthesis, characterization and *in vitro* biological studies of substituted 2-phenylbenzimidazoles (H, Cl, CH_3 and CF_3) ligands and iridium, rhodium and ruthenium complexes was carried out by Rylands *et al(Figure 11).*[52] The antiplasmodial activity of the ligands and complexes were evaluated against *P. falciparum* NF54 CQS strain. The derivatized ligands **1.4.6a** – **1.4.6d** showed weak antimalarial activity (IC_{50} = 17.66 – 22.32 μM) against the NF54 strain.

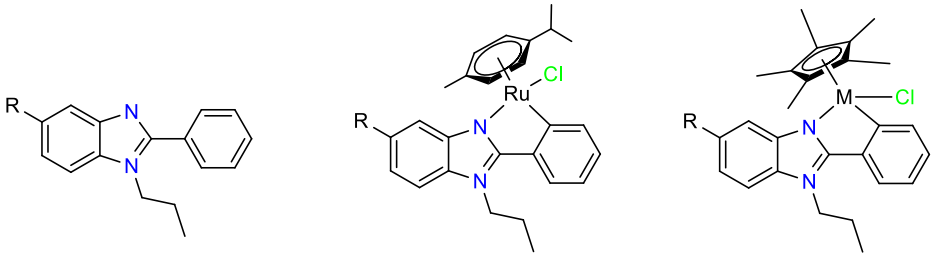

1.4.6a : R = H
1.4.6b : R = Cl
1.4.6c : R = CH_3
1.4.6d : R = CF_3

1.4.6.1a : R = H
1.4.6.1b : R = Cl
1.4.6.1c : R = CH_3
1.4.6.1d : R = CF_3

1.4.6.2a : R = H i/ii
1.4.6.2b: R = Cl i/ii
1.4.6.2c : R = CH_3 i/ii
1.4.6.2d : R = CF_3 i/ii
M = Ir or Rh

Figure 11: Structures of 2-phenylbenzimidazoles ligands and complexes reported by Rylands et al.[52]

Incorporation of the metals onto the substituted 2-phenylbenzimidazole ligands significantly improved their antiplasmodial activity resulting in a low range of inhibitory concentrations of 0.12 – 5.17 μM. It was observed that the substituents did not seem to have a great impact on the antiplasmodial activities of the complexes. Cyclometallated complexes showed activity in the order Ru>Ir>Rh across all the series of complexes. As a result, further screening of the ruthenium and iridium complexes was carried out against the CQR *P. falciparum* strain, K1, which is also resistant to multiple other drugs. Activity of the complexes against this strain showed the ruthenium analogues to be twice more active than the iridium complexes. A loss of activity observed against K1 strain compared to activity against NF45 was attributed to reduced ability to target the resistant strains. Cytotoxicity studies of the hydrogen substituted ruthenium (IC_{50} = 50.92 $\pm$ 0.81 μM) and iridium complexes (IC_{50} = 20.71 $\pm$ 0.23 μM) performed against the Chinese Hamster Ovarian (CHO) cells displayed low toxicity. In an attempt to investigate the potential MOA, the -haematin inhibition studies did not show any activity up to 500 μM implying a different MOA. The activity of these complexes, their relatively low cytotoxicity and resistance indices (RI) indicates their promising application as new antimalarials, thus further studies are required for this class of compounds.[52]

The synthesis and study of 7-nitrobenzoxadiazole (NBD) ligands and *N,N* ruthenium half-sandwich complexes as antiplasmodials were reported by Milheiro and co-workers (*Figure 12*).[53] The *in vitro* antiplasmodial activity of the complexes was evaluated against the blood stage CQS 3D7-GFP, CQR Dd2 as well as artemisinin-resistant IPC5202 *P. falciparum* strains with CQ, DHA and primaquine used as a reference. Thereafter, the antimalarial activity of the complexes against the human hepatic cells, HepG2, their relative cytotoxicity and theirs SI's were evaluated. Ruthenium complexes **1.4.7a** – **1.4.7c** (IC_{50} = 7.69-12 nM) exhibited high potency against the CQS 3D7-GFP strain of *P. falciparum* parasites in the order 2>1>3 whereas **1.4.7d** and **1.4.7e** (IC_{50} = 219 $\pm$ 62 nM and IC_{50} = 139 $\pm$ 54 nM respectively) were weakly active. Low potency was observed for all complexes against CQR Dd2 strains, however, the activities were still better than that of CQ. **1.4.7a-c** also displayed better activity in comparison to **1.4.7d** and **1.4.7e** against artemisinin-resistant IPC5202 *P. falciparum* strains, even so, lower RIs were obtained for **1.4.7d** and **1.4.7e**. The bulkier pentamethylcyclopentadientyl moiety of **1.4.7c** compared to the less bulky cyclopentadiene of **1.4.7b** did not pay any significant role in the activity against the *P. falciparum* strains even with increased lipophilicity. A measure of the complexes' cytotoxicity against the human hepatic cells, HepG2, revealed that complexes **1.4.7a-c** were not highly toxic. It was reported that these complexes are amongst the most promising cyclometallated antimalarials to date.[53]

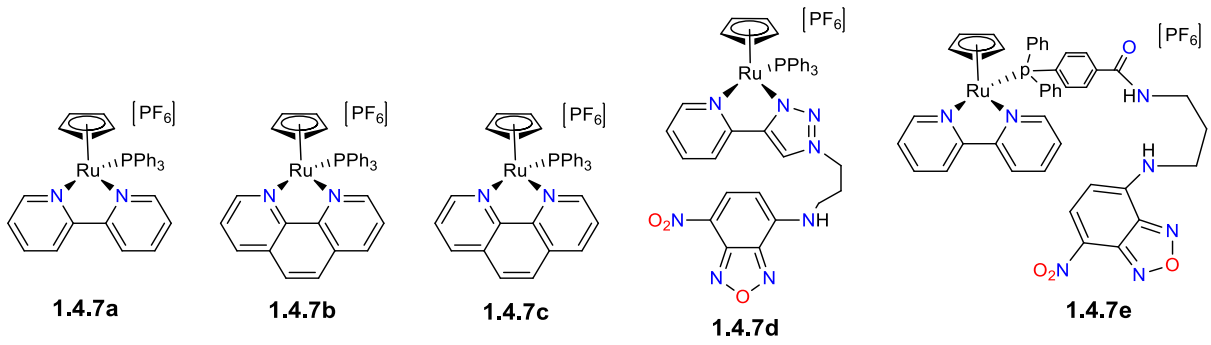

Figure 12: Structure of N,N ruthenium half-sandwich complexes. [53]

1.5. Summary

Reports of widespread reduced efficacy of current drugs due to the growing resistance of malaria parasites is one of the biggest issues in the management of the malaria endemic. It is thus important to design and study new compounds for the treatment of malaria. For many years, the discovery and development of antiplasmodials against malaria was predominantly focused on the derivatisation of known antimalarials in an effort to overcome resistance. Extensive studies of the biological activity of CQ derivatized metal complexes aimed at discovering new and effective antimalarials has been done. These efforts have resulted in the discovery of ferroquine, a drug candidate which has reached Phase II clinical trials. Recently, increasingly more research has gone into the development of metal complexes containing organic scaffolds as several reports have observed an improvement in their biological activity against malaria parasites once incorporated with a metal. Incorporating a metal into and organic scaffold results in complexes with great properties as they include both an organic pharmacophore as well as a metal offering different properties. The nature of the cyclometallated complexes allows for adaptations that can improve the compound's activity and its physicochemical properties. Thus, this area of research continues to thrive and in this thesis we discuss the study of dipyridylamino complexes of the PGMs Ru(II), Ir(III) and Rh(III) as antiplasmodials.

2,2-Dipyridylamine, is a versatile ligand and it's chlorido and iodide complexes with ruthenium,[54] rhodium and iridium[55] have been evaluated for *in vitro* biological activity against a human ovarian cancer cell line, A2780. No data has been reported on their applicability as antiplasmodials. In this thesis the synthesis, characterization and biological activity of the same six complexes as well as six more nitrate complexes will be studied.

1.6. Aims and objectives:

1.6.1. Aims

The aim of this project was to synthesize and characterize a library of iridium (Ir), rhodium (Rh) and ruthenium (Ru) half-sandwich organometallic complexes from 2,2-dipyridylamine (dpa), where the complexes were isolated with either a PF_6^- counterion or NO_3^- counterion. The intention was to observe whether the counterion will influence biological activity. The aqueous solubility and interaction with water and DMSO of the ligand and complexes would then be studied, and they would be screened for in vitro biological activity against malaria strains.

1.6.2. Objectives:

1.6.2.1. Twelve cationic *N,N'*-chelated half-sandwich organometallic complexes of 2,2-dipyridylamine were synthesized according to scheme 1 below. **C1**-**C6** were synthesized and underwent counterion exchange to PF_6^-. **C7**-**C12**(novel) also underwent a counterion exchange to NO_3^-.

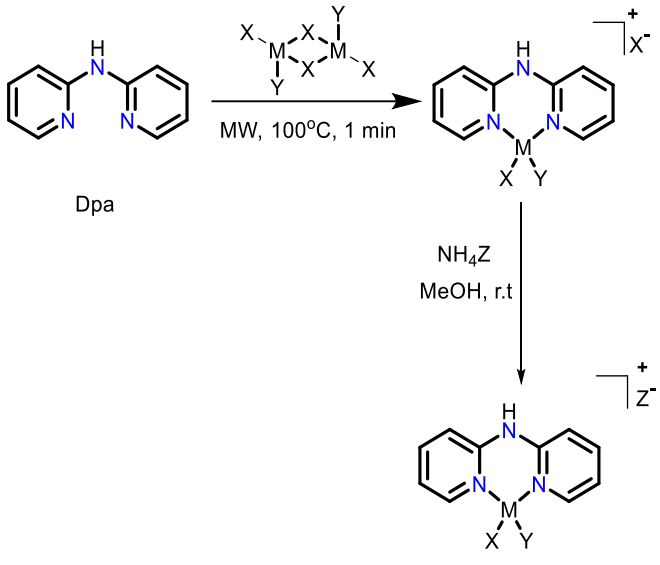

C1: M = Ir, X = Cl, Y = Cp*, Z = PF_6
C2: M = Ir, X = I, Y = Cp*, Z = PF_6
C3: M = Rh, X = Cl, Y = Cp*, Z = PF_6
C4: M = Rh, X = I, Y = Cp*, Z = PF_6
C5: M = Ru, X = Cl, Y = p-cymene, Z = PF_6
C6: M = Ru, X = I, Y = p-cymene, Z = PF_6
C7: M = Ir, X = Cl, Y = Cp*, Z = NO_3
C8: M = Ir, X = I, Y = Cp*, Z = NO_3
C9: M = Rh, X = Cl, Y = Cp*, Z = NO_3
C10: M = Rh, X = I, Y = Cp*, Z = NO_3
C11: M = Ru, X = Cl, Y = p-cymene, Z = NO_3
C12: M = Ru, X = I, Y = p-cymene, Z = NO_3

*Scheme 1: Synthetic route for the synthesis of complexes **C1**-**C12**.*

1.6.2.2. Characterization was done using the following analytical techniques; infrared spectroscopy (ATR-FTIR), nuclear magnetic resonance (NMR) spectroscopy, mass spectrometry (MS), high performance liquid chromatography (HPLC), cyclic voltammetry (CV) and single crystal X-ray diffraction (XRD) discussed in Chapter 2.

1.6.2.3. The aqueous solubility of the complexes was studied using turbidimetric assay which will we discussed in detail in chapter 3.

1.6.2.4. The hydrolysis studies of the complexes was done under biologically relevant conditions. The results of this study will be analysed in Chapter 3.

1.6.2.5. *In vitro* biological activity of the ligand and complexes against CQS 3D7 strain and the drug sensitive NF54 strain of the *P. falciparum* parasite was investigated. The inhibitory concentrations of these compounds are discussed in detail in chapter 3.

1.7. References:

(1) Nkoana, W.; Nyoni, D.; Chellan, P.; Stringer, T.; Taylor, D.; Smith, P. J.; Hutton, A. T.; Smith, G. S. Heterometallic Half-Sandwich Complexes Containing a Ferrocenyl Motif : Synthesis , Molecular Structure , Electrochemistry and Antiplasmodial Evaluation. *J. Organomet. Chem.* **2014**, *752*, 67–75. https://doi.org/10.1016/j.jorganchem.2013.11.025.

(2) Marcelino, P. R. F.; Moreira, M. B.; Lacerda, T. M.; da Silva, S. S. Metal-Based Drugs for Treatment of Malaria. In *Biomedical Applications of Metals*;, **2018**; pp 167–193. https://doi.org/10.1007/978-3-319-74814-6_8.

(3) Zheng, J.; Rubin, E. J.; Bifani, P.; Mathys, V.; Lim, V.; Au, M.; Jang, J.; Nam, J.; Dick, T.; Walker, J. R.; Pethe, K.; Camacho, L. R. Para-Aminosalicylic Acid Is a Prodrug Targeting Dihydrofolate Reductase in Mycobacterium Tuberculosis. *J. Biol. Chem.* **2013**, *288* (32), 23447–23456. https://doi.org/10.1074/jbc.M113.475798.

(4) Bruijnincx, P. C.; Sadler, P. J. New Trends for Metal Complexes with Anticancer Activity. *Curr. Opin. Chem. Biol.* **2008**, *12* (2), 197–206. https://doi.org/10.1016/j.cbpa.2007.11.013.

(5) WHO. *Malaria Report 2018*; **2018**.

(6) WHO. *World Malaria Report 2018: Guinea*; **2018**.

(7) Doolan, D. L.; Doban, C.; Baird, J. K. Acquired Immunity to Malaria. *Clin. Microbiol. Rev.* **2009**, *22* (1), 13–36. https://doi.org/10.1128/CMR.00025-08.

(8) Malaria| Frequently Asked Questions (FAQs) www.cdc.gov/malaria/about/faqs.html#/ (accessed Jul 24, 2018).

(9) Fact Sheet: World Malaria Report http://www.who.int/news-room/fact-sheets/detail/malaria / (accessed Jun 1, 2020).

(10) Malaria | Malaria's impact wordlwide https://www.cdc.gov/malaria/malaria_worldwide/impact.html (accessed Jul 24, 2018).

(11) Q&A on artemisinin resistance https://www.who.int/malaria/media/artemisinin_resistance_qa/en/ (accessed Jan 21, 2020).

(12) Hempelmann, E. History of Malaria. **2017**, No. July 2010.

(13) Mutabingwa, T.; Nzila, A.; Mberu, E.; Nduati, E.; Winstanley, P.; Hills, E.; Watkins, W. Chlorproguanil-Dapsone for Treatment of Drug-Resistant Falciparum Malaria in Tanzania. *Lancet* **2001**, *358* (9289), 1218–1223. https://doi.org/10.1016/S0140-6736(01)06344-9.

(14) International travel and health https://www.who.int/ith/diseases/malaria/en/.

(15) Lifecycle https://www.cdc.gov/malaria/about/biology/index.html# (accessed Nov 26, 2019).

(16) Breman, J. G.; Mills, A.; Snow, R. W.; Mulligan, J.; Lengeler, C.; Mendis, K.; Sharp, B.; Morel, C.; Marchesini, P.; White, N. J.; Steketee, R. W.; Doumbo, O. K. Chapter 21 Conquering Malaria. In *Disease Control Priorities in Developing Countries. 2nd edition.*; Jamison DT, Breman JG, Measham AR, et al., Ed.; Oxford University Press: Washington (DC), **2006**; pp 413–431.

(17) Nagaraj, V. A.; Sundaram, B.; Varadarajan, N. M. Malaria Parasite-Synthesized Heme Is Essential in the Mosquito and Liver Stages and Complements Host Heme in the Blood Stages of Infection. *PLoS Pathog.* **2013**, *9* (8). https://doi.org/10.1371/journal.ppat.1003522.

(18) Coronado, L. M.; Nadovich, C. T.; Spadafora, C. *Malarial Hemozoin : From Target to Tool*; Elsevier B.V., **2014**; Vol. 1840. https://doi.org/10.1016/j.bbagen.2014.02.009.

(19) Meibalan, E.; Marti, M. Biology of Malaria Transmission. **2017**, *7* (3), 1–16. https://doi.org/10.1101/cshperspect.a025452.

(20) Summers, K. A Structural Chemistry Perspective on the Antimalarial Properties of Thiosemicarbazone Metal Complexes. *Mini-Reviews Med. Chem.* **2019**, *9* (7). https://doi.org/10.2174/1389557518666181015152657.

(21) Tse, E. G.; Korsik, M.; Todd, M. H. The Past, Present and Future of Anti-Malarial Medicines. *Malar. J.* **2019**, *18* (1), 1–21. https://doi.org/10.1186/s12936-019-2724-z.

(22) LiverTox: Clinical and Research Information on Drug-Induced Liver Injury https://www.ncbi.nlm.nih.gov/books/NBK547866/ (accessed Jan 21, 2020).

(23) Bouchaud, O.; Imbert, P.; Touze, J. E.; Dodoo, A. N.; Danis, M.; Legros, F. Fatal Cardiotoxicity Related to Halofantrine: A Review Based on a Worldwide Safety Data Base. *Malar. J.* **2009**, *8* (1). https://doi.org/10.1186/1475-2875-8-289.

(24) Davis, T. M. E.; Hung, T. Y.; Sim, I. K.; Karunajeewa, H. A.; Ilett, K. F. Piperaquine: A Resurgent Antimalarial Drug. *Drugs* **2005**, *65* (1), 75–87. https://doi.org/10.2165/00003495-200565010-00004.

(25) Cox, F. E. History of the Discovery of the Malaria Parasites and Their Vectors. *Malar. J.* **2006**, *5* (48). https://doi.org/10.1186/1475-2875-5-48.

(26) WHO. *World Health Organization Model List of Essential Medicines*; **2019**.

(27) Ouji M, Augereau JM, Paloque L, B.-V. F. Plasmodium Falciparum Resistance to Artemisinin-Based Combination Therapies: A Sword of Damocles in the Path toward Malaria Elimination. *Parasite* **2018**, *25* (24). https://doi.org/10.1051/parasite/2018021.

(28) Overview of malaria treatment https://www.who.int/malaria/areas/treatment/overview/en/ (accessed Jan 21, 2020).

(29) Kuhlmann, M. F, Fleckenstein, J. M. Antiparasitic Agents. In *Infectious diseases (4th edition)*; Jonathan Cohen, William G. Powderly, S. M. O., Ed.; Elsevier, **2017**; pp 1345–1372. https://doi.org/10.1016/B978-0-7020-6285-8.00157-X.

(30) Hoffman, L. S , White, N. J. Malaria. In *Tropical Infectious Diseases*; Richard L. Guerrant, David H. Walker, P. F. W., Ed.; Elsevier, **2011**; pp 646–675. https://doi.org/https://doi.org/10.1016/C2009-0-40410-0.

(31) Vinayak, S.; Alam, T.; Mixson-Hayden, T.; McCollum, A. M.; Sem, R.; Shah, N. K.; Lim, P.; Muth, S.; Rogers, W. O.; Fandeur, T.; Barnwell, J. W.; Escalante, A. A.; Wongsrichanalai, C.; Ariey, F.; Meshnick, S. R.; Udhayakumar, V. Origin and Evolution of Sulfadoxine Resistant Plasmodium Falciparum. *PLoS Pathog.* **2010**, *6* (3). https://doi.org/10.1371/journal.ppat.1000830.

(32) Gatton, M. L.; Martin, L. B.; Cheng, Q. Evolution of Resistance to Sulfadoxine-Pyrimethamine in Plasmodium Falciparum. *Antimicrob. Agents Chemother.* **2004**, *48* (6), 2116–2123. https://doi.org/10.1128/AAC.48.6.2116-2123.2004.

(33) Elamin, S. B.; Malik, E. M.; Abdelgadir, T.; Khamiss, A. H.; Mohammed, M. M.; Ahmed, E. S.; Adam, I. Artesunate plus Sulfadoxine-Pyrimethamine for Treatment of Uncomplicated Plasmodium Falciparum Malaria in Sudan. *Malar. J.* **2005**, *4*, 3–6. https://doi.org/10.1186/1475-2875-4-41.

(34) Lippert, B. *Uses of Metal Compounds in Medicine*; Elsevier Inc., **2013**. https://doi.org/10.1016/b978-0-12-409547-2.05375-0.

(35) Mbaba, M.; Golding, T. M.; Smith, G. S. Recent Advances in the Biological Investigation of Organometallic Platinum-Group Metal (Ir, Ru, Rh, Os, Pd, Pt) Complexes as Antimalarial Agents. *MDPI* **2020**, *25* (22), 1–18.

(36) Franz, K. J.; Metzler-Nolte, N. *Introduction: Metals in Medicine*; **2019**; Vol. 119. https://doi.org/10.1021/acs.chemrev.8b00685.

(37) Gichumbi, J. M.; Holger, F. B. Half-Sandwich Complexes of Platinum Group Metals (Ir, Rh, Ru and Os) and Some Recent Biological and Catalytic Applications. *J. Organomet. Chem.* **2018**, *866*, 123–143. https://doi.org/10.1016/j.jorganchem.2018.04.021.

(38) Deo, K. M.; Ang, D. L.; Mcghie, B.; Rajamanickam, A.; Dhiman, A.; Khoury, A.; Holland, J.; Bjelosevic, A.; Pages, B.; Gordon, C.; Aldrich-wright, J. R. Platinum Coordination Compounds with Potent Anticancer Activity. *Coord. Chem. Rev.* **2018**, *375*, 148–163. https://doi.org/10.1016/j.ccr.2017.11.014.

(39) Tas, D.; Balzarini, J. Novel Platinum(II) and Palladium(II) Complexes of Thiosemicarbazones Derived from 5-Substitutedthiophene-2-Carboxaldehydes and Their Antiviral and Cytotoxic Activities. *Eur. J. Med. Chem.* **2011**, *46* (11), 5616–5624. https://doi.org/10.1016/j.ejmech.2011.09.031.

(40) Rajapakse, C. S. K.; Martı, A.; Naoulou, B.; Jarzecki, A. A.; Sua, L.; Deregnaucourt, C.; Schre, J.; Musi, E.; Ambrosini, G.; Schwartz, G. K.; Sa, R. A. Synthesis , Characterization , and in Vitro Antimalarial and Antitumor Activity of New Ruthenium (II) Complexes of Chloroquine. *Inorg. Chem.* **2009**, *48* (3), 1122–1131. https://doi.org/10.1021/ic802220w.

(41) Wani, W. A.; Jameel, E.; Baig, U.; Mumtazuddin, S.; Hun, L. T. Ferroquine and Its Derivatives: New Generation of Antimalarial Agents. *Eur. J. Med. Chem.* **2015**, *101*, 534–551. https://doi.org/10.1016/j.ejmech.2015.07.009.

(42) Navarro, M.; Pekerar, S.; Pe, H. A. Synthesis , Characterization and Antimalarial Activity of New Iridium – Chloroquine Complexes. *Polyhedron* **2007**, *26* (12), 2420–2424. https://doi.org/10.1016/j.poly.2006.12.010.

(43) Ma, D. L.; Wang, M.; Mao, Z.; Yang, C.; Ng, C. T.; Leung, C. H. Rhodium Complexes as Therapeutic Agents. *Dalt. Trans.* **2016**, *45* (7), 2762–2771. https://doi.org/10.1039/c5dt04338g.

(44) Sa, R. A.; Navarro, M.; Pe, H. Toward a Novel Metal-Based Chemotherapy against Tropical Diseases . 2 . Synthesis and Antimalarial Activity in Vitro and in Vivo of New Ruthenium - and Rhodium - Chloroquine Complexes. **1996**, 1095–1099.

(45) Ekengard, E.; Kumar, K.; Fogeron, T.; De Kock, C.; Smith, P. J.; Haukka, M.; Monari, M.; Nordlander, E. Pentamethylcyclopentadienyl-Rhodium and Iridium Complexes Containing (N^N and N^O) Bound Chloroquine Analogue Ligands: Synthesis, Characterization and Antimalarial Properties. *Dalt. Trans.* **2016**, *45* (9), 3905–3917. https://doi.org/10.1039/c5dt03739e.

(46) Glans, L.; Ehnbom, A.; De Kock, C.; Martínez, A.; Estrada, J.; Smith, P. J.; Haukka, M.; Sánchez-Delgado, R. A.; Nordlander, E. Ruthenium(Ii) Arene Complexes with Chelating Chloroquine Analogue Ligands: Synthesis, Characterization and in Vitro Antimalarial Activity. *Dalt. Trans.* **2012**, *41* (9), 2764–2773. https://doi.org/10.1039/c2dt12083f.

(47) Melis, D. R.; Barnett, C. B.; Wiesner, L.; Nordlander, E.; Smith, G. S. Quinoline-Triazole Half-

Sandwich Iridium(Iii) Complexes: Synthesis, Antiplasmodial Activity and Preliminary Transfer Hydrogenation Studies. *Dalt. Trans.* **2020**, *49* (33), 11543–11555. https://doi.org/10.1039/d0dt01935f.

(48) Chellan, P.; Avery, V. M.; Duffy, S.; Triccas, J. A.; Nagalingam, G.; Tam, C.; Cheng, L. W.; Liu, J.; Land, K. M.; Clarkson, G. J.; Romero-Canelón, I.; Sadler, P. J. Organometallic Conjugates of the Drug Sulfadoxine for Combatting Antimicrobial Resistance. *Chem. - A Eur. J.* **2018**, *24* (40), 10078–10090. https://doi.org/10.1002/chem.201801090.

(49) Saify, Z. S.; Azim, M. K.; Ahmad, W.; Nisa, M.; Goldberg, D. E.; Hussain, S. A.; Akhtar, S.; Akram, A.; Arayne, A.; Oksman, A.; Khan, I. A. New Benzimidazole Derivatives as Antiplasmodial Agents and Plasmepsin Inhibitors: Synthesis and Analysis of Structure-Activity Relationships. *Bioorganic Med. Chem. Lett.* **2012**, *22* (2), 1282–1286. https://doi.org/10.1016/j.bmcl.2011.10.018.

(50) Doğan, U.; Özcan, Ö.; Alaca, G.; Arı, A.; Günnaz, S.; Yalçın, H. T.; Şahin, O.; İrişli, S. Novel Benzimidazole- Platinum(II) Complexes: Synthesis, Characterization, Antimicrobial and Anticancer Activity. *J. Mol. Struct.* **2021**, *1229*. https://doi.org/10.1016/j.molstruc.2020.129785.

(51) Pribut, N.; Basson, A. E.; Van Otterlo, W. A. L.; Liotta, D. C.; Pelly, S. C. Aryl Substituted Benzimidazolones as Potent HIV-1 Non-Nucleoside Reverse Transcriptase Inhibitors. *ACS Med. Chem. Lett.* **2019**, *10* (2), 196–202. https://doi.org/10.1021/acsmedchemlett.8b00549.

(52) Rylands, L.; Welsh, A.; Maepa, K.; Stringer, T.; Taylor, D.; Chibale, K.; Smith, G. S. Structure-Activity Relationship Studies of Antiplasmodial Cyclometallated Ruthenium(II), Rhodium(III) and Iridium(III) Complexes of 2-Phenylbenzimidazoles. *Eur. J. Med. Chem.* **2019**, *161*, 11–21. https://doi.org/10.1016/j.ejmech.2018.10.019.

(53) Milheiro, S. A.; Gonçalves, J.; Lopes, R. M. R. M.; Madureira, M.; Lobo, L.; Lopes, A.; Nogueira, F.; Fontinha, D.; Prudêncio, M.; M. Piedade, M. F.; Pinto, S. N.; Florindo, P. R.; Moreira, R. Half-Sandwich Cyclopentadienylruthenium(II) Complexes: A New Antimalarial Chemotype. *Inorg. Chem.* **2020**, *59* (17), 12722–12732. https://doi.org/10.1021/acs.inorgchem.0c01795.

(54) Štarha, P. Half-Sandwich Ru(II) Halogenido, Valproato and 4-Phenylbutyrato Complexes Containing 2,2 -Dipyridylamine: Synthesis, Characterization, Solution Chemistry and In Vitro Cytotoxicity. *molecules* **2016**, *21* (12), 1725. https://doi.org/10.3390/molecules21121725.

(55) Štarha, P.; Dvořák, Z.; Trávníček, Z. Half-Sandwich Ir(III) and Rh(III) 2,2'-Dipyridylamine Complexes: Synthesis, Characterization and in Vitro Cytotoxicity against the Ovarian Carcinoma Cells. *J. Organomet. Chem.* **2018**, *872*, 114–122. https://doi.org/10.1016/j.jorganchem.2018.07.035.

Chapter 2

Synthesis and characterisation of complexes C1-C12

2.1. Introduction

The emergence of resistant plasmodium strains to currently used antimalarial drugs has brought about extensive research in finding new chemotypes effective in treating malaria. As discussed in Chapter 1, one area of drug discovery in the field of malaria is focused on incorporating metals into already existing drugs in an attempt to improve their efficacy since the most effective current antimalarial being chloroquine, has proven to be less effective and even ineffective in some parts of the world.[123] Incorporating metals, especially PGMs, into organic pharmacophores has proven to have an effect on the ligand's antiplasmodial activity, i.e., improving its efficacy [4,5,6], etc. The ligand 2,2'-dipyridylamine (**Dpa**), an organic pharamacophore, is a metal complexing agent that is normally used as a bidentate nitrogen donor ligand. **Dpa** has been employed in various fields of research including catalysis, [7,8] and in medicinal chemistry. Ŝtarha *et al.* studied their *in vitro* cytotoxicity against the A2780 ovarian carcinoma cells.[9,10] They reported the synthesis and study of ruthenium(Ru) *para*-cymene (*p*-cym) half sandwich organometallic complexes with a PF_6^- counterion and the effect of replacing their chlorido ligand with different halogenido ligands(see *Figure 2.1*).[10] This work was later expanded with iridium(Ir) and rhodium(Rh) cyclopentadienyl (Cp*) bidentate metal complexes[9] (see *Figure 2.1*). It was found that the iridium-chlorido ($Ir(\eta^5\text{-}Cp^*)(dpa)Cl]PF_6$), iridium-iodido ($Ir(\eta^5\text{-}Cp^*)(dpa)I]PF_6$) and rhodium-iodido ($Rh(\eta^5\text{-}Cp^*)(dpa)I]PF_6$) complexes were active against the A2780 human cancer cell line while the rhodium-chlorido ($Rh(\eta^5\text{-}Cp^*)(dpa)Cl]PF_6$), ruthenium-chlorido [Ru(η^5-(*p*-cymene))(dpa)Cl]PF_6 and ruthenium-iodido [Ru(η^5-(*p*-cymene))(dpa)I]PF_6 complexes were inactive.[9,10]

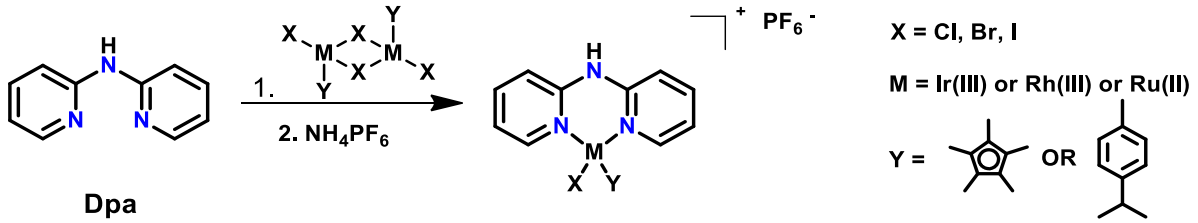

*Figure 2.1: **Dpa** complexes reported by Ŝtarha.*[9,10]

This chapter focuses on the synthesis and characterization of twelve iridium, rhodium and ruthenium half- sandwich organometallic complexes of the ligand **Dpa**. Six of them (**C1**-**C6**) have the PF_6^- counterion and were previously reported by Ŝtarha *et al.,* and the other six (**C7**-**C12**) have a NO_3^- counterion. A previous study of cationic metal complexes bearing a different counterion shows an effect on several of its properties including solubility, kinetic stability as well as its bioavailability.[11] Additionally, varying the halogenido ligand from chlorido to iodido also showed an increase in bioactivity.[12] It has been reported that exchanging a chlorido ligand for an iodido ligand has as effect on the polarization[12] of the complex as well as its redox potential.[13,14] The replacement results in an increase in the positive charge polarization on the metal complex, where chlorido is less positive than iodido. This has resulted in more potent complexes that are also more selective.[12] Thus, we wished to investigate whether changing the counterion for these PGM complexes of **Dpa** would also affect its properties and antimalarial potency. In this chapter, the synthesis and characterisation of Ir(III), Rh(III) and Ru(II) complexes with either a PF_6^- or NO_3^- counterion respectively will be discussed.

2.2. Results and Discussion

2.2.1. Synthesis of the complexes

Dpa is a bidentate ligand that chelates to a metal using the nitrogen atoms of the pyridyl rings.[15] Cationic PF_6^- organometallic complexes of Ir(III), Rh(III) and Ru(II) have all been previously synthesized and reported in literature.[8-10] The organometallic complexes **C1**-**C12** were made following an adapted microwave reaction reported by Ŝtarha, *et al*. according to *Scheme 2.1*.[10] **Dpa** is combined with appropriate metal dimer to produce the cationic Cl^- complexes. These are not isolated and are simply carried to the next step. To displace the Cl^-/I^- counterion, each complex is stirred in methanol with ammonium hexafluorophosphate (**C1**-**C6**) or ammonium nitrate (**C7**-**C12**) in order to yield the final product. The complexes **C1**-**C6** are isolated as red, orange or yellow crystalline powders in moderate to good yields. They were found to be soluble in acetone, acetonitrile, DCM, DMSO and methanol (with heat). Complexes **C7**-**C12** on the other hand were isolated as yellow or orange crystalline powders in moderate to good yields and are soluble in water, acetonitrile, DCM, DMSO and methanol (with heat). The synthesis of the starting material, i.e. metals dimers $[Ir(Cp^*)Cl_2]_2$, $[Ir(Cp^*)I_2]_2$, $[Rh(Cp^*)Cl_2]_2$, $[Rh(Cp^*)I_2]_2$, $[Ru(p\text{-cymene})Cl_2]_2$ and $[Ru(p\text{-cymene})I_2]_2$ were adapted from reported methods.[16,17]

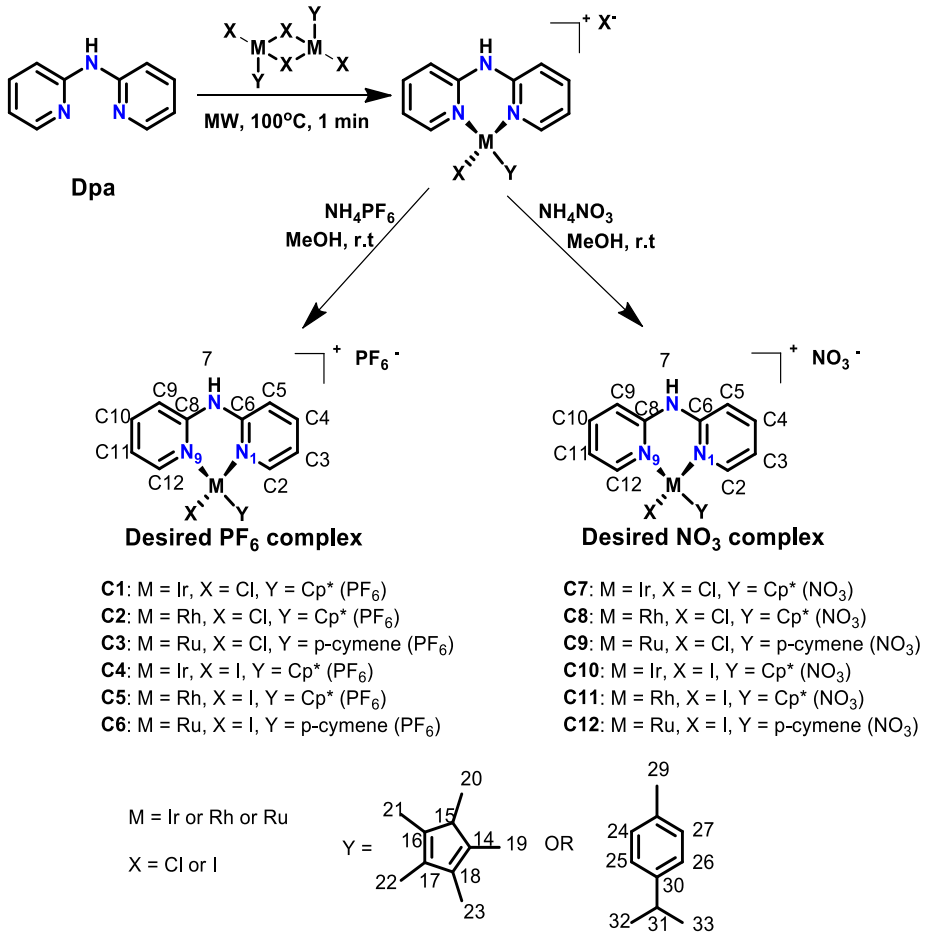

*Scheme 2.2: Reaction scheme for the synthesis of cationic **Dpa** complexes.*

2.2.2. Characterisation of complexes C1-C12

FTIR was used to confirm the coordination of the metals to **Dpa**. The complexes **C1**-**C6** were characterized with reference to the literature.[10,11] The FTIR spectra of complexes **C1**-**C6** were very similar. A summary of distinctive bands of complexes **C1**-**C6** are summarised on *Table 2.1* below. A strong band between 827-832 cm^{-1}, distinctive of the PF_6^- stretch, was observed for complexes **C1**-**C6** signifying successful exchange of the Cl^-/ I^- counterion. The C=N stretching vibrations were observed between 1624-1628 cm^{-1}, a shift of about 33-37 cm^{-1} from 1591 cm^{-1} of the **Dpa** (see *Figure 2.2* below). This is attributed to the fact that electron distribution in the pyridyl rings has changed. Electron density is being pulled away from the pyridine rings by the electropositive metal thus making the C=N bond stronger and consequently shorter. Strengthening of the other bonds in the pyridine ring can also be observed in the slight increase in frequency for C-N aromatic stretches from 1139 cm^{-1} for the ligand to 1158-1162 cm^{-1} for the complexes. Additionally, this proves that coordination took place through the N atoms. The C-H aliphatic stretches of the cyclopentadienyl ring (Cp*) and *para*-cymene (*p*-cym) were observed for complexes **C1**, **C4**, **C5** and **C3** between 2918-2984 cm^{-1} and not observed for **C2** and **C6**, however, these were detected using proton NMR which will be discussed. No significant differences between the spectra for the chlorido (**C1**-**C3**) versus iodido (**C4**-**C6**) complexes was observed.

*Table 2.1: Significant IR frequencies for **Dpa** ligand and hexafluorophosphate (PF_6^-) complexes.*

Complex	**(PF_6) (cm^{-1})**	**(C=N) (cm^{-1})**	**$(C\text{-}H)_{aliphatic}$ (cm^{-1})**	**$(C\text{-}N)_{aromatic}$ (cm^{-1})**	**$(C\text{-}H)_{aliphatic}$ (Cp*/ p-cym) (cm^{-1})**
Dpa		1591		1139	
C1	832	1628	1472	1162	2918, 2984
C2	823	1625	1467	1161	(not visible)
C3	830	1625	1465	1161	2979
C4	829	1626	1471	1161	2980
C5	827	1624	1469	1159	2980
C6	834	1626	1467	1158	(not visible)

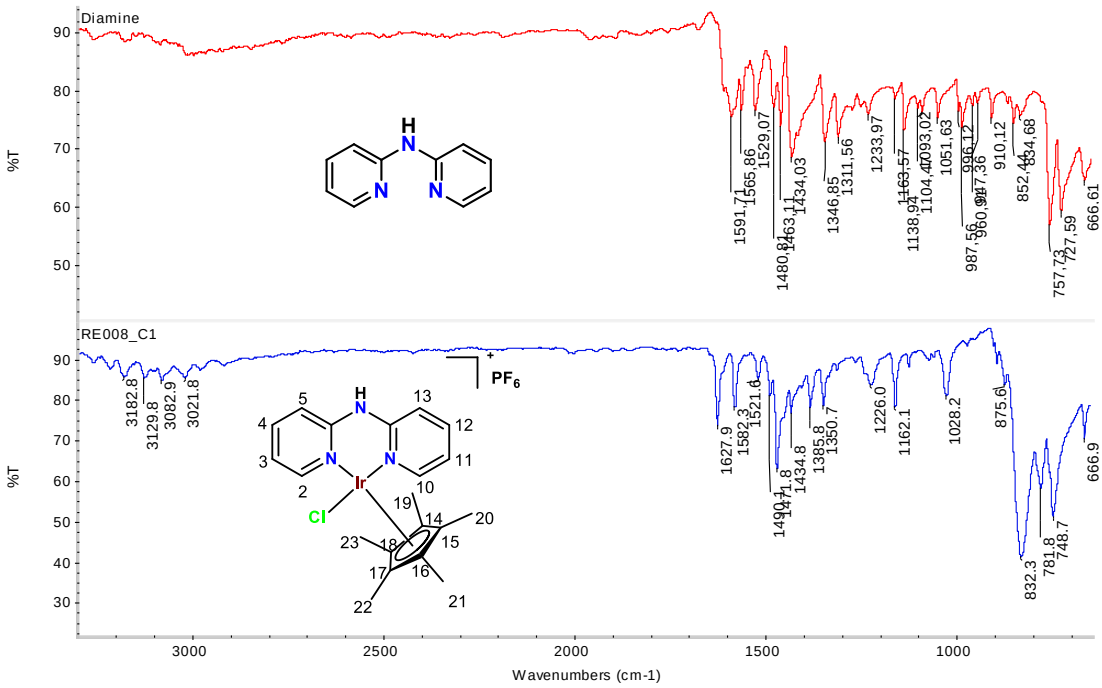

*Figure 2.2: FTIR (ATR) spectra of **Dpa** (top) and **C1** (bottom).*

From the IR spectra obtained for complexes **C7**-**C12**, the complexation and counterion exchange appears to have taken place. This is observed at wavelengths 1299-1317 cm^{-1} and 764-771 cm^{-1} where the nitrate symmetric and asymmetric stretch absorptions, respectively, are found (see *Table 2.2* below). A clear shift of the C=N stretch is also observed for the nitrate complexes as indicated on *Table 2.2*, suggesting coordination through the nitrogen atoms of the pyridine rings. Further evidence of metalation is the emergence of the C-H bending and stretching bands attributed to the Cp^* and *p*-cymene moiety.

*Table 2.2: Significant IR frequencies for **Dpa** ligand and nitrate (NO_3^-) complexes).*

Complex	**$_{as}$ (NO_3) (cm^{-1})**	**$_{s}$ (NO_3) (cm^{-1})**	**(C=N) (cm^{-1})**	**$(C\text{-}H)_{aliphatic}$ (cm^{-1})**	**$(C\text{-}N)_{aromatic}$ (cm^{-1})**	**$_{s}$ $(C\text{-}H)_{aliphatic}$ (Cp*/ *p*-cym)(cm^{-1})**
Dpa			1591		1139	
C7	770	1310	1637	1470	1157	2916, 2958
C8	771	1311	1634	1467	1156	2916, 2953
C9	766	1315	1634	1469	1158	2963
C10	766	1299	1625	1470	1154	2909, 2953
C11	768	1301	1623	1468	1153	2956
C12	764	1317	1623	1466	1155	2971

The ^1H NMR spectra of the ligand (**Dpa**) and complexes **C1**-**C12** were all run in methanol-d_4 (summary of shifts in *Table 2.3 and Table 2.4*). The amino proton H_7 was not observed for either the ligand or the

complexes**.** This is because the amino proton is readily and rapidly exchangeable for the protons of the deuterated methanol which makes it difficult to detect. Due to symmetry, all the peaks in the aromatic region are assigned to two protons of each pyridyl proton at the same positions. For complexes **C1**, **C2**, **C4**, **C5**, **C7**, **C8**, **C10** and **C11**, a singlet at 1.46-1.63 ppm integrated for 15 protons, H_{19}-H_{23}, allocated to the methyl groups of the Cp* moiety was observed. The shift in resonances attributed to the pyridyl ring protons for the complexes compared to the **Dpa** ligand confirm metalation. For all complexes, a downfield shift is observed for the protons of the pyridyl rings that are *ortho* (H_2 and H_{10}), *meta* (H_3 and H_{11}) and *para* (H_4 and H_{12}) to the pyridyl nitrogens (indicated by green arrows in *Figure 2.3*). As previously mentioned, coordination of the electron-withdrawing metals to the ligand results in electron density being donated by the pyridine rings to the metal centre and resulting in the protons being less shielded. For the protons on the carbons in the meta position to the pyridyl nitrogens, a downfield shift is noted for H_3 and H_{11} and an upfield shift for H_5 and H_{13}. Although in similar positions, these four protons experience different electron environments. The amine is an *ortho* and *para* directing electron-donating group and is situated in the *ortho* position relative to the protons H_5 and H_{13}. As a consequence, these protons are being more shielded due to its electron donating ability. The same phenomenon is expected for H_3 and H_{11} since they are positioned *para* to the amino group. However, their position relative to the pyridyl nitrogens, where the metal is chelated, has a stronger effect on their shielding. The de-shielding effect from electron density being pulled away from the pyridyl rings by the metal surpasses the shielding effect resulting from the *para* directing amine. This was expected and it is consistent with literature reporting on complexes **C1**-**C6.**[9,10] Protons H_2 and H_{10} resonate as a doublet since they couple to protons H_3 and H_{11} (see ^{1}H spectrum of **C1** on Figure 2.4). Two triplets attributed to protons H_4 and H_{12}, and H_3 and H_{11} resonate at 7.96-8.03 ppm and 7.25-7.34 ppm respectively, as a result of coupling to each other and to their neighbouring protons H_5 and H_{13}, and H_2 and H_{10}. The doublet resonating at 7.28-7.47 ppm is assigned to H_5 and H_{13} since they only couple to H_4 and H_{12}. The resonances for protons H_5 and H_{13}, and H_3 and H_{11}, which should be observed as a doublet and a triplet respectively, overlap and appear as a multiplet between 7.18-7.34 ppm for the Rh- and Ru-chlorido complexes **C2, C3, C8,** and **C9**. The ^{1}H spectra of **C3**, **C6**, **C9** and **C12** displays signals for all protons of the *para*-cymene moiety (*Figure 2.5*).

*Table 2.3: ^{1}H NMR shifts (ppm) of the **Dpa** ligand and the PF_6^- complexes **C1**-**C6** in methanol-d4.*

	Proton	Dpa	C1	C2	C3	C4	C5	C6
Pyridyl protons	**H_2 and H_{10} (d)**	8.20	8.43	8.44	8.63	8.65	8.67	8.80
	H_4 and H_{12} (t)	7.66	7.95	7.98	7.92	7.91	7.98	7.89
	H_5 and H_{13} (d)	7.59	7.30	7.28 - 7.32 (m)	7.18-7.23 (m)	7.30	7.28	7.16
	H_3 and H_{11} (t)	6.90	7.25			7.15	7.25	7.12
Cp*	**$H_{Cp^*(19\text{-}23)}$**		1.47	1.49		1.58	1.62	
para-cymene	**H_{24} and H_{27} (d)**				5.66			5.67
	H_{25} and H_{26} (d)				5.56			5.61
	H_{31} (sep)				2.61			2.65
	H_{29} (s)				2.09			2.22
	H_{32} and H_{33} (d)				1.22			1.22

*Table 2.4: ^{1}H NMR shifts (ppm) of the **Dpa** ligand and the PF_6^- complexes **C7**-**C12** in methanol-d4.*

	Proton	Dpa	C7	C8	C9	C10	C11	C12
Pyridyl protons	H_2 and H_{10} (d)	8.20	8.43	8.45	8.63	8.66	8.66	8.81
	H_4 and H_{12} (t)	7.66	7.96	8.00	7.93	7.93	7.98	7.89
	H_5 and H_{13} (d)	7.59	7.32	7.30 - 7.34 (m)	7.19-7.22 (m)	7.30	7.31	7.19
	H_3 and H_{11} (t)	6.90	7.24			7.16	7.25	7.12
Cp*	$H_{Cp^*(19-23)}$		1.47	1.50		1.55	1.63	
para-cymene	H_{24} and H_{27} (d)				5.67			5.68
	H_{25} and H_{26} (d)				5.57			5.62
	H_{31} (sep)				2.62			2.65
	H_{29} (s)				2.10			2.22
	H_{32} and H_{33} (d)				1.23			1.22

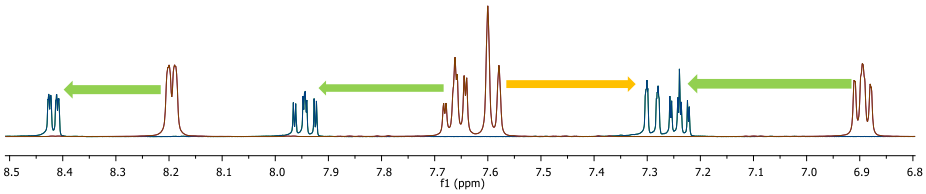

*Figure 2.3: Aromatic region of the overlapped ^{1}H NMR spectra of **Dpa** (red) and **C1** (blue) in methanol-d4 (CD_3OD).*

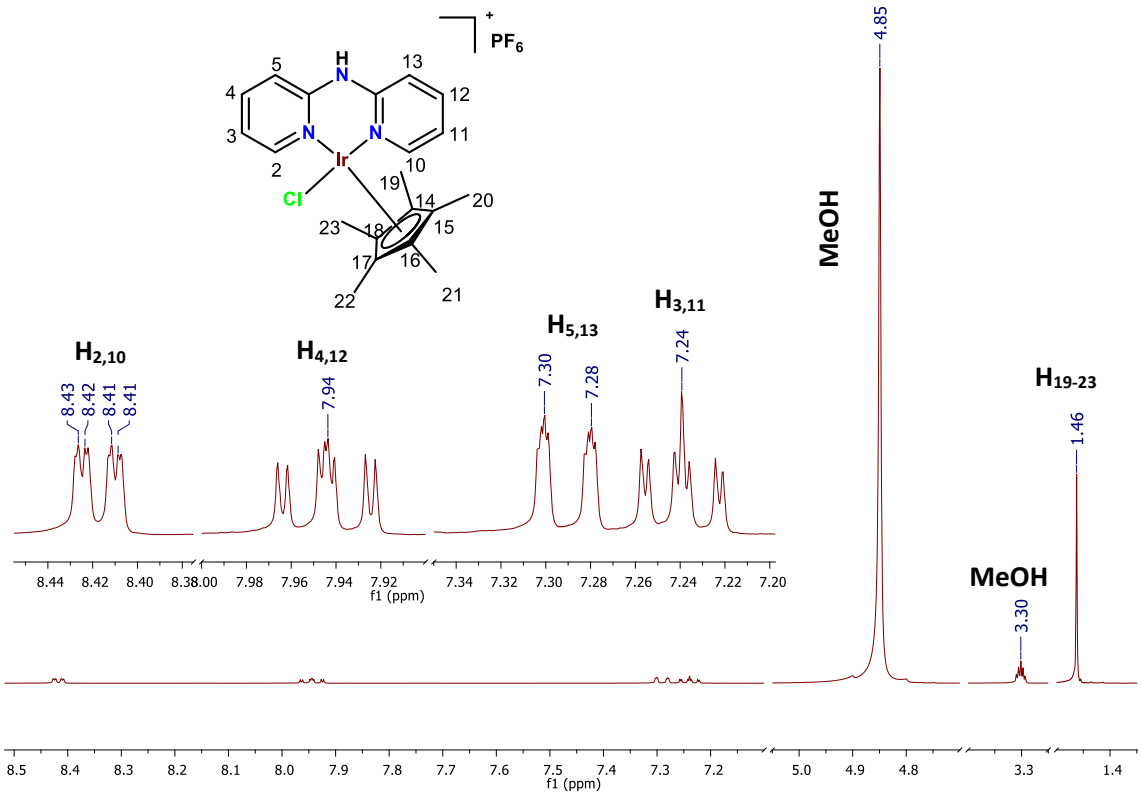

*Figure 3.4: ^{1}H NMR spectra of **C1** in methanol-d4.*

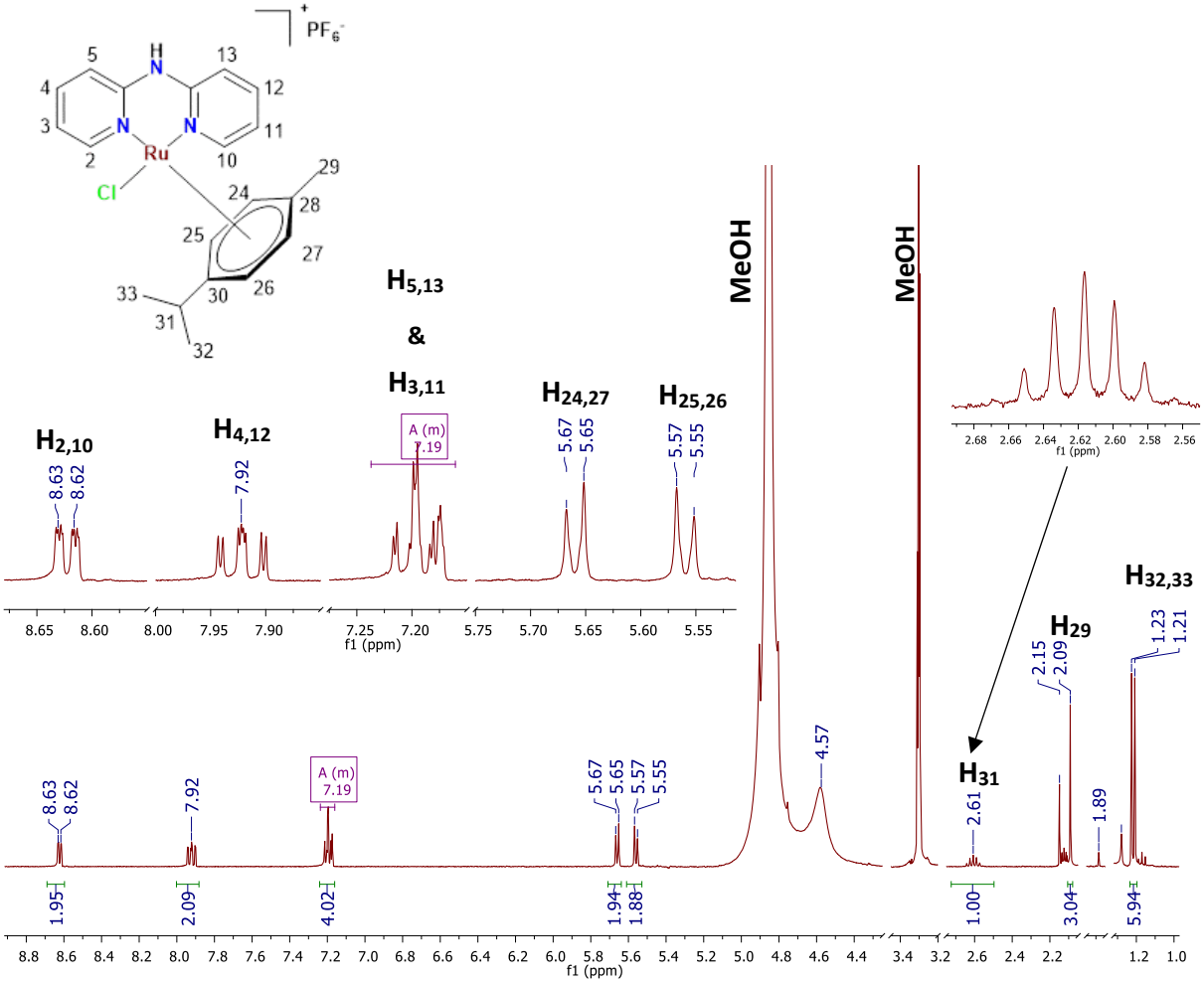

*Figure 2.5: ^{1}H NMR spectra of **C3** in methanol-d4.*

The *para*-cymene moiety shows seven peaks attributed to fourteen protons in different chemical environments for **C3**, **C6**, **C9** and **C12**. The protons of the tertiary carbon of the isopropyl group for the *para*-cymene moiety was expected to resonate as a septet since it couples to protons H_{32} and H_{33} contributing three protons each:

For I = 6, the N(number of neighbouring protons) + 1 rule eludes that:

multiplicity = 6 + 1 = 7 signals (**septet**)

C3 has the proton H_{31} signal resonating at 2.61 ppm as a quintet with weak intensity (*Figure 2.5*). However, a septet is observed for complexes **C6**, **C9** and **C12**. In the ^{1}H spectra of **C3**, **C6**, **C9** and **C12**, two doublets at 5.66-5.68 ppm and 5.56-5.62 ppm are assigned to nuclei H_{24} and H_{27}, and H_{24} and H_{27} respectively. A singlet at 2.09-2.22 ppm integrated for 3 protons belongs to the methyl of the *p*-cymene moiety, H_{29}. The protons H_{32} and H_{33} of the isopropyl group resonate as doublets at 1.22-1.23 ppm as they couple to H_{31}. A comparison of the chlorido complexes (**C1, C2, C3, C7, C8 and C9**) to their respective and iodido complexes (**C4, C5, C6, C10, C11 and C12**) reveals that the protons *ortho* to the pyridyl nitrogen (H_2 and H_{10}) are more deshielded for the iodido complexes. This is expected since iodine is higher in the nephelauxetic series than chlorine. Therefore, this generates a stronger pull on the electrons closest to the metal centre, thus protons become less shielded.

For the purpose of further substantiating successful metal coordination, ^{13}C NMR of the novel nitrate complexes was conducted, ^{13}C NMR was not done for known PF_6^- complexes **C1**-**C6**. From the spectra acquired, all carbons were assigned (see *Table 2.4*). The ^{13}C NMR of all complexes were recorded in methanol-d_4. The Ir and Rh complexes **C7**, **C8**, **C10** and **C11** have the carbons *ortho* to the two pyridyl protons (C_6, C_8, C_2 and C_{10}) as the most deshielded, with the quaternary carbons being more downfield as demonstrated in *Figure 2.7* with the spectra of **C9**. Other pyridyl carbons all resonate in the aromatic region as singlets. The carbons of the Cp* moiety resonate at different positions (see *Figure 2.6*), those of the five-membered ring resonate at a higher frequency (89.55-98.50 ppm) whereas the methyl carbons are in the lower aliphatic region between 8.74-9.85 ppm. As seen for the proton NMR, the *para*-cymene moiety of complexes **C9** and **C12** gives rise to more peaks in the spectra (see *Figure 2.7*). The isopropyl and methyl group on the *para*-cymene creates a different chemical environment for the carbons on the benzene ring. Two quaternary carbons, C_{28} and C_{30}, are seen as weak signals resonating at 101.34-100.81 ppm and 108.13-109.77 ppm respectively. Methyl carbon, C_{29}, is observed at lower frequencies (18.36 and 19.59 ppm) in the aliphatic region whereas the isopropyl carbons resonate at a higher frequency of 22.34 and 22.43 ppm for ruthenium complexes **C9** and **C12**.

*Table 2.4: ^{13}C NMR shifts (ppm) of the NO_3^- counterion complexes **C7**-**C12** in methanol-d4.*

	Carbon	C7	C8	C9	C11	C12
Pyridyl carbons	$C_{6,8}$	153.62	153.81	155.72	156.02	158.81
	$C_{2,10}$	153.37	152.71	154.45	153.80	154.39
	$C_{4,12}$	142.38	142.21	141.77	142.11	141.58
	$C_{3,11}$	122.2	122.06	120.66	121.80	120.32
	$C_{5,13}$	115.35	115.65	115.02	115.33	114.69
Cp*	$Cp^*_{(14-18)}$	89.55	97.95		98.50	
	$Cp^*_{(14-18)}$	8.57	8.74		9.85	
para-cymene	C_{30}			108.13		109.77
	C_{28}			101.34		100.81
	$C_{24,27}$			86.83		87.50
	$C_{25,26}$			85.21		84.92
	C_{31}			32.18		32.63
	$C_{32,33}$			22.34		22.43
	C_{29}			18.36		19.59

As seen for the ^1H NMR spectra discussed above, the same phenomenon was observed when comparing the chlorido complexes (**C8** and **C9**) to their respective iodido complexes (**C11** and **C12**). The carbons *ortho* to the pyridyl nitrogen (C_6, C_8, C_2 and C_{10}) were found to be more deshielded for the iodido complexes. A comparison of differences in shifts between PF_6^- complexes, **C1-C6**, and NO_3^- complexes **C7-C12** showed that the complexes had very similar shifts, very small inconsistent differences were be observed and could not be rationalised.

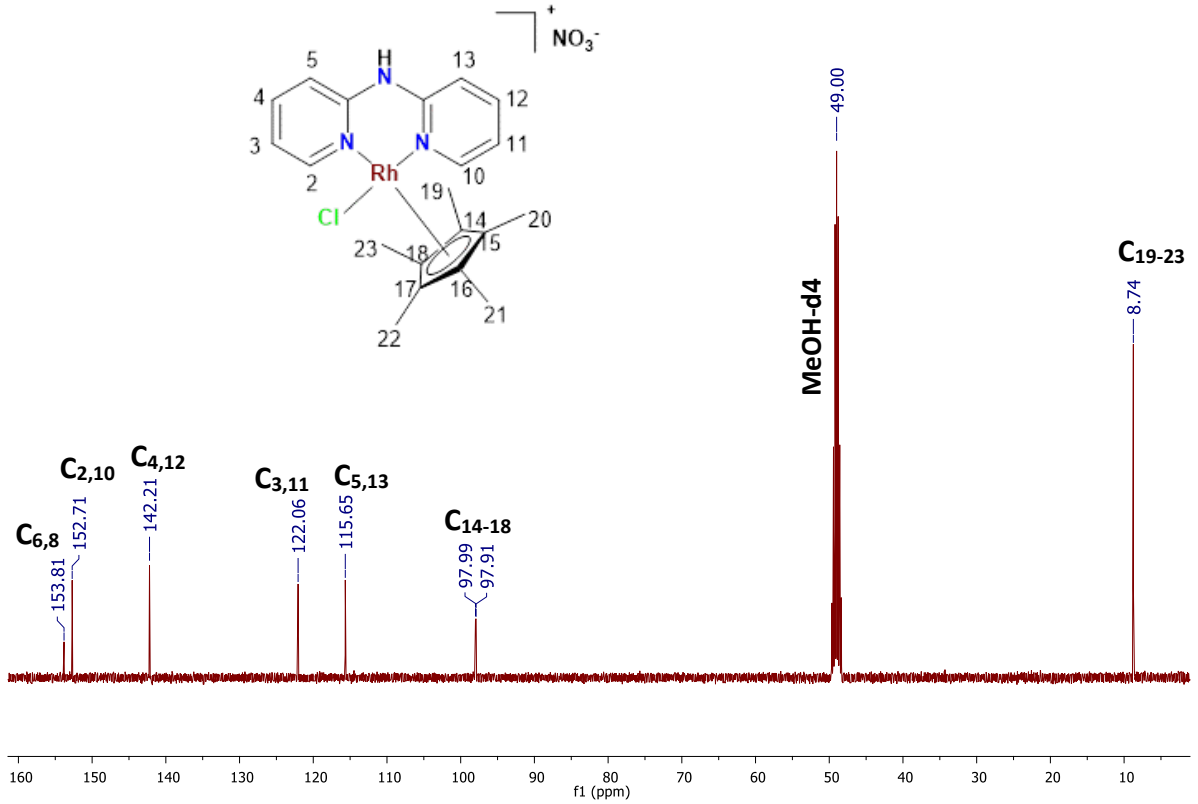

*Figure 2.6: ^{13}C NMR spectra of **C8** in methanol-d4.*

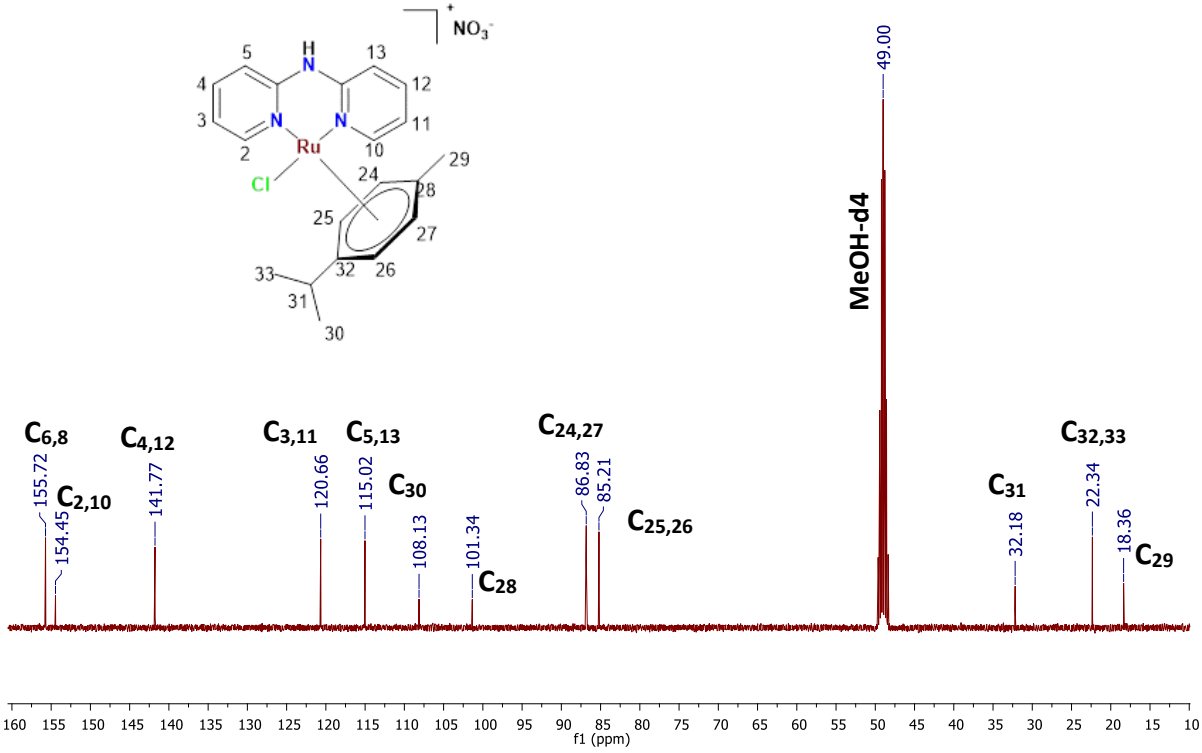

*Figure 2.7: ^{13}C NMR spectra of **C9** in methanol-d4.*

Mass spectra of the nitrate complexes **C7**-**C12** were collected using the positive electrospray ionisation (ESI) mode. The base peaks corresponding to the metal cation species($[M]^+$) with loss of the NO_3^- counterion were observed for each complex (see *Table 2.5).*

*Table 2.5: m/z values of the base peaks seen in the mass spectra of the nitrate complexes **C7**-**C12** in the positive ionisation mode.*

Complex	m/z	ESI+
C7	534.1286	$[Ir(\eta^5\text{-Cp*})(dpa)Cl]^+$
C8	444.0718	$[Rh(\eta^5\text{-Cp*})(dpa)Cl]^+$
C9	442.0929	$[Ru(\eta^5\text{-}(p\text{-cym})(dpa)Cl]^+$
C10	626.0641	$[Ir(\eta^5\text{-Cp*})(dpa)I]^+$
C11	538.073	$[Rh(\eta^5\text{-Cp*})(dpa)I]^+$
C12	533.9994	$[Ru(\eta^5\text{-}(p\text{-cym})(dpa)I]^+$

Single crystals of **C1** and **C2** were grown from a solution of acetone and diethyl ether and single crystals of complexes **C7** and **C9** were grown from a solution of methanol and diethyl ether. The crystal structures were solved by single crystal X-ray diffraction and had not been reported at the time of the thesis write-up. The $[Ir(\eta^5\text{-Cp*})(dpa)Cl]PF_6$ complex **C1** crystallised in the orthorhombic space group $P2_12_12_1$ whereas the $[Ir(\eta^5\text{-Cp*})(dpa)Cl]NO_3$ complex **C7** crystallised in the monoclinic $P21/c$ space group. Rh complex **C2**, crystallised similar to **C1** in the orthorhombic space group $P2_12_12_1$. The Ru-nitrate complex **C9** crystallised in the triclinic *P*-1 space group with a molecule of water.

Half-sandwich organometallic complexes are known to adopt the pseudo-octahedral piano-stool geometry, which was also the case for complexes **C1, C2, C7 and C9.**[5,18,19] A summary of the recorded bond lengths and angles is tabulated below in *Table 2.6* and *Table 2.7*. Bond lengths and bond angles were calculated using Mercury 4.3.1. software. Centroids in *Table 2.6* and *Table 2.7* were created for the pentamethylcyclopentadienyl and para-cymene rings using Mercury 4.3.1. software. The centroidal bond lengths and bond angles between the centroid and adjacent angles was calculated using Mercury 4.3.1. thus standard errors could not be obtained for those values. The centroids are not included in *Figure 2.9* above. Structurally similar complexes were reported by Liu *et al.* where iridium is cyclometallated to 2-phenylquinoline and has a PF_6^- counterion is used for comparison.[20] Reported complex,[20] and complex **C1** were both found to have crystallized in the same space group. The bond length between Ir and the centroid of Cp* of complex **C1** was found to be 1.775Å which was comparable to that of the reported complex which was 1.829 Å. Complex **C7**, the nitrate analogue of **C1**, also had a comparable metal-centroid (Ir- Cp*) bond length of 1.782Å to **C1** and it was also comparable to the reported complex, a comparison is made to evaluate whether the complexes had generally accepted values in comparison to known similar complexes. This was also observed for the metal-halide (Ir-Cl) and metal-nitrogen (Ir-N1/ Ir-N9) bonds for complexes **C1** and **C7** which were in the range 2.395(7)-2.936(3)Å and 2. 017(2) -2. 084(8) Å respectively. The bond lengths of complex **C2** were found to be in agreement with those of complexes **C1** and **C7**. The crystal structures show that the metals coordinate through the nitrogen atoms N1 and N9. The crystal structure of complex **C3** of the form $[Ru(\eta^5\text{-(p-cymene)})(dpa)Cl]PF_6$, that is similar to complex **C9** was reported by Romain *et al* and was used for comparison.[8] The Ru- $\mathbf{C_{centroid}}$ = 1.677Å, Ru-Cl= 2.422(4) Å, and the N-C bonds in the

range 1.345(2)-1.38(2) Å are in agreement with reported values in literature of a similar complex. The structure of the crystals are shown in *Figure 2.8* below, the counterions and hydrogen atoms have been omitted for clarity. From the results obtained, the complexes prove that the intended complexes were synthesized successfully. A comparison to reported compounds which are structurally similar gives details of how the bonds lengths and angles calculated were within reasonable ranges.

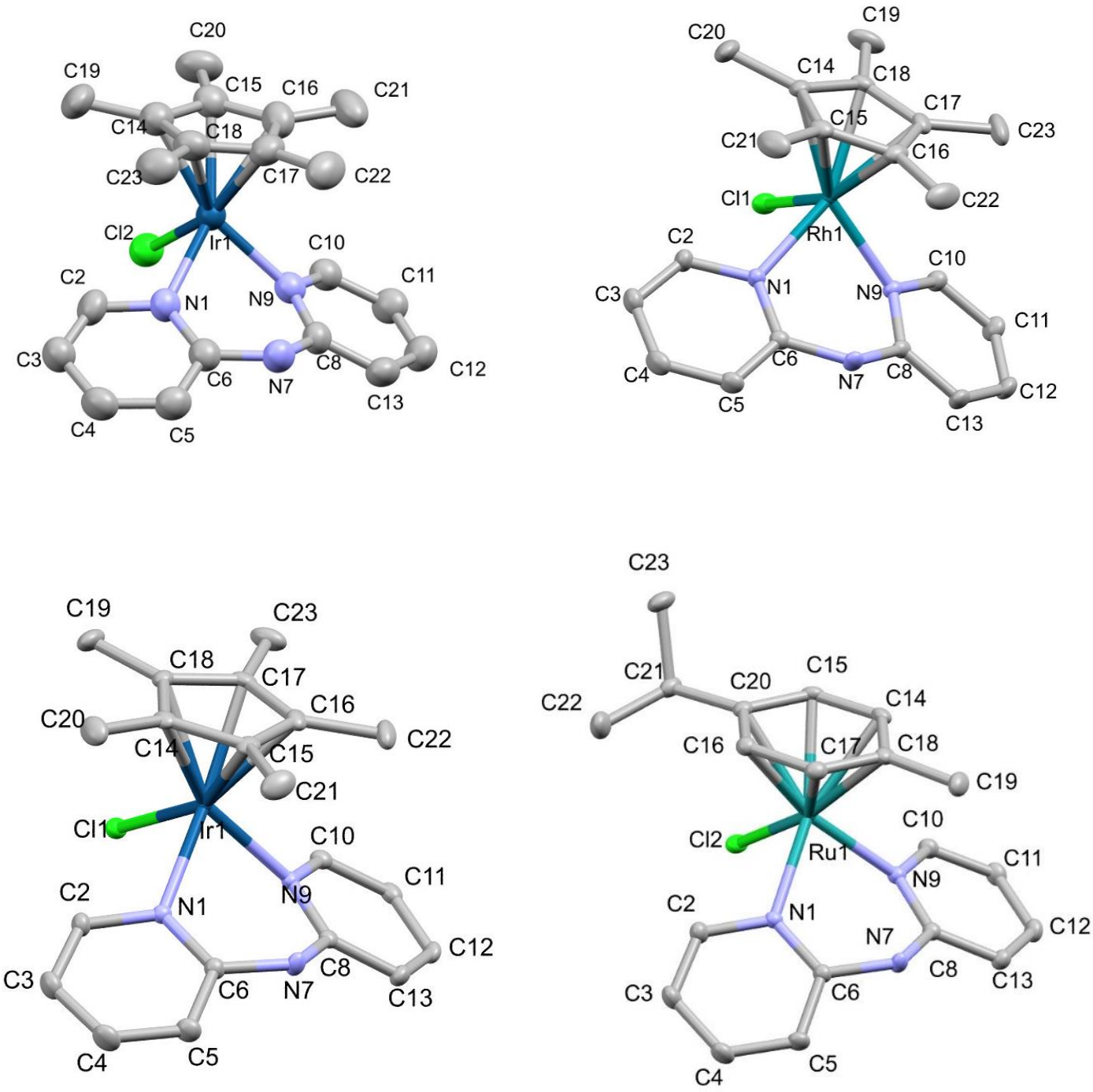

*Figure 2.8: Crystallographic structure of complexes **C1**, **C2**, **C7** and **C9**. Hydrogen atoms, solvents and the counterions have been omitted for clarity. Ellipsoids at 50% probability.*

*Table 2.6: Bond lengths for complexes **C1**, **C2**, **C7** and **C9** ($C_{centroid}$ of Cp* ring).*

	Complexes			
	PF_6^-		NO_3^-	
Bond	**C1 (Å) (M=Ir1, X2=Cl2)**	**C2 (Å) (M=Rh1, X2=Cl1)**	**C7 (Å) (M=Ir1, X2=Cl2)**	**C9 (Å) (M=Ru1, X2=Cl2)**
M- $C_{centroid}$	1,775	1.779	1.782	1.677
M-X	2.396(3)	2.3928(6)	2.395(7)	2.422(4)
M-N1	2.086(9)	2.094(2)	2.086(2)	2.107(1)
M-N9	2.084(8)	2.093(2)	2.107(2)	2.093(1)
N1-C2	1.370(1)	1.342(2)	1.359 (3)	1.358(2)
N1-C6	1.360(1)	1.356(3)	1.349(3)	1.345(2)
N9-C8	1,350(1)	1.347(3)	1.350(3)	1.346(2)
N9-C10	1.360(1)	1.353(3)	1.361(3)	1.363(2)

*Table 2.7: Bond angles for complexes **C1**, **C2**, **C7** and **C9**.*

	Complexes			
	PF_6^-		NO_3^-	
Bond	**C1 (M=Ir1, X2=Cl2)**	**C2 (M=Rh1, X2=Cl1)**	**C7 (M=Ir1, X2=Cl2)**	**C9 (M=Ru1, X2=Cl2)**
N1-M-N9	83.7(3)	84.10(7)	83.28(7)	84.54(5)
N1-M-X	86.6(3)	89.32(5)	88.08(5)	86.74(3)
N1-M-$C_{centroid}$[a]	128.62	128.08	128.77	129.27
N9-M-X	87.3(2)	88.26(5)	88.45(5)	87.11(3)
N9-M-$C_{centroid}$[a]	128.79	127.82	127.10	126.94
X-M-$C_{centroid}$[a]	127.04	125.72	126.97	127.64

[a] Distances and angles were calculated using Mercury software version 4.3.1.

2.2.3. DMSO interaction studies

The aprotic solvent, DMSO, is known to interact with some metal complexes which could result in dissociation of a ligand from the complex or cleavage of metal-halide bonds.[21] This is especially important to study since DMSO is used to prepare the compound stock solutions prior to use in *in vitro* biological assays. In order to investigate whether any interaction between the complexes and DMSO

takes place, a study using ^{1}H NMR was conducted. This was done by preparing a sample of each complex in DMSO-d_6 and immediately running ^{1}H NMR and again after 24 hours. For these complexes, an interaction could occur with the metal whereby DMSO-d_6 displaces the Cl/I ligand. On condition that this occurs, a change would be observed between a NMR spectrum run immediately and one run after 24 hours as the chemical environment around the metal would be different with DMSO-d_6 coordinated to it. The two spectra of each complex were compared by overlapping the spectra run at 0 hours and that run after 24 hours. No differences in the spectra was observed (see a fragment, i.e., pyridyl protons region, of overlapped spectra for **C3** on *Figure 2.9*). However, whether interaction occurred or not cannot be concluded since the reaction could be instantaneous and thus not detectable.

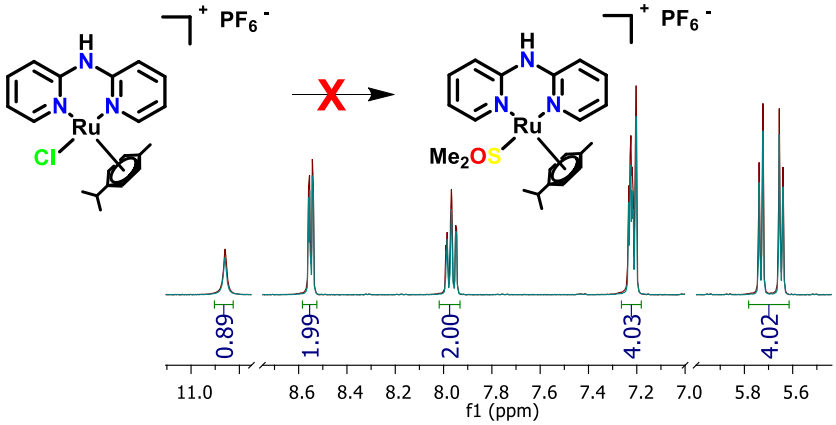

*Figure 2.9: Overlapped pyridyl protons fragment of the ^{1}H NMR spectra of **C3** (red: 0hrs, blue: 24hrs).*

A study reporting the synthesis of complexes **C3** and **C6** conducted a similar study by running ^{1}H NMR in DMSO-d_6 immediately after preparing the sample and again after 48 hours They also reported that no changes were detected from which they concluded that no interaction takes place.[22] Before it can be concluded that the **Dpa** complexes are stable in DMSO-d_6 even after standing for 24 hours at room temperature, further investigations were necessary. A DMSO titration study was done on complex **C2**. A 1mM stock solution of **C2** was prepared in dichloromethane (DCM). In a quartz cuvette, 1ml of the stock solution was transferred and a 4mM stock solution of DMSO was added in small increments from 1-100 equivalents. After each addition, the UV-Vis spectrum of the sample was obtained between 220-1000 nm. This was performed in order to determine whether any interaction does occur, and if so, after how many equivalents of DMSO added would the reaction reach its endpoint. The spectra was corrected for dilution and it was found that after each addition, the spectrum was different from the previous run (see *Figure 2.10*) indicating that some interaction does take place yet not to completion.

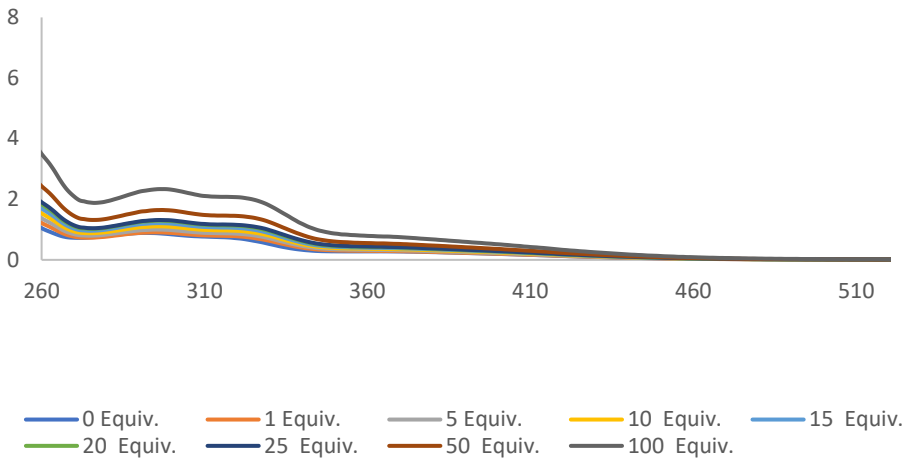

*Figure 2.10: Overlapped UV-Vis spectra of **C2** (1mM) after each addition of DMSO from 0-100 equivalents.*

Another study was conducted where **C2** was combined with 100 equivalents of DMSO and UV-Vis spectra were recorded over a period of 18 hours. The reaction still did not reach completion according to the absorbance recorded. The conditions could not be modified any further due to time constraints. Further investigations will be done in future.

2.2.4. Cyclic voltammetry

Electrochemistry is an important factor to consider in drug development since it predicts what active species is formed and how it behaves once it has been administered. It can also be used to probe how a drug will be metabolized, how it will interact with DNA, what binding interactions will occur between compounds and proteins *in vitro*, etc.[23] An electrochemical technique, i.e. cyclic voltammetry, was used to study the electron transfer processes of a solution of complexes **C1**-**C6** in acetonitrile using 0.2 M $TBAPF_6$ as the supporting electrolyte across a wide range of potential energy (-2500 – 2500 mV) that covers the cell potential range of -40 – 70 mV. The working electrode used was the glassy carbon, whereas the reference electrode was an $Ag/AgNO_3$ electrode and platinum wire as the counter electrode. The scans were conducted on a full scale of 100 μA at a scan rate of 100 mV/s.

*Table 2.8: Potential (mV) of oxidation and reductions obtained for **Dpa** and the chlorido complexes **C1**, **C2** and **C3** (↔ = reversible electron transfer reaction).*

	Potential range (mV)	Dpa	C1	C2	C3
Reductions	**-1000-1499**		-1121	-1485 -1222	
	-1500-1999	-1862	-1830		-1724↔ -1364
	-2000-2500		-2356	-2008 -2097	-2241 ↔-1874
Oxidation		1021	1318	1119 1805	1266

*Table 2.9: Potential (mV) of oxidation and reductions obtained for iodido complexes **C4**, **C5** and **C6** (↔ = reversible reductions).*

	Potential range (mV)	C4	C5	C6
Reductions	**-1000-1499**	-1452	-1020	-1488
	-1500-1999	-1855	-1428 ↔ -1238	-1736
	-2000-2500	-2271	-2057	
Oxidation		1056	1063	1032

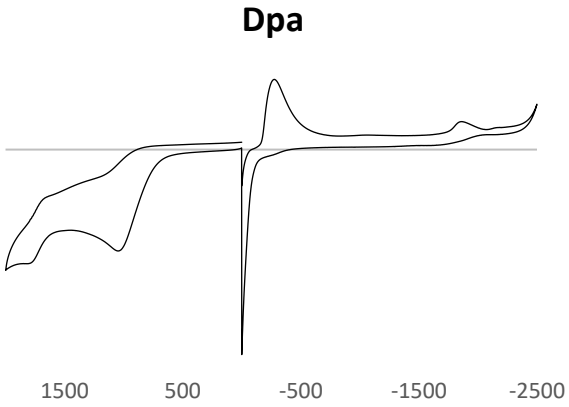

*Figure 2.11: Voltammogram (reduction-oxidation) of **Dpa** ligand at a scan rate of 100 mV/s.*

From the voltammogram of the **Dpa** ligand (see *Figure 2.11* above), we can deduce that the ligand induces redox activity however it does not undergo any reduction or oxidation. A redox active ligand then binds a metal centre that readily undergoes change in oxidation state to make the complexes, this results in a change of the redox activity of the ligand. This is seen on the voltammogram of complexes **C1**-**C6**. The potentials at between -70 and -640 mV are due to PF_6^- and are not involved in the redox potential of the complexes. The voltammogram of Ir complexes **C1** and **C4** both show irreversible oxidations at two potentials, E_{pa} = 1318 mV for **C1** and at E_{pa} = 1056 mV for **C4**. These oxidations may be attributed to Ir(III) → Ir(IV). Ru complexes **C3** and **C6** also undergo an oxidation process at E_{pa} = 1266 mV and E_{pa} = 1032 mV respectively, an oxidation associated with the Ru(II) → Ru(III). An oxidation of the metals of complexes **C2** and **C5** to a higher oxidation state, Rh(III) → Rh(IV), is also observed at anodic potentials of 1119 mV and 1063 mV respectively. The oxidation observed for complexes **C1**-**C6** are not reversible, this suggests that once the metals undergo the electron transfer process, the oxidated species is not stable and rapidly undergoes another reaction. From the results obtained, it is evident that the oxidation of the iodido complexes is a relatively facile process in comparison to the chlorido complexes since they oxidise at lower potentials. This is related to the donating ability of the halogen ligand. Iodine is less electronegative than chlorine i.e., it is a better electron donor, this means that loss of electrons of this complex will occur easier than for the chlorido complexes. The voltammograms of complexes **C1**-**C6** (see *Figure 2.12* below), show reduction and quasi-reversible processes (indicated by ↔ on *Table 2.8* and **2.9**) which can be attributed to the

halogenido ligands being cleaved off. A study of the electrochemistry of complexes **C7**-**C12** was not performed due to time constraints.

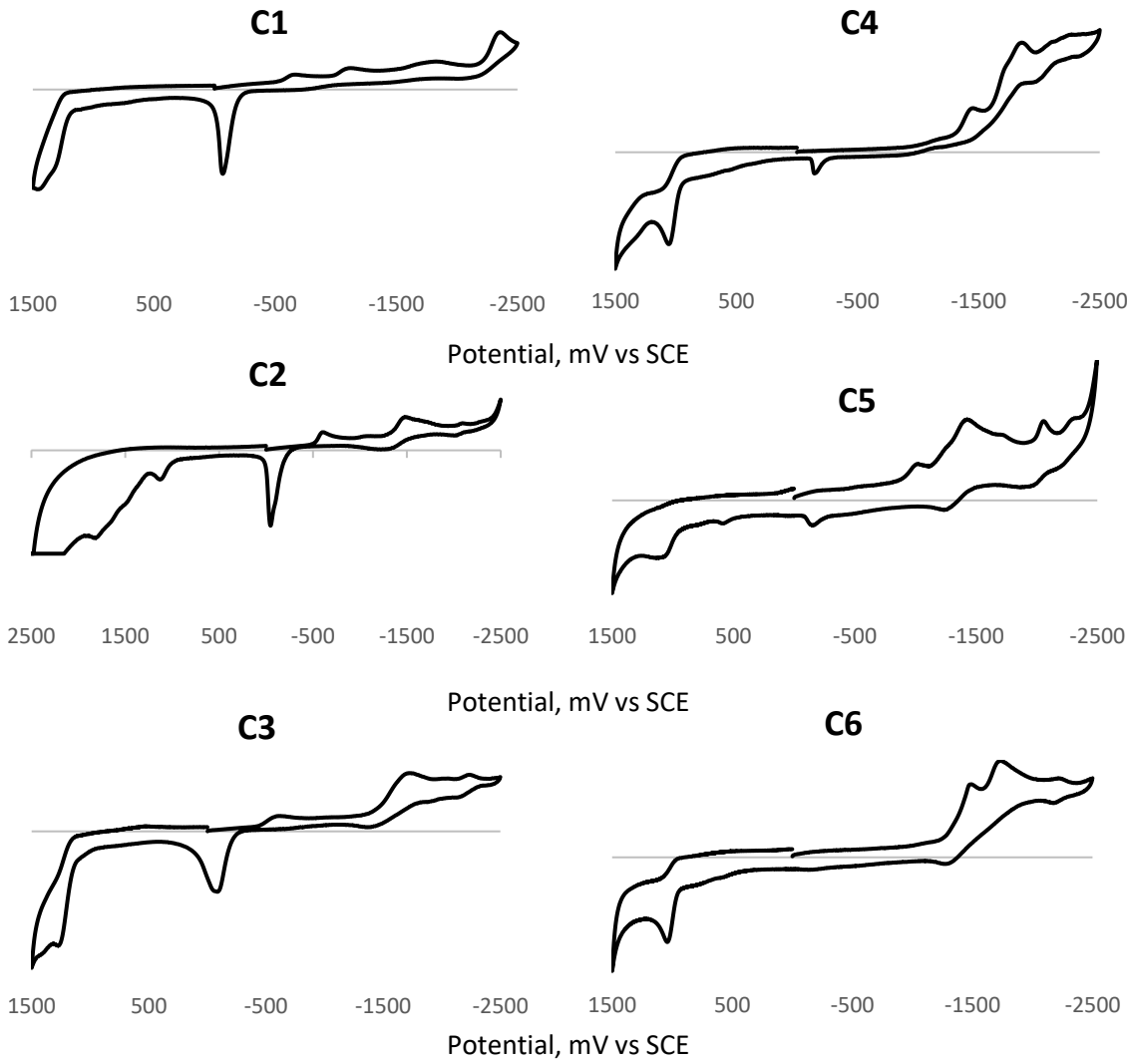

*Figure 2.12: Cyclic voltammogram (reduction-oxidation) of **C1**-**C6** ligand at a scan rate of 100 mV/s.*

Using HPLC, the purity analysis of the complexes was done and good (95-99%) HPLC traces were obtained. All complexes but **C2** was analysed using trifluoroacetic acid (TFA) in methanol as an ion pairing agent. Complexes **C2** and **C8** did not generate good traces using TFA, this may be due to TFA decomposing the complex or driving the complexes to hydrolyse. HPLC of complex C2 was then done in H_2O/ MeCN using a high concentration of sodium chloride (NaCl) to supress any hydrolysis. HPLC of C8 could not be obtained due to time constraints, the same HPLC method will be used to analyse it. A representative HPLC chromatogram of complex **C10** showing its purity is shown on Figure 2.14 on the next page.

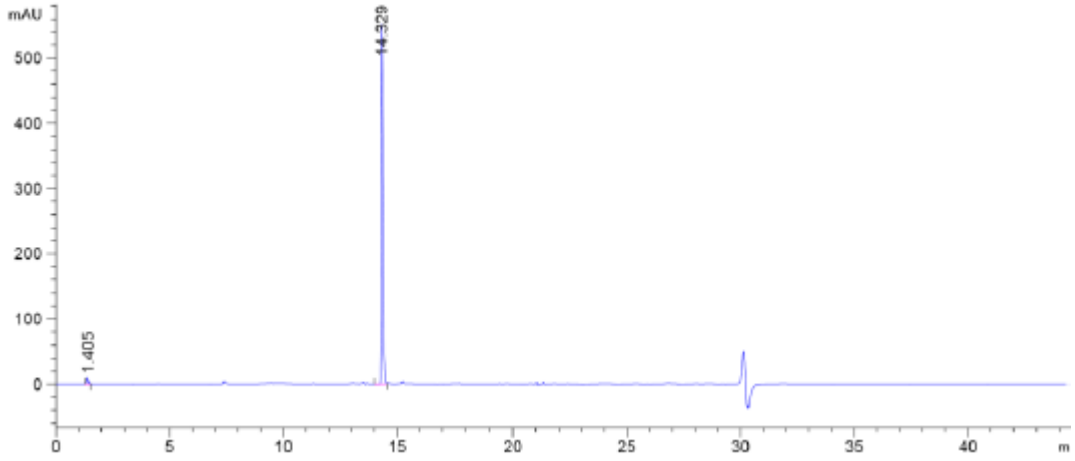

*Figure 2.14: HPLC chromatogram of complex **C10** with 98% purity.*

2.3. Summary

Twelve complexes (**C1**-**C12**) of the ligand 2,2'-dipyridylamine (**Dpa**), of which six were new, were synthesized successfully in moderate to good yields. They were characterized using FTIR, ^{1}H NMR, ^{13}C NMR (**C7**-**C12**), ESI-mass spectrometry (**C7**-**C12**), XRD (**C2**, **C5**, **C7** and **C9**), HPLC and CV (**C1**-**C6**). To obtain the purity of the complexes, HPLC studies were conducted in methanol. It was found that complexes were 95-99 % pure. XRD proved beyond reasonable doubt that the metal coordinates to **Dpa** via the nitrogen atoms of the pyridyl rings. DMSO interaction studies using NMR suggested that all complexes may be stable in DMSO even after 24 hours of standing at room temperature, however, UV-Vis studies suggest otherwise. More studies are required in order to confirm the reactivity of complexes **C1**-**C12** with DMSO. Cyclic voltammetry showed that complexes **C1**-**C6** undergo irreversible oxidation reactions due to the unstable nature of the oxidated species that may be involved in other reactions immediately after the electron transfer preventing it from reversing the oxidation.

2.4. Experimental Section

2.4.1. Materials and Instrumentation

Chemicals and reagents. Metal dimer starting material $IrCl_3{\cdot}3H_20$, $RhCl_3{\cdot}H_2O$ and $RuCl_3.3H_2O$ were all purchased from Heraeus Metals. 2,2'-dipyridylamine (95 %), 1,2,3,4,5-cyclopentadiene, ammonium hexafluorophosphate, ammonium nitrate, trifluoroacetic acid (TFA), sodium chloride, Tetra-*n*-butyl ammonium perchlorate ($TBAClO_4$) and all reagent solvents (analytical grade) were obtained from Sigma Aldrich (Merck). Methanol used for reactions was distilled before use, all other solvents and reagents were used as received. Deuterated solvents methanol-d4 and dimethylsulfoxide-d6 were obtained from Cambridge. HPLC solvents, i.e., H_2O, MeOH and MeCN, were also used as received.

Instrumentation. IR spectroscopy was performed using a NICOLET FTIR with an ATR accessory. ^{1}H and ^{13}C NMR was recorded on a 400 MHz Varian Unity Inova spectrometer. Mass spectrometry was performed using a Waters Synapt G2 instrument in the positive ionisation mode.

HPLC was conducted on an Agilent 1200 system with a quad pump and DAD detector using a Kinetex C180 100 Å, 150 x 4.6 mm diameter with 5μM pore sizes. For **C1, C3, C4-C7**, **C9-C11,** H_2O 0.1 % TFA / MeOH 0.1 % TFA was used at gradients of t = 0 min 10 % A, t = 20 min 90 % A, t = 30 min 90 % A, t =

31 min 10 % A and t = 45 min 10 % A over a 45 min period. Flow rate was 1 mL min^{-1}, and the detection wavelength was set at 254 nm, 260 nm and 300 nm with the reference wavelength at 360 nm. Sample injections were half the loop volume (50 µL) with needle washes of 50 % H_2O/MeOH between injections. It was assumed that all species have the same extinction coefficient at 254 nm, 260 nm and 300 nm. All peaks were manually integrated to gain the percentage area. Samples were dissolved in 10 % MeOH / 90 % H_2O at ca. 100 µM. The mobile phase for **C2** was 50mM NaCl in H_2O/ MeCN 3:1 50mMNaCl at gradients t = 0 min 10 % B, t = 10 min 20 % B, t = 20 min 60 % B, t = 25 min 100 % B, t = 30 min 100 % B, t = 35 min 10% B and t = 40 min 10% over a 40 min period. Flow rate was 1 mL min^{-1}, and the detection wavelength was set at 254 nm, 290 nm, 300 nm and 320 nm with the reference wavelength at 360 nm. Sample injections were half the loop volume (50 µL) with needle washes of 50 % H_2O/MeCN between injections. It was assumed that all species have the same extinction coefficient at 254 nm, 290 nm, 300 nm and 320 nm. All peaks were manually integrated to gain the percentage area. Samples were dissolved in 10 % MeCN / 90 % H_2O at ca. 100 µM.

UV-Vis was analysed using a Macro Cell 110-QS cuvette with a 10mm light path and SPECTROstar Nano Microplate reader.

Electrochemical measurements were recorded using Basi Epsilon Eclipse Electrochemical Analyzer Potentiostat/Galvanostat. A three-electrode system consisting of a glassy carbon disk as the working electrode, a platinum wire as the counter/auxiliary electrode and $Ag/AgNO_3$ as the reference electrode. The electrodes were mounted in a single-compartment cell configuration. Cyclic voltammograms were obtained from a 10^{-3} M stock solution of analyte in acetonitrile containing 0.1 M of the supporting electrolyte, i.e., TBAP (tetra-n-butylammonium fluoride).

2.4.2. General Method for synthesis of C1-C6

2,2'-dipyridylamine (1 equiv.) was dissolved in dry methanol (4 mL) and the appropriate metal dimer (0.5 equiv.) was added. The mixture was reacted in a microwave for 1 minute at 100°C. Solution was cooled to room temperature and NH_4PF_6 (1 equiv.) was added. The reaction was stirred at room temperature. The reaction was monitored with TLC to see the consumption of starting material. When starting material could no longer be detected, reaction mixture was stirred for a further 2 hours. Crude precipitate at the end of the reaction was filtered off, redissolved in acetone and filtered through celite. The volume of the filtrate was reduced and recrystallised through the addition of diethyl ether and the complexes precipitated out as crystalline powders. Complexes were isolated in moderate to good yields (70-78 %) as yellow, orange and red crystalline powders.

2.4.2.1. $[Ir(\eta^5\text{-}Cp^*)(dpa)Cl]PF_6$ (C1)

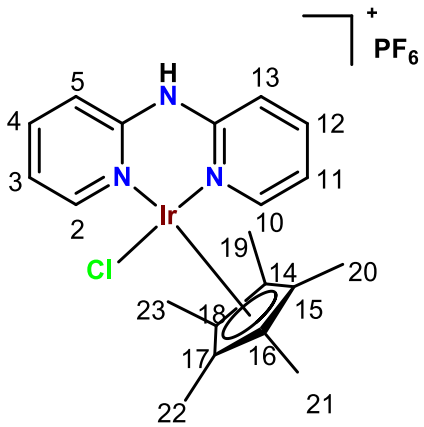

The dimer $[Ir(\mu\text{-}Cl)(\eta^5\text{-}(Cp^*))Cl_2]$ (50 mg, 0.063 mmol) was reacted with **Dpa** (23 mg, 0.134 mmol) for 3 hours and NH_4PF_6 (24 mg, 0.147 mmol) was then added. The product (**C1**) was isolated as a yellow

crystalline solid (61 mg, 72% yield).IR (ATRcm^{-1}): 667, 749, 782, 832, 876, 1028, 1162, 1226, 1351, 1386, 1435,1472, 1490, 1522, 1582, 1628, 3022, 3083, 3130, 3183. ^{1}H NMR (400 MHz, methanol-d4) δ 8.43 (d, *J*(H_4 and H_{12}) 5.8 Hz , 2H, H_2 and H_{10}), 7.95 (t, *J*(H_3, H_5, H_{11} and H_{13}) = 8 Hz, 2H, H_4 and H_{12}), 7.30 (d, *J*(H_4 and H_{12}) = 8.2 Hz, 2H, H_5 and H_{13}), 7.25 (t, *J* (H_2, H_4, H_{10} and H_{12})= 6.1 Hz, 2H, H_3 and H_{11}), 1.47 (s, 15H, H_{19} – H_{23}). HPLC: retention time of 11.25 min = 98% pure.

2.4.2.2. [Rh(η^5-Cp*)(dpa)Cl]PF_6 C2:

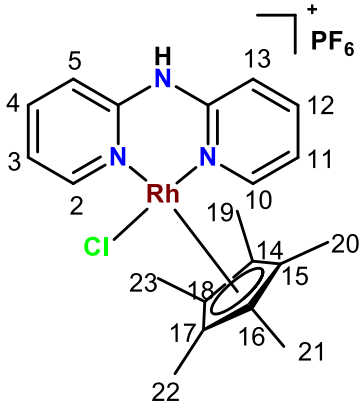

The dimer [Rh(μ-Cl)(η^5-(Cp*))Cl_2] (50 mg, 0.081 mmol) was reacted with **Dpa** (27 mg, 0.157 mmol) for 3 hours and NH_4PF_6 (28 mg, 0.171 mmol) was then added. The product (**C2**) was isolated as a yellow crystalline solid (68 mg, 72% yield). IR (ATR, cm^{-1}): 681, 739, 772, 834, 904, 1021, 1078, 1126, 1161, 1233, 1352, 1376, 1470, 1518, 1584, 1624, 2922, 3384. ^{1}H NMR (400 MHz, methanol-d4) δ 8.44 (d, *J*(H_4 and H_{12}) 4.8 Hz , 2H, H_2 and H_{10}), 7.98 (t, *J*(H_3, H_5, H_{11} and H_{13}) = 7.8 Hz, 2H, H_4 and H_{12}), 7.28-7.32 (m, 4H, H_3, H_5 , H_{11} and H_{13}), 1.49 (s, 15H, $H_{19\text{-}23}$). HPLC: retention time of 18.889 min = 99% pure.

2.4.2.3. [Ru(η^5-(p-cymene))(dpa)Cl]PF_6 C3:

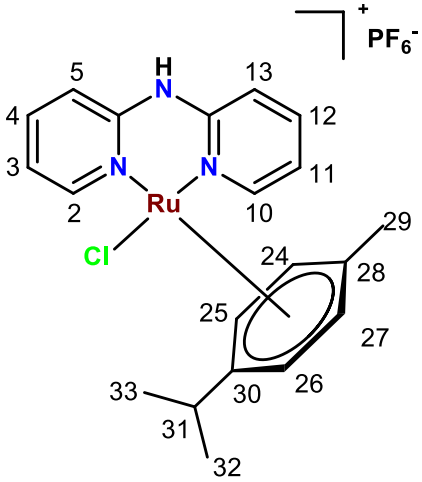

The dimer [Ru(μ-Cl)(η^5-(p-cymene))Cl_2]$_2$ (50 mg, 0.082 mmol) was reacted with **Dpa** (29 mg, 0.169 mmol) for 2 hours and NH_4PF_6 (29 mg, 0.178 mmol) was then added. The product (**C3**) was isolated as an orange powder (0.035 mg, 74% yield). IR (ATR, cm^{-1}): 677, 763, 829, 878, 965, 1024, 1058, 1091, 1160, 1233, 1279, 1341, 1436, 1464, 1489, 1522, 1582, 1625, 2362, 3084, 3160, 3230.^{1}H NMR (400 MHz, methanol-d4) δ 8.63 (d, *J*(H_4 and H_{12}) 5.8 Hz , 2H, H_2 and H_{10}), 7.92 (t, *J*(H_3, H_5, H_{11} and H_{13}) = 7.8 Hz, 2H, H_4 and H_{12}), 7.16-7.24 (m, 4H, H_3, H_5 , H_{11} and H_{13}), 5.66 (d, *J* (H_{25} and H_{26})= 6 Hz, 2H, H_{24} and H_{27}), 5.56 (d, *J* (H_{24} and H_{27})= 6 Hz, 2H, H_{25} and H_{26}), 2.65 (s, 1H, H_{31}), 2.09 (s, 3H, H_{29}), 1.22 (d, *J* (H_{31})= 7.2 Hz, 6H, H_{32} and H_{33}). HPLC: retention time of 10.188 min = 95% pure.

2.4.2.4. [Ir(η^5-Cp*)(dpa)I]PF$_6$: C4:

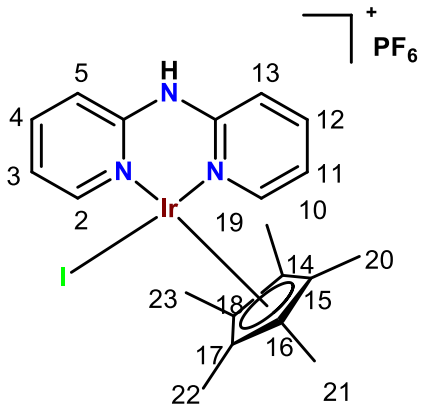

The dimer [Ir(μ-I)(η^5-(Cp*))I$_2$]$_2$ (50 mg, 0.043 mmol) was reacted with **Dpa** (15 mg, 0.093 mmol) for 3 hours and NH_4PF_6 (13 mg, 0.080 mmol) was then added. The product (**C4**) was isolated as a yellow crystalline powder (52 mg, 78% yield).IR (ATR, cm^{-1}): 683, 740, 768, 831, 875, 906, 1025, 1079, 1125, 1161, 1231, 1359, 1384, 1431, 1471, 1520, 1583, 1626, 1702, 2359, 2912, 3363. ^{1}H NMR (400 MHz, methanol-d4) δ 8.65 (d, *J*(H_4 and H_{12}) 6 Hz , 2H, H_2 and H_{10}), 7.98 (t, *J*(H_3, H_5, H_{11} and H_{13}) = 7.2 Hz, 2H, H_4 and H_{12}), 7.28 (d, *J*(H_4 and H_{12}) = 8 Hz, 2H, H_5 and H_{13}), 7.25 (t, *J* (H_2, H_4, H_{10} and H_{12})= 65.8 Hz, 2H, H_3 and H_{11}), 1.62 (s, 15H). HPLC: retention time of 13.925 min = 95% pure.

2.4.2.5. [Rh(η^5-Cp*)(dpa)I]PF$_6$ C5:

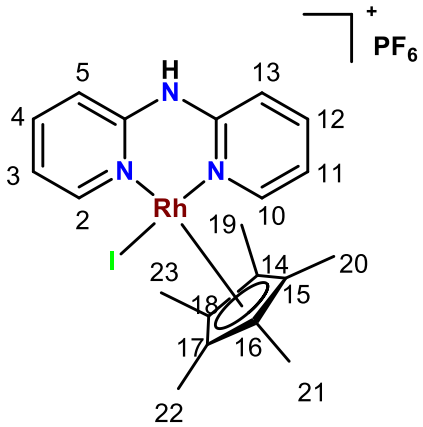

The dimer [Rh(η^5-Cp*)(dpa)I]PF$_6$ (50 mg, 0.051 mmol) was reacted with **Dpa** (17 mg, 0.099 mmol) for 3 hours and NH_4PF_6 (18 mg, 0.114 mmol) was then added. The product (**C5**) was isolated as orange shiny crystalline powder (49 mg, 71% yield).IR (ATRcm^{-1}): 680, 739, 768, 827, 870, 1020, 1079, 1123, 1159, 1124, 1213, 1266, 1356, 1378, 1469, 1489, 1519, 1583, 1624, 1696, 2980, 3377. ^{1}H NMR (400 MHz, methanol-d4) δ 8.67 (d, *J*(H_4 and H_{12}) 1.6 Hz , 2H, H_2 and H_{10}), 7.98 (t, *J*(H_3, H_5, H_{11} and H_{13}) = 7.8 Hz, 2H, H_4 and H_{12}), 7.28 (d, *J*(H_4 and H_{12}) = 8.4 Hz, 2H, H_5 and H_{13}), 7.25 (t, *J* (H_2, H_4, H_{10} and H_{12})= 6.6 Hz, 2H, H_3 and H_{11}), 1.62 (s, 15H, H_{19} – H_{23}). HPLC: retention time of 13.175 min = 96% pure.

2.4.2.6. [Ru(η^5-(p-cymene))(dpa)I]PF_6 C6:

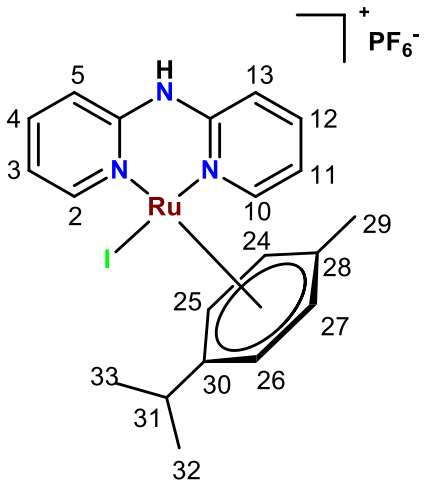

The dimer [Ru(μ-I)(η^5-(p-cymene))I_2]$_2$ (50 mg, 0.051 mmol) was reacted with **Dpa** (17 mg, 0.099 mmol) for 2 hours and NH_4PF_6 (19mg, 0.117 mmol) was then added. The product (**C6**) was isolated as a red shiny crystalline powder (0.045 mg, 70% yield). IR (ATR, cm^{-1}): 671, 747, 766, 832, 881, 1033, 1058, 1087, 1119, 1159, 1169, 1232, 1347, 1381, 1433, 1466, 1523, 1583, 1625, 1916, 2966, 3321, 3368, 3852.^{1}H NMR (400 MHz, methanol-d4) δ 8.81 (d, *J*(H_4 and H_{12}) 6 Hz , 2H, H_2 and H_{10}), 7.89 (t, *J*(H_3, H_5, H_{11} and H_{13}) = 7.9 Hz, 2H, H_4 and H_{12}), 7.16 (d, 2H, J (H_4 and H_{12}) = H_5 and H_{13}, 2H, H_5 and H_{13}), 7.12 (t, *J* (H_2, H_4, H_{10} and H_{12}) 7.9 Hz , 2H, H_3 and H_{11}), 5.66 (d, *J* (H_{25} and H_{26})= 6.4 Hz, 2H, H_{24} and H_{27}), 5.56 (d, *J* (H_{24} and H_{27})= 6.4 Hz, 2H, H_{25} and H_{26}), 2.65 (s, 1H, H_{31}), 2.09 (s, 3H, H_{29}), 1.22 (d, *J* (H_{31})= 6.8 Hz, 6H, H_{32} and H_{33}). HPLC: retention time of 13.312 min = 97% pure.

2.4.3. General Method for synthesis of C7-C12

2,2'-dipyridylamine (1 equiv.) was dissolved in dry methanol (4 mL) and the appropriate metal dimer (0.5 equiv.) was added. The mixture was reacted in a microwave for 1 minute at 100°C. Solution was cooled to room temperature and NH_4NO_3 (1 equiv.) was added. The reaction was stirred at room temperature. The reaction was stirred overnight for a further ~18 hours. The volume of filtrate was reduced and recrystallised through the addition of diethyl ether and the complexes precipitated out as crystalline powders. Complexes were isolated in moderate to good yields (41-86 %) as yellow and orange and crystalline powders.

2.4.3.1. [Ir(η^5-Cp*)(dpa)Cl]NO_3 C7:

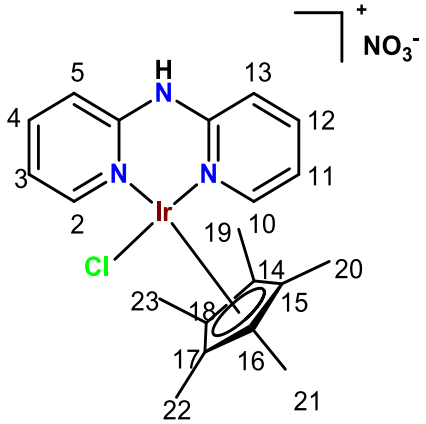

The dimer [Ir(μ-Cl)(η^5-(Cp*))Cl$_2$] (107 mg, 0.134 mmol) was reacted with **Dpa** (46 mg, 0.269 mmol) for 18 hours and NH_4NO_3 (23 mg, 0.287 mmol) was then added. The product (**C7**) was isolated as a yellow a powder (134 mg, 86% yield).IR (ATRcm^{-1}): 669, 700, 770, 780, 827, 843, 873, 906, 1035, 1073, 1109, 1124, 1157, 1213, 1234, 1262, 1310, 1362, 1391, 1440, 1470, 1487, 1528, 1580, 1614, 1637, 2918, 3065, 3179. ^{1}H NMR (400 MHz, methanol-d4) δ 8.42 (d, *J*(H_4 and H_{12}) 6 Hz , 2H, H_2 and H_{10}), 7.95 (t, *J*(H_3, H_5, H_{11} and H_{13}) = 7.8 Hz, 2H, H_4 and H_{12}), 7.32 (d, *J*(H_4 and H_{12}) = 8.2 Hz, 2H, H_5 and H_{13}), 7.24 (t, *J* (H_2, H_4, H_{10} and H_{12})= 6.7 Hz, 2H, H_3 and H_{11}), 1.47 (s, 15H, H_{19} – H_{23}). ^{13}C NMR (400 MHz, methanol-d4) δ 153.62 ($C_{6,8}$), 153.37 ($C_{2,10}$), 142.38 ($C_{4,12}$), 122.20 ($C_{3,11}$), 115.35 ($C_{5,13}$), 89.55 ($C_{14\text{-}18}$), (49.00 methanol CH_3)8.57 ($C_{19\text{-}23}$). ESI+ MS (*m/z*) 534.1289 [M]$^+$. HPLC: retention time of 11.25 min = 98% pure

2.4.3.2. [Rh(η^5-Cp*)(dpa)Cl]NO$_3$ C8:

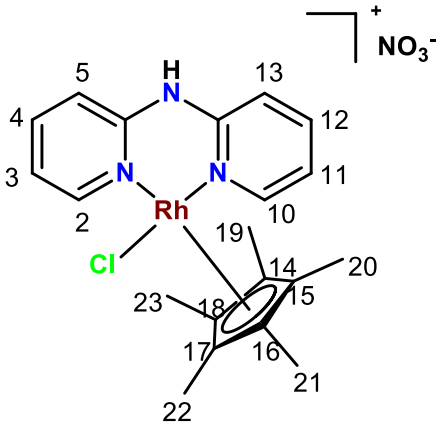

The dimer [Rh(μ-Cl)(η^5-(Cp*))Cl$_2$] (100 mg, 0.162 mmol) was reacted with **Dpa** (50 mg, 0.292 mmol) for 18 hours and NH_4NO_3 (26 mg, 0.325 mmol) was then added. The product (**C8**) was isolated as a yellow powder (0.138 mg, 84% yield). IR (ATR, cm^{-1}): 667, 699, 741, 771, 827, 842, 873, 904, 1019, 1036, 1084, 1122, 1156, 1234, 1262, 1311, 1356, 1389, 1437, 1467, 1527, 1579, 1634, 2955. ^{1}H NMR (400 MHz, methanol-d4) δ 8.45 (d, *J*(H_4 and H_{12}) 6.8 Hz , 2H, H_2 and H_{10}), 8.09 (t, *J*(H_3, H_5, H_{11} and H_{13}) = 7.9 Hz, 2H, H_4 and H_{12}), 7.30-7.34 (m, 4H, H_3, H_5 , H_{11} and H_{13}), 1.50 (s, 15H, $H_{19\text{-}23}$). HPLC: retention time of 18.889 min = 99% pure. ^{13}C NMR (400 MHz, methanol-d4) δ 153.81 ($C_{6,8}$), 152.71 ($C_{2,10}$), 142.21 ($C_{4,12}$), 122.06 ($C_{3,11}$), 115.65 ($C_{5,13}$), 97.95 ($C_{14\text{-}18}$), (49.00 methanol CH_3) 9.85 ($C_{19\text{-}23}$). ESI+ MS (*m/z*) 444.0718 [M]$^+$.

2.4.3.3. [Ru(η^5-(p-cymene))(dpa)Cl]NO$_3$ C9:

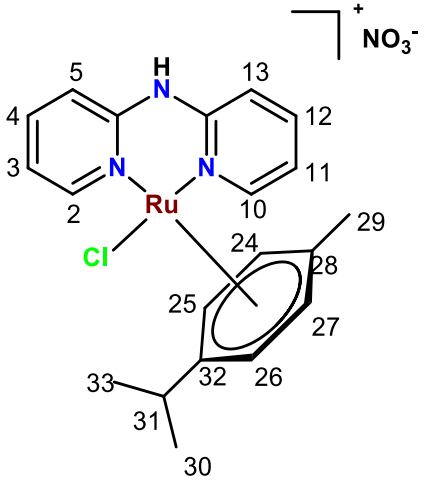

The dimer $[Ru(\mu\text{-}Cl)(\eta^5\text{-}(p\text{-cymene}))Cl_2]_2$ (100 mg, 0.163 mmol) was reacted with **Dpa** (56 mg, 0.327 mmol) for 18 hours and NH_4NO_3 (26 mg, 0.325 mmol) was then added. The product (**C9**) was isolated as an orange powder (68 mg, 41% yield). IR (ATR, cm^{-1}): 662, 766, 826, 869, 886, 922, 996, 1024, 1062, 1088, 1120, 1158, 1223, 1315, 1354, 1382, 1431, 1469, 1528, 1582, 1613, 1634, 2965.^{1}H NMR (400 MHz, methanol-d4) δ 8.63 (d, *J*(H_4 and H_{12}) 6.2 Hz , 2H, H_2 and H_{10}), 7.92 (t, *J*(H_3, H_5, H_{11} and H_{13}) = 5.8 Hz, 2H, H_4 and H_{12}), 7.19-7.22 (m, 4H, H_3, H_5 , H_{11} and H_{13}), 5.67 (d, *J* (H_{25} and H_{26})= 6.4 Hz, 2H, H_{24} and H_{27}), 5.57 (d, *J* (H_{24} and H_{27})= 6.4 Hz, 2H, H_{25} and H_{26}), 2.62 (s, 1H, H_{31}), 2.10 (s, 3H, H_{29}), 1.23 (d, *J* (H_{31})= 4 Hz, 6H, H_{32} and H_{33}). ^{13}C NMR (400 MHz, methanol-d4) δ 155.72 ($C_{6,8}$), 15.45 ($C_{2,10}$), 141.77 ($C_{4,12}$), 120.66 ($C_{3,11}$), 115.02 ($C_{5,13}$), 108.13 (C_{30}) 101.34 (C_{28}), 86.83 ($C_{24,27}$), 85.21 ($C_{25,26}$), (49.00 methanol CH_3) 32.18 (C_{31}), 22.34 ($C_{32,33}$), 18.36 (C_{29}). ESI+ MS (*m/z*) 442.0929 $[M]^+$, HPLC: retention time of 10.257 min = 94% pure.

2.4.3.4. $[Ir(\eta^5\text{-}Cp^*)(dpa)I]NO_3$ C10:

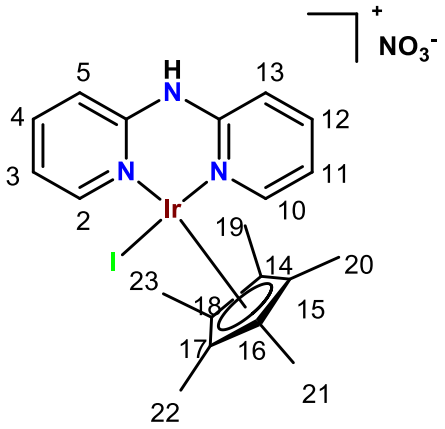

The dimer $[Ir(\mu\text{-}I)(\eta^5\text{-}(Cp^*))I_2]_2$ (44 mg, 0.038 mmol) was reacted with **Dpa** (13 mg, 0.076 mmol) for 18 hours and NH_4NO_3 (7 mg, 0.087 mmol) was then added. The product (**C10**) was isolated as a yellow crystalline powder (35 mg, 67% yield).IR (ATR, cm^{-1}): 672, 702, 739, 766, 840, 876, 906, 950, 1022, 1079, 1122, 1154, 1231, 1244, 1300, 1363, 1383, 1398, 1429, 1470, 1488, 1523, 1579, 1625, 1645, 2909, 2954. ^{1}H NMR (400 MHz, methanol-d4) δ 8.66 (d, *J*(H_4 and H_{12}) 6.8 Hz , 2H, H_2 and H_{10}), 7.93 (t, *J*(H_3, H_5, H_{11} and H_{13}) = 7.90 Hz, 2H, H_4 and H_{12}), 7.16 (d, *J*(H_4 and H_{12}) = 8.2 Hz, 2H, H_5 and H_{13}), 7.16 (t, *J* (H_2, H_4, H_{10} and H_{12})= 9.2 Hz, 2H, H_3 and H_{11}), 1.55 (s, 15H, H_{19}-H_{23}). ESI+ MS (*m/z*) 626.0641 $[M]^+$, HPLC: retention time of 14.329 min = 98% pure.

2.4.3.5. $[Rh(\eta^5\text{-}Cp^*)(dpa)I]NO_3$ C11:

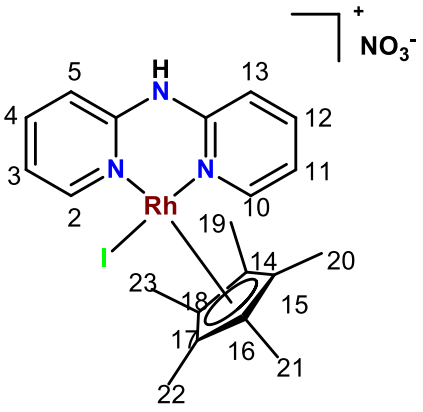

The dimer [Rh(μ-I)(η^5-Cp*)I_2]$_2$ (100 mg, 0.102 mmol) was reacted with **Dpa** (34 mg, 0.0.199 mmol) for 18 hours and NH_4NO_3 (17 mg, 0.212 mmol) was then added. The product (**C11**) was isolated as an orange shiny crystalline powder (94 mg, 78% yield). IR (ATR cm^{-1}): 707, 740, 768, 839, 877, 905, 965, 1018, 1036, 1076, 1120, 1153, 1231, 1261, 1301, 1360, 1382, 1427, 1468, 1487, 1523, 1578, 1623, 2956, 3054, 3154.^{1}H NMR (400 MHz, methanol-d4) δ 8.66 (d, *J*(H_4 and H_{12}) 6 Hz , 2H, H_2 and H_{10}), 7.98 (t, *J*(H_3, H_5, H_{11} and H_{13}) = 7.9 Hz, 2H, H_4 and H_{12}), 7.31 (d, *J*(H_4 and H_{12}) = 8.4 Hz, 2H, H_5 and H_{13}), 7.25 (t, *J* (H_2, H_4, H_{10} and H_{12})= 6.5 Hz, 2H, H_3 and H_{11}), 1.63 (s, 15H, H_{19} – H_{23}). ^{13}C NMR (400 MHz, methanol-d4) δ 156.02 ($C_{6,8}$), 153.80 ($C_{2,10}$), 142.11 ($C_{4,12}$), 121.80 ($C_{3,11}$), 115.33 ($C_{5,13}$), 98.50 ($C_{14\text{-}18}$), (49.00 methanol CH_3) 9.85 ($C_{19\text{-}23}$). ESI+ MS (*m/z*) 538.0073 $[M]^+$, HPLC: retention time of 13.413 min = 97% pure.

2.4.3.6. [Ru(η^5-(p-cymene))(dpa)I]NO_3 C12:

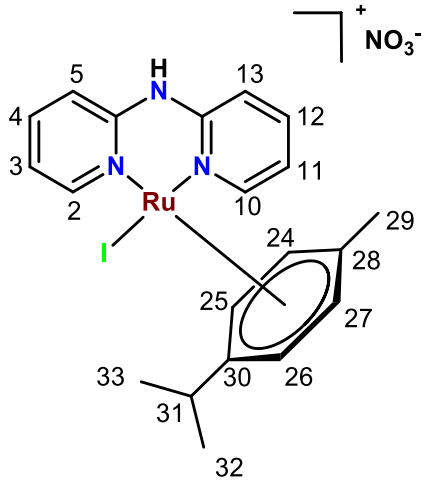

The dimer [Ru(μ-I)(η^5-(p-cymene))I_2]$_2$ (100 mg, 0.102 mmol) was reacted with **Dpa** (35 mg, 0.204 mmol) for 18 hours and NH_4PF_6 (19 mg, 0.249 mmol) was then added. The product (**C12**) was isolated as a red shiny crystalline powder (85 mg, 70% yield). IR (ATR, cm^{-1}): 670, 746, 764, 802, 826, 558, 1024, 1056, 1085, 117, 1155, 1233, 1317, 1345, 1376, 1432, 1466, 1489, 1520, 1580 ,1623, 2966, 2966, 3051, 3150. ^{1}H NMR (400 MHz, methanol-d4) δ 8.81 (d, *J*(H_4 and H_{12}) 4.2 Hz , 2H, H_2 and H_{10}), 7.89 (t, *J*(H_3, H_5, H_{11} and H_{13}) = 6.8 Hz, 2H, H_4 and H_{12}), 7.19 (d, 2H, J (H_4 and H_{12}) = 6 H_5 and H_{13}, 2H, H_5 and H_{13}), 7.12 (t, *J* (H_2, H_4, H_{10} and H_{12}) 6.6 Hz , 2H, H_3 and H_{11}), 5.68 (d, *J* (H_{25} and H_{26})= 6.4 Hz, 2H, H_{24} and H_{27}), 5.62 (d, *J* (H_{24} and H_{27})= 6.4 Hz, 2H, H_{25} and H_{26}), 2.66 (s, 1H, H_{31}), 2.22 (s, 3H, H_{29}), 1.22 (d, *J* (H_{31})= 3.2 Hz, 6H, H_{32} and H_{33}). ^{13}C NMR (400 MHz, methanol-d4) δ 158.81.72 ($C_{6,8}$), 154.36 ($C_{2,10}$), 141.58 ($C_{4,12}$), 120.32 ($C_{3,11}$), 114.69 ($C_{5,13}$), 109.77 (C_{30}) 100.81 (C_{28}), 87.50 ($C_{24,27}$), 84.52 ($C_{25,26}$), (49.00 methanol CH_3) 32.63 (C_{31}), 22.43 ($C_{32,33}$), 19.59 (C_{29}). ESI+ MS (*m/z*) 533.9994 $[M]^+$.

2.4.4. Single crystal X-ray diffraction:

Single crystals of **C1** and **C2** were grown from a solution of acetone and diethyl ether and single crystals of complexes **C7** and **C9** were grown from a solution of methanol and diethyl ether. Single-crystal X-ray intensity data were collected on a Bruker 3-circle Apex II DUO X-ray diffractometer equipped with an INCOATEC IμS HB microfocus sealed tube (MoKα radiation λ = 0.71073 Å) fitted with a multilayer monochromator. Data were captured with a CCD (charge-coupled device) area detector. Data collection was carried out at 100 K using an Oxford Cryosystems cryostat (700 series Cryostream Plus) attached to the diffractometer. Data collection and reduction were carried out using the Bruker software package APEX3, using standard procedures. All structures were solved and refined using SHELX-2016 employed within the X-Seed3, environment. Hydrogen atoms were placed in calculated

positions using standard riding models. X-ray diffraction data are summarised in *Table 2.10* and *2.11*. Distances and angles were calculated using Mercury software version 4.3.1.

*Table 2.10.: Crystal data and structure refinement details of complexes **C1** and **C7**.*

		C1	**C7**
Empirical formula		$C_{20}H_{24}ClF_6IrN_3P$	$C_{20}H_{25}ClN_4O_4Ru$
Formula weight		679.04	596.08
Temperature (K)		100(2)	100(2)
Wavelength (Å)		0.71073	0.71073
Crystal system		Orthorhombic	monoclinic
Space group		$P2_12_12_1$	$P21/c$
Unit cell dimensions (Å, °)	***a***	9.0227(7)	*a*8.4482(14)
	b	15.3290(12)	16.812(3)
	c	16.4996(13)	14.096(2)
	α	90	90
	β	90	100.321(2)
	γ	90	90
Volume (Å)		2282.0(3)	2071.3(6)
Z		4	4
Calculated density (g. cm^{-3})		1.976	1,911
Absorption coefficient (mm^{-1})		6.100	6,604
***F*$_{000}$**		1312	1160
Crystal size (mm^3)		0.200 ´ 0.069 ´ 0.047	0.204 ´ 0.121 ´ 0.056
q range for data collection (°)		1.813 to 28.372	1.904 to 29.664
Miller index ranges		$-12 \leq h \leq 12$, $-20 \leq k \leq 20$, $-21 \leq l \leq 22$	$-12 \leq h \leq 12$, $-23 \leq k \leq 23$, $-19 \leq l \leq 19$
Reflections collected		32000	53743
Independent reflections		5700 [R_{int} = 0.0387]	5856 [R_{int} = 0.0529]
Completeness to q$_{max}$ (%)		0.998	0.999
Max. and min. transmission		0.118 and 1.000	0.680 and 1.000
Refinement method		Full- matrix least-squares on F^2	Full-matrix least-squares on F^2

Data/ restraints/ parameters	5700/ 25/ 362	5856 / 0 / 271
Goodness-of-fit on F^2	1.105	1.039
Final R indices [I>2s(I)]	R1 = 00478, *w*R2 = 0.1119	*R*1 = 0.0179, *wR*2 = 0.0390
R indices (all data)	R1 = 00493, *w*R2 = 0.1129	*R*1 = 0.0223, *wR*2 = 0.0403
Largest diff. peak and hole ($eÅ^{-3}$)	3.225 and -0.414	0.622 and -0.535
Absolute structure parameter	0.0064(4)	

*Table 2.11.: Crystal data and structure refinement details of complexes **C2** and **C9**.*

		C2	**C9**
Empirical formula		$C_{20}H_{24}ClF_6N_3PRh$	$C_{20}H_{25}ClN_4O_4Ru$
Formula weight		589.72	521.96
Temperature (K)		100(2)	100(2)
Wavelength (Å)		0.71073	0.71073
Crystal system		Orthorhombic	triclinic
Space group		$P2_12_12_1$	*p-1*
Unit cell dimensions (Å, °)	***a***	9.0227 (7)	8.4482(14)
	b	15.3290 (12)	16.812(3)
	c	16.4996 (13)	14.096(2)
	α	90	96.622(2)
	β	90	106.129(2)
	γ	90	93.986(2)
Volume (Å)		2275.0(4)	1034.81(19)
Z		4	2
Calculated density ($g.\ cm^{-3}$)		1.722	1.675
Absorption coefficient (mm^{-1})		1.001	0.922
F_{000}		1184	532
Crystal size (mm^3)		0.246 ´ 0.228 ´ 0.158	0.157 ´ 0.145 ´ 0.140
q range for data collection (°)		1.812 to 30.501	1.739 to 29.635
Miller index ranges		$-12 \leq h \leq 12$, $-21 \leq k \leq 21$, $-23 \leq l \leq 23$	$-11 \leq h \leq 11$, $-14 \leq k \leq 14$, $-17 \leq l \leq 17$

Reflections collected	42571	59403
Independent reflections	6935 [R_{int} = 0.0387]	5830 [R_{int} = 0.0329]
Completeness to q_{max} (%)	0.999	0.998
Max. and min. transmission	0.876 and 1.000	0.950 and 1.000
Refinement method	Full- matrix least-squares on F^2	Full-matrix least-squares on F^2
Data/ restraints/ parameters	6935/ 138/ 362	5830 / 4 / 286
Goodness-of-fit on F^2	1.043	1.059
Final R indices [I>2s(I)]	R1 = 0.0174, *w*R2 = 00421	*R*1 = 0.0190, *wR*2 = 0.0487
R indices (all data)	R1 = 0.0179, *w*R2 = 0.0423	*R*1 = 0.0201, *wR*2 = 0.0493
Largest diff. peak and hole (eÅ^{-3})	0.437 and -0.345	0.459 and -0.674
Absolute structure parameter	0.010(7)	

2.5. References:

(1) Mutabingwa, T.; Nzila, A.; Mberu, E.; Nduati, E.; Winstanley, P.; Hills, E.; Watkins, W. Chlorproguanil-Dapsone for Treatment of Drug-Resistant Falciparum Malaria in Tanzania. *Lancet* **2001**, *358* (9289), 1218–1223. https://doi.org/10.1016/S0140-6736(01)06344-9.

(2) WHO. *Q&A on artemisinin resistance*. http://www.who.int/malaria/media/artemisinin_resistance_ga/en/ (accessed Oct 16, 2020).

(3) WHO. *World Health Organization Model List of Essential Medicines*; **2019**.

(4) Rajapakse, C. S. K.; Martı, A.; Naoulou, B.; Jarzecki, A. A.; Sua, L.; Deregnaucourt, C.; Schre, J.; Musi, E.; Ambrosini, G.; Schwartz, G. K.; Sa, R. A. Synthesis , Characterization , and in Vitro Antimalarial and Antitumor Activity of New Ruthenium (II) Complexes of Chloroquine. *Inorg. Chem.* **2009**, *48* (3), 1122–1131. https://doi.org/10.1021/ic802220w.

(5) Chellan, P.; Avery, V. M.; Duffy, S.; Triccas, J. A.; Nagalingam, G.; Tam, C.; Cheng, L. W.; Liu, J.; Land, K. M.; Clarkson, G. J.; Romero-Canelón, I.; Sadler, P. J. Organometallic Conjugates of the Drug Sulfadoxine for Combatting Antimicrobial Resistance. *Chem. - A Eur. J.* **2018**, *24* (40), 10078–10090. https://doi.org/10.1002/chem.201801090.

(6) Navarro, M.; Pekerar, S.; Pe, H. A. Synthesis , Characterization and Antimalarial Activity of New Iridium – Chloroquine Complexes. *Polyhedron* **2007**, *26* (12), 2420–2424. https://doi.org/10.1016/j.poly.2006.12.010.

(7) Wang, S.; Bruneau, C.; Renaud, J. L.; Gaillard, S.; Fischmeister, C. 2,2′-Dipyridylamines: More than Just Sister Members of the Bipyridine Family. Applications and Achievements in Homogeneous Catalysis and Photoluminescent Materials. *Dalt. Trans.* **2019**, *48* (31), 11599–11622. https://doi.org/10.1039/c9dt02165e.

(8) Romain, C.; Gaillard, S.; Elmkaddem, M. K.; Toupet, L. New Dipyridylamine Ruthenium Complexes for Transfer Hydrogenation of Aryl Ketones in Water. *Organometallics.* **2010**, *13*, 1992–1995. https://doi.org/10.1021/om100127f.

(9) Štarha, P.; Dvořák, Z.; Trávníček, Z. Half-Sandwich Ir(III) and Rh(III) 2,2'-Dipyridylamine Complexes: Synthesis, Characterization and in Vitro Cytotoxicity against the Ovarian Carcinoma Cells. *J. Organomet. Chem.* **2018**, *872*, 114–122. https://doi.org/10.1016/j.jorganchem.2018.07.035.

(10) Štarha, P. Half-Sandwich Ru(II) Halogenido, Valproato and 4-Phenylbutyrato Complexes Containing 2,2 -Dipyridylamine: Synthesis, Characterization, Solution Chemistry and In Vitro Cytotoxicity. *molecules* **2016**, *21* (12), 1725. https://doi.org/10.3390/molecules21121725.

(11) Agharkar, S.; Lindenbaum, S.; Higuchi, T. Enhancement of Solubility of Drug Salts by Hydrophilic Counterions: Properties of Organic Salts of an Antimalarial Drug. *J. Pharm. Sci.* **1976**, *65* (5), 747–749. https://doi.org/10.1002/jps.2600650533.

(12) Romero-Canelón, I.; Salassa, L.; Sadler, P. J. The Contrasting Activity of Iodido versus Chlorido Ruthenium and Osmium Arene Azo- and Imino-Pyridine Anticancer Complexes: Control of Cell Selectivity, Cross-Resistance, P53 Dependence, and Apoptosis Pathway. *J. Med. Chem.* **2013**, *56* (3), 1291–1300. https://doi.org/10.1021/jm3017442.

(13) Jungwirth, U.; Kowol, C. R.; Keppler, B. K.; Christian, G. Anticancer Activity of Metal Complexes : Involvement of Redox Processes. *Antioxd Redox Signal.* **2011**, *15* (4), 1085–1127. https://doi.org/10.1089/ars.2010.3663.Anticancer.

(14) Wondrak, G. T. *Redox-Directed Cancer Therapeutics: Molecular Mechanisms and Opportunities.* antioxid Redox Signal; **2009**, 11 (12), 3013-69. https://doi.org/10.1089/ars.2009.2541.

(15) Brogden, D. W.; Berry, J. F. Coordination Chemistry of 2,2'-Dipyridylamine: The Gift That Keeps on Giving. *Comments on Inorganic Chemistry*. **2016**, No. 1, 17–37. https://doi.org/10.1080/02603594.2015.1079522.

(16) Tönnemann, J.; Risse, J.; Grote, Z.; Scopelliti, R.; Severin, K. Efficient and Rapid Synthesis of Chlorido-Bridged Half- Sandwich Complexes of Ruthenium , Rhodium , and Iridium by Microwave Heating. *Eur. J. Inorg. Chem.* **2013**, *2013* (24), 4558–4562. https://doi.org/10.1002/ejic.201300600.

(17) Compounds, C. Metal - Ligand Bifunctional Catalysis: A Nonclassical Mechanism for Asymmetric Hydrogen Transfer between Alcohols and Carbonyl Compounds. *J. Org. Chem.* **2001**, *66* (24).

(18) Gichumbi, J. M.; Friedrich, H. B.; Omondi, B.; Chenia, H. Y. Synthesis, Characterization, and Antimicrobial Studies of Half-Sandwich H6-Toluene Ruthenium Complexes with N,N'-Bidentate Ligands. *J. Coord. Chem.* **2020**, *73* (12), 1833–1847. https://doi.org/10.1080/00958972.2020.1795146.

(19) Wirth, S.; Rohbogner, C. J.; Cieslak, M.; Kazmierczak-Baranska, J.; Donevski, S.; Nawrot, B.; Lorenz, I. P. Rhodium(III) and Iridium(III) Complexes with 1,2-Naphthoquinone-1-Oximate as a Bidentate Ligand: Synthesis, Structure, and Biological Activity. *J. Biol. Inorg. Chem.* **2010**, *15* (3), 429–440. https://doi.org/10.1007/s00775-009-0615-4.

(20) Liu, Z.; Habtemariam, A.; Pizarro, A. M.; Clarkson, G. J.; Sadler, P. J. Organometallic Iridium(III) Cyclopentadienyl Anticancer Complexes Containing C,N-Chelating Ligands. *Organometallics* **2011**, *30* (17), 4702–4710. https://doi.org/10.1021/om2005468.

(21) Shvartsburg, A. A.; Wilkes, J. G. Fragmentation Chemistry of DMSO Complexes of Metal Dications. *J. Phys. Chem. A*. **2002**, 4543–4551.https//doi.org/10.1021/jp020292l.

(22) Starha, P. Half-Sandwich Ir (III) and Rh (III) 2,2'-Dipyridylamine Complexes : Synthesis ,

Characterization and in Vitro Cytotoxicity against the Ovarian Carcinoma Cells. *J. Organ. Chem.* **2018**, *872*, 114–122. https://doi.org/10.1016/j.jorganchem.2018.07.035.

(23) Mandić, Z. Electrochemical Methods in Drug Discovery and Development. Bulgarian Chemical Communications. **2017**, *49* (C), 65–73.

Chapter 3

Biological screening of organometallic complexes

3.1. Introduction

As mentioned in Chapter 1, the study of metal complexes as new and effective medicines is advancing. With a global increase of reduced efficacy due to growing resistance, the necessity for viable new antiplasmodial drugs is evident. To combat this, researchers proposed incorporating metals into current drugs with the aim of improving their efficacy as well as overcoming resistance. This research led to the successful synthesis of the most advanced organometallic antimalarial drug today, i.e., ferrocene derivative of chloroquine, ferroquine. Drug discovery has now advanced past this stage of incorporating metals only into current drugs since it has been reported that incorporating metals into organic pharamacophores can improve their therapeutic efficacy.[1,2] Complexes **C1**-**C6** have previously been synthesized and evaluated against human ovarian cancer cell line, A2780, by Ŝtarha and co-workers. It was found that complexes **C1**, **C4** and **C5** were active.[3,4] The applicability of known complexes **C1**-**C6** as antiplasmodials has not been reported. The study of similar *N, N'* organometallic complexes of the ligand picolinamide, reported by Almodares *et al.,* evaluated for antitumor activity reports varying IC_{50} values with one ruthenium complex showing better potency than cisplatin on tested cells HT-29 (human colon cancer cell line) and MCF-7 (breast cancer cell line).[5]

To make the complexes **C7**-**C12**, the halogenido counterions are exchanged for NO_3^-. Salt formation is an important property in drug discovery. One of the most important factors to consider when addressing the aqueous solubility of a compound is to consider salt formation. The formation of salts do not only influence a compound's solubility, it may also affect its physicochemical, and biological properties such as toxicity and gastrointestinal absorption.[6] The PF_6^- counterion is widely used in the synthesis of half-sandwich organometallic complex for antiplasmodial application. NO_3^- on the other hand, a biologically friendly species that is found in the body, is not used extensively. A study of the complexes with different counterions is done to investigate whether hexafluorophosphate or nitrate complexes would have better activity.

Drug discovery is highly guided by pharmacology since the study of a potential drug candidates' pharmacodynamic and pharmacokinetic properties is very important.[7] During drug development, the physicochemical profiling of a drug with poor properties has proven to be a very costly mistake. The use of efficient and reliable high throughput *in vitro* assays to determine important properties of a drug have become crucial in the early stages of drug discovery.[8] It is thus important that these properties need to be optimized before a drug could be classified as a drug candidate.[9] Thorough investigations are required to gain a complete understanding of a drug's therapeutic efficacy as well as its physicochemical properties to determine the drug's fate. Amongst others, these properties influence how a drug will be delivered to its target site (method of delivery), as well as formulation.[8]

In this chapter, the turbidimetric solubility, aquation studies and *in vitro* biological activity of the ligand (**Dpa**) and complexes (**C1**-**C12**) (*Figure 3.1*) will be discussed.

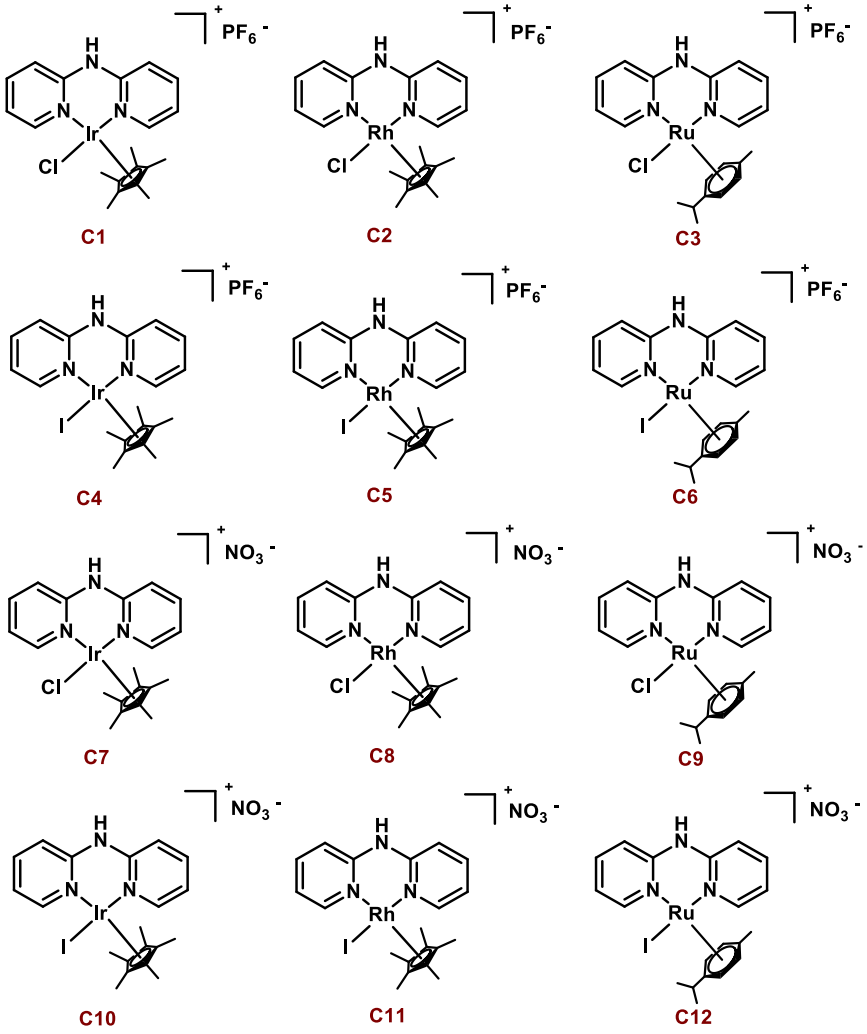

*Figure 3.1.: Structure of complexes **C1**-**C12**.*

Due to COVID-19 delays, the evaluation of complexes **C7**-**C12** against two chloroquine sensitive *P. falciparum* strains of 3D7 and NF45 wa not done.

3.2. Results and Discussion

3.2.1. *Turbidimetric assay*

The solubility of a compound in aqueous based medium is one of the most important physicochemical properties to consider during drug discovery and development amongst others.[10'11] The dose of administered drug that is able to enter the systemic circulation and still have therapeutic effect is influenced by the solubility.[12-13] Low solubility in aqueous media can cause a drug candidate to be eliminated during the early stages of drug discovery, even before functional assessment as a potential drug candidate.[10,14] Additionally, should the drug precipitate at concentration lower than the IC_{50} value, the bioassays will be unreliable.[12,14] Solubility of a compound is dependent on two factors which are the conditions of the solvent within which the compound is dissolved, and its structure pertaining to its physicochemical properties.[12]

Drug developers usually employ medium to high throughput screening techniques to measure the solubility of potential candidates. The kinetic assay is a high throughput assay normally used for

determining *in vitro* solubility.[15] The aqueous solubility of the **Dpa** ligand and the 12 complexes (**C1**-**C12**) were measured with hydrocortisone and reserpine as positive and negative control, respectively with the use of a kinetic assay.

A detailed protocol is given in the experimental section (3.4.2). Briefly, a stock solution of each compound in DMSO was added to phosphate-buffered saline (PBS) which mimics physiological conditions and 4-(2-hydroxyethyl)-1-piperazineethanesulfonic acid (HEPES) buffer which is normally used in the *in vitro P. falciparum assays* in a 96-well plate. The plates were incubated at 25 °C, thereafter, the formation of any precipitate is determined by measuring the absorbance at 620 nm to produce the compound solubility range. A compound is considered to have poor solubility if it is lower than 10 µg/mL, if it ranges between 10-60 µg/mL then is has moderate solubility. Good solubility criterion is > 60 µg/mL. The solubility ranges of all compounds are summarized in *Table 3.1* below.

*Table 3.1.: A summary of solubility ranges of **Dpa** ligand, its complexes (**C1**-**C12**) and the control drugs Reserpine and Hydrocortisone in PBS and HEPES buffer.*

Compound	Concentration			
	PBS		HEPES	
	µM	µg/mL	µM	µg/mL
Dpa	80-120	14-21	80-120	14-21
Reserpine	20-40	12-24	40-80	24-49
Hydrocortisone	>160	>60	>160	>60
C1	80-120	54-81	40-80	27-54
C2	40-80	24-47	40-80	24-47
C3	20-40	12-23	40-80	24-47
C4	40-80	31-62	40-80	31-62
C5	80-120	54-82	20-40	14-27
C6	40-80	27-54	10-20	7-14
C7	>160	95	>160	95
C8	>160	81	>160	82
C9	>160	81	>160	81
C10	>160	110	80-120	55-83
C11	>160	96	>160	96
C12	>160	95	>160	95

All the complexes demonstrated good aqueous solubility in DMSO up to a maximum concentration of 200 µM. **Dpa** was moderately soluble up to 80 µM in both buffer solutions. As expected, reserpine showed moderate solubility whereas hydrocortisone was highly soluble even at maximum concentration in solution in both PBS and HEPES (see *Figure 3.2* for demonstration in PBS).

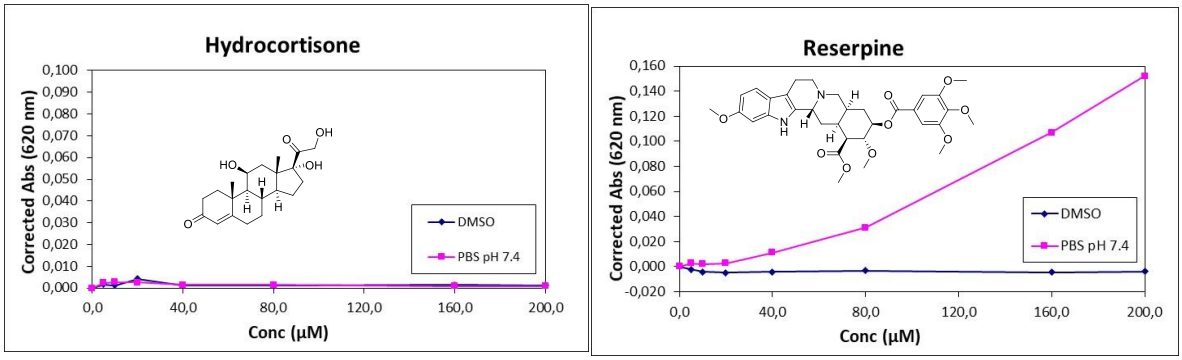

Figure 3.2.: Absorbance curve of hydrocortisone and reserpine in DMSO (blue) and in PBS buffer (pink).

Complexes with the PF_6^- counterion (**C1**-**C6**) presented varying solubility ranges. **C1** showed moderate solubility in the HEPES buffer and showed slightly higher solubility in the PBS buffer. The same phenomenon is seen for rhodium iodido complex, **C5**. The solubility range in both buffer solutions was observed to be indistinguishable for complexes **C4** and **C2** at 40-80 µM. Although displaying varying poor to moderate solubilities, ruthenium complexes **C3** and **C6** showed the least aqueous solubility in comparison to the iridium (**C1** and **C4**) and rhodium (**C2** and **C5**) complexes. The reason why the ruthenium complexes were less soluble is not immediately clear, however, it could be due to the para-cymene ligand. It could also be due to the strength of the interaction between the cation and the counterion, if the interaction is much stronger, it would be harder for the water molecule to solvate the ions causing it to go into solution. From these results, it shows that complexation improved the aqueous solubility of the ligand **dpa** except for complexes **C3** and **C6**. On the contrary, complexes with the NO_3^- counterion (**C7**-**C12**) shows significantly improved solubility in comparison to the PF_6^- complexes. Complexes **C7**-**C12** were soluble up to 200 µM with the exception of **C10** presenting moderate to good solubility in the HEPES buffer. There is no significant pattern observed for chlorido vs iodido complexes which have the same metal for **C1**-**C6**. Complex **C1**, which has a chlorido ligand displays better solubility compared to its iodido counterpart (**C4**) in PBS buffer. The rhodium (**C5**) and ruthenium (**C6**) iodido complexes exhibit better solubility than their chlorido analogues in PBS buffer. However, the opposite is observed in the HEPES buffer.

3.2.2. Hydrolysis studies

When a drug is administered a number of processes could occur that alters the structure of the compound. Metal complexes can undergo ionization (oxidation/ reduction of the ligand or complex), ring opening of metal chelates or a labile ligand such as a halide bound to the metal is displaced by a water molecule.[16] These interactions can either activate or deactivate a drug. For metallodrugs, the metal centre is susceptible to interaction with other molecules present in biological media such as water. Aqua complexes have been reported to be more reactive than their chlorido derivatives.[17] Additionally, this displacement of the chlorido atom by a water molecule serves as an activation step for some organometallic complexes aimed at the treatment of cancer.[18] Reaction of metal complexes with water is especially important since it has been reported that the aqua species is likely the dominant species in *in vitro* biological assays. The hydrolysis of organoiridium *C,N'* chelated complexes reported by Liu *et al*. was monitored by ^{1}H NMR and it was found that all the complexes underwent rapid hydrolysis (less than ~ 5 minutes).[19] This was important since the aqua adduct was found to be the active species. These complexes were then tested against A2780 human ovarian cancer cell line. Three of the complexes were found to show promising activity against the tested

strain, A2780.[19] In this case, the ability of the complexes to undergo hydrolysis plays a role in the bioavailability of the active species. A small library of four N, N chelating half sandwich organometallic complexes were reported by Soldevila-Barreda *et al*.[20] Stability of these complexes in aqueous medium was analysed with a hydrolysis study. Results obtained showed that hydrolysis of the metal-ligand bond occurs instantaneously. *In vitro* screening of the complexes against A2780 cancer cell line illustrated that these complexes were moderately active.[20] Thus, it is important to confirm whether complexes **C1**-**C12** readily react with water.

First, each complex was incubated in D_2O in the presence of $AgNO_3$ for 18 hours at 37°C (see *Scheme 3.1*). $AgNO_3$ is a known halide abstractor and was used to ensure that the aqua complex would be produced.

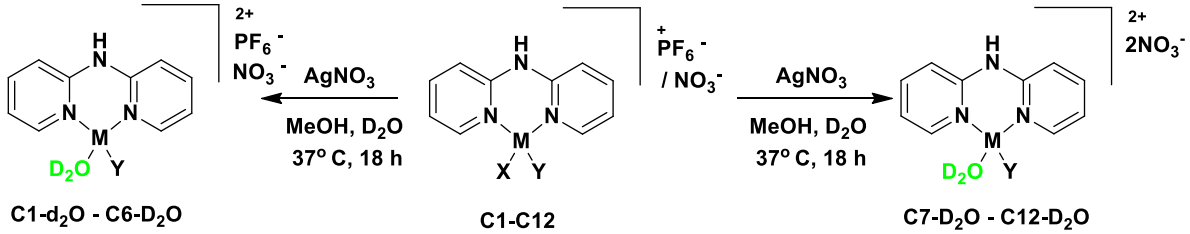

C1-D_2O: M = Ir, X = D_2O, Y = Cp* (PF_6)
C2-D_2O: M = Rh, X = D_2O, Y = Cp* (PF_6)
C3-D_2O: M = Ru, X = D_2O, Y = p-cymene (PF_6)
C4-D_2O: M = Ir, X = D_2O, Y = Cp* (PF_6)
C5-D_2O: M = Rh, X = D_2O, Y = Cp* (PF_6)
C6-D_2O: M = Ru, X = D_2O, Y = p-cymene (PF_6)

C7-D_2O: M = Ir, X = D_2O, Y = Cp* 2(NO_3)
C8-D_2O: M = Rh, X = D_2O, Y = Cp* 2(NO_3)
C9-D_2O: M = Ru, X = D_2O, Y = p-cymene2(NO_3)
C10-D_2O: M = Ir, X = D_2O, Y = Cp* 2(NO_3)
C11-D_2O: M = Rh, X = D_2O, Y = Cp* 2(NO_3)
C12-D_2O: M = Ru, X = D_2O, Y = p-cymene2(NO_3)

*Scheme 3.1: Synthesis of aqua species **C1-D_2O** – **C12-D_2O**.*

After 18 hours, each solution was filtered through celite, a drop or two of TMS (internal reference) was added and ^{1}H NMR analysis was done on the filtrate. The proton spectra obtained was presumed to be that of the aqua species **C1-D_2O** – **C12-D_2O** where the chlorido or iodido ligand is displaced and a D_2O molecule is subsequently bound to the metal. This zero-net charge of D_2O results in the metal centre being doubly charged with PF_6^- and NO_3^- as counterions for complexes **C1**-**C6** and two NO_3^- counterions for **C7**-**C12**. Secondly, each complex was then incubated in 75% D_2O/ 25% MeOD-d_4 (to solubilize less soluble complexes) at 37°C in the absence of $AgNO_3$. Solutions were then filtered through celite before a drop of TMS was added and ^{1}H NMR analysis was done on the filtrates. The spectra of the aqua species generated in the presence of $AgNO_3$ was compared to that of each complex incubated without $AgNO_3$ in order to examine whether the complexes readily undergo aquation.

According the ^{1}H spectra, iridium chlorido complex **C1** (see *Figure 3.3* below) does not undergo any aquation in a 75% D_2O/25% MeOD-d_4 solution after 18 hours of incubation. The generated aqua species, C1-H_2O (red) does not overlap with the incubated species in the absence of $AgNO_3$(blue). A shift of all pyridyl protons downfield for the incubated species without $AgNO_3$ is observed, this signifies successful generation of the aqua adduct by incubation with $AgNO_3$. The coordination of D_2O to the metal centre changes the chemical environment of the pyridyl protons making them less shielded due to the increased positive nature of the metal centre. However, this indicates that complex **C1** does not readily undergo hydrolysis in the absence of a halide abstractor. This is also observed for complexes **C5**, **C6**, **C7**, **C10** as well as **C11**.

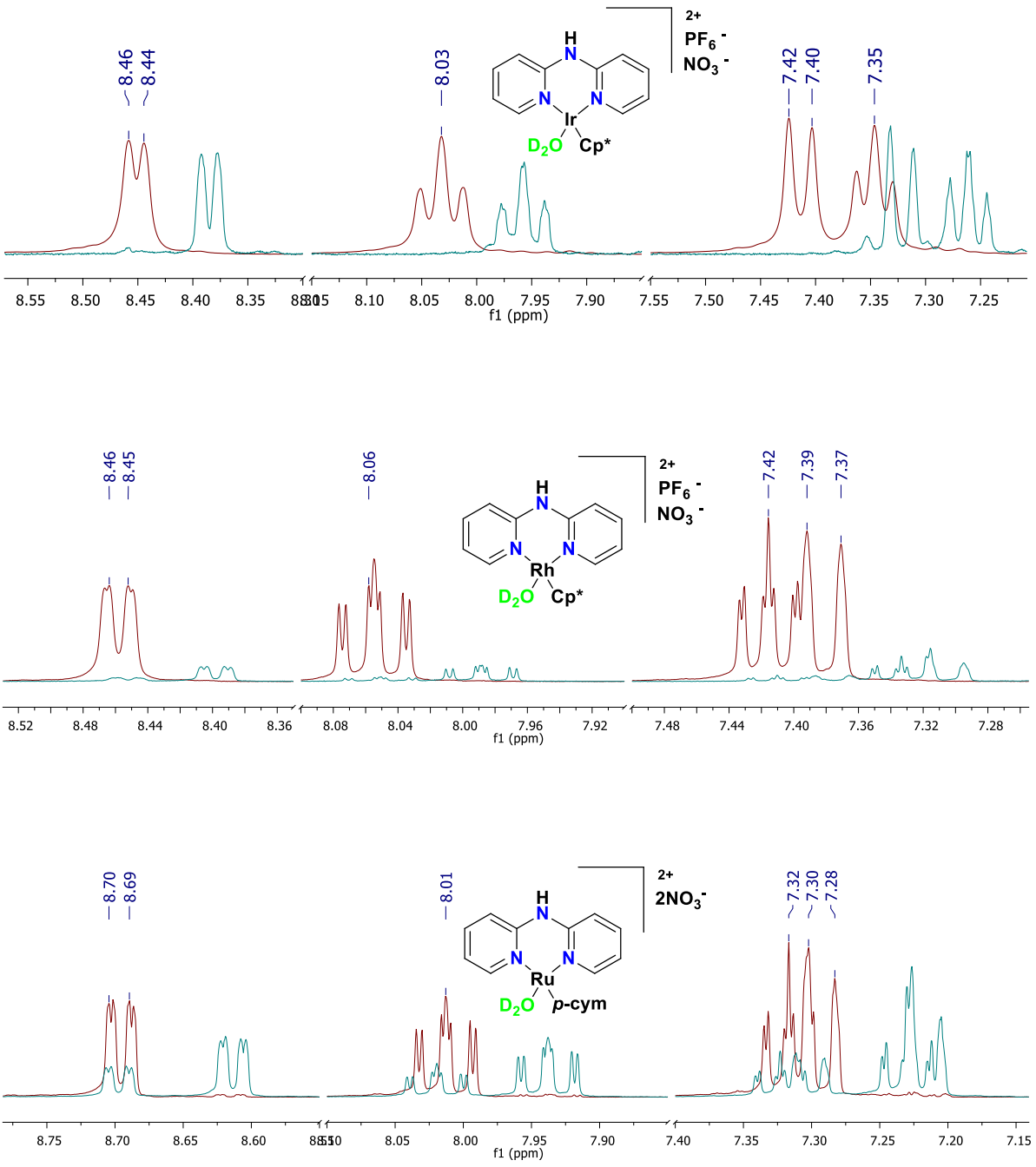

*Figure 3.3.: An overlap of the proton spectra (only pyridyl protons shown) of generated aqua species (red), i.e., complexes **C1-D₂O** (no hydrolysis), **C2-D₂O** (trace amounts of aqua species) and **C9-D₂O** (~30% hydrolyse species), and that of incubated organometallic without $AgNO_3$ (blue).*

Some aquation was observed for complexes **C2**, **C3**, **C8** and **C9**. This was confirmed by the set of peaks that occur at similar shifts to the generated aqua species in the NMR spectra. For **C2** and **C8**, only a small amount of the halogenido-complexes react with water. For **C3**, based on the peak intensity, there is a higher ratio of the aqua species **C3-D₂O** to chlorido complex at approximately 2.4: 1. Complex **C9,** on the other hand, displayed of the chlorido species in comparison to the aqua species with an approximated ratio of 1:1.5. Two sets of pyridyl protons attributed to two different species are observed for complex **C12**. The major species did not overlap with that of the aqua species suggesting that **C12** does not undergo hydrolysis to completion. A summary of the result obtained for the

hydrolysis of complexes **C1**-**C12** (*Table 3.2*) shows that the chlorido complexes undergo hydrolysis relatively faster than their iodido derivatives. A study of organoiridium complexes discussed above investigated the effect of exchanging a chloride ligand with pyridine on the rate of hydrolysis, in vitro activity as well as reactivity.[17] The rapidly hydrolysable iridium chloride complex was evaluated against a pyridine derivative and it was found that pyridine complex does not undergo hydrolysis. This was attributed to the pyridine blocking the site required by the water molecule to bind. It was concluded that the type of ligand sets binding to iridium will determine its reactivity. With an ionic radius of 0.181 nm, chlorine is relatively smaller than iodine that has an ionic radius of 0.220 nm. This leads to an increase in the nephelauxetic effect, therefore, a greater electron cloud expansion of the metal onto the iodide ligand occurs. As a result, the bond between the metal and iodide ligand is more covalent, whereas that of the metal and chlorine is more ionic. In this way, iodine may be blocking aquation of the metals.

Table 3.2.: Summary of Cl and I complexes that underwent aquation vs. those that did not.

	NO aquation		Aquation	
	Cl	**I**	**Cl**	**I**
PF_6		**C1**	**C2**	
		C5	**C3**	
		C6		
NO_3	**C7**	**C10**	**C8**	**C12**
		C11	**C9**	

From the results shown above, all but one iodido complex, **C12**, did not undergo aquation. Additionally, **C7**, was the only chloride ligand bearing complex that did not generate an aqua species in the absence of $AgNO_3$. Complexes **C2, C3, C8, C9** and **C12** appear to hydrolyse in the presence of deuterium oxide over a period of 18 hours. Since bioassays normally conduct drugs testing in aqueous medium, it is possible that the active species of these complexes is the aqua complex.

3.2.3. Antiplasmodial activity against *P. falciparum*

The *in vitro* biological antimalarial activity of **Dpa** and complexes **C1**-**C6** was evaluated against 3D7 CQ-sensitive strain of *P. falciparum* parasite at Griffith University in the research group of Prof. Vicky Avery. Evaluation of the complexes **C7**-**C12** was not done due to time constraints.

The antimalarial activity of known antimalarials, i.e., artesunate, chloroquine and pyrimethamine, were also analysed (see *figure 3.3*) as reference standards. It was found that **Dpa** was not active, however, complexes **C1**-**C6** showed some activity. The rhodium-chlorido complex **C2** (IC_{50} = 4.72 μM) showed the best activity relative to the other complexes whereas iridium-chlorido complex **C1** (IC_{50} = 8.93 μM) showed the least activity.

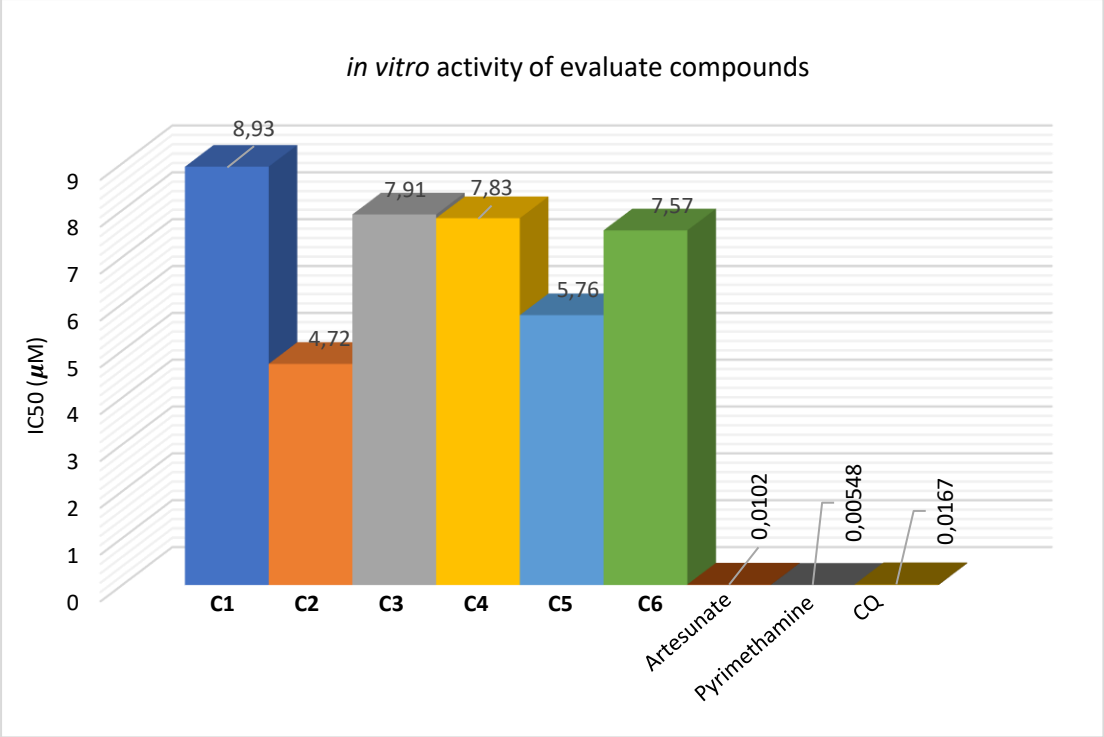

Figure 3.4.: Preliminary *in vitro biological activity results of ligand* ***Dpa****, complexes* ***C1****-****C6*** *and other known antimalarials against 3D7 P. falciparum* strain.

The iridium-iodido, derivative **C4** (IC_{50} = 7.83 μM), was more active than its chlorido derivative. This is also observed for the ruthenium complexes **C3** (IC_{50} = 7.91 μM) and **C6** (IC_{50} = 7.57 μM). For rhodium complexes **C2** and **C5**, the chlorido derivative (**C2)** showed higher activity. This is postulated to be attributed to the complexes' solubility in aqueous medium shown in *table 3.1* since *in vitro* testing takes place in aqueous based medium. Romero-Canelón *et al.* conducted a study of the activity of iodido versus chlorido ruthenium and osmium complexes. The study showed that the iodido complexes exhibited better antiproliferative activity compared to the chlorido analogues.[21] This difference in activity was attributed to charge distribution of the complexes. A comparison of the electrostatic potential surfaces of the chlorido and iodido complex highlights that the iodine ligand is more positively charged resulting in higher potency. The same can be proposed for the greater activity observed for the iodide complexes of iridium and ruthenium. In the parasite assay preparation, a 25 mM solution of HEPES was used in the culture medium for the *P. falciparum* 3D7 strains. From the results of aqueous solubility of complexes in HEPES buffer, **C4** (31-62 μg/mL) is slightly more soluble than **C1** (24-47 μg/mL). This could mean that a higher concentration of **C4** is still in solution than that of **C1** after 72 hours of incubation which might result in more of **C4** being transported into the parasite resulting in the complex having better activity. This rationalization can be used for the rhodium complexes as well, **C2** (24-47 μg/mL) is slightly more soluble than **C5** (14-27 μg/mL) resulting in better activity to some extent. Furthermore, the lower solubility of **C6** (7-14 μg/mL) compared to that of **C3** (24-47 μg/mL) is compromising to its activity. In comparison to known antimalarials (IC_{50} = 0.00548-0.0167 μM), these complexes did not show good activity. Incorporation of the metals to the organic scaffold, **Dpa**, certainly improved its activity against 3D7 CQ-sensitive strains. The antiproliferative activity of the complexes showed that rhodium (**C2** and **C5**) was the most active, followed by ruthenium (**C6** and **C4**), and lastly, the least active, the iridium complexes (**C4** and **C1**).

We were also able to carry out antiplasmodial testing for **Dpa** ligand, complexes (**C1**-**C6**) and dimers ($[Ir(Cp^*)Cl_2]_2$, $[Ir(Cp^*)I_2]_2$, $[Rh(Cp^*)Cl_2]_2$, $[Rh(Cp^*)I_2]_2$, $[Ru(p\text{-cymene})Cl_2]_2$ and $[Ru(p\text{-cymene})I_2]_2$) was done against the drug sensitive strain of *P. falciparum*, NF54, in the lab of Prof. Lubbe Wiesner at the University of Cape Town. The known antimalarials, CQ and artesunate were also screened as reference standards. Both a two- and a three- day assay was conducted in order to observe whether the incubation period would alter the compounds efficacy. A summary of the mean (two tests) IC_{50} values and their standard deviations were summarized on *table 3.3* below.

*Table 3.3.: Mean antiplasmodial activity of tested dimers, complexes (**C1**-**C6**) and known antimalarials CQ and artesunate against NF54, a drug sensitive strain of Plasmodium falciparum.*

Sample	Mean IC_{50} (ng/mL)	Standard Deviation (ng/mL)	Mean IC_{50} (ng/mL)	Standard Deviation (ng/mL)
Dpa	>5000	NA	>5000	NA
C1	>5000	NA	>5000	NA
C2	>5000	NA	>5000	NA
C3	>5000	NA	>5000	NA
C4	>5000	NA	>5000	NA
C5	>5000	NA	>5000	NA
C6	>5000	NA	>5000	NA
$[Ir(Cp^*)Cl_2]_2$	4802.7	160.1	>5000	NA
$[Ir(Cp^*)I_2]_2$	>5000	NA	>5000	NA
$[Rh(Cp^*)Cl_2]_2$	4955.7	25.1	>5000	NA
$[Rh(Cp^*)I_2]_2$	>5000	NA	>5000	NA
$[Ru(p\text{-cymene})Cl_2]_2$	>5000	NA	>5000	NA
$[Ru(p\text{-cymene})I_2]_2$	>5000	NA	>5000	NA
Chloroquine	8.1	3.3	4.9	0.0
Artesunate	2.9	1.4	4.1	0.6

Following two- and three-day incubation, none of the complexes showed any activity at a concentration range of 5.00 – 0.31 µg/ mL. Subsequent to the two-day incubation, dimers $[Ir(Cp^*)Cl_2]_2$ and $[Rh(Cp^*)Cl_2]_2$ displayed weak antiplasmodial activity with IC_{50} values of 4802.7 ± 160.1 ng/mL and 4955.7 ± 25.1 ng/mL respectively (see *table 3.3*). This activity was not observed after the three-day incubation. The reference standards, CQ and artesunate, displayed very good activity. Complexes displayed weak activities against the NF54 strain above. This may be due to the fact that the growth media was supplemented with hypoxanthine which could counter the compounds' MOA resulting in a lag time, thus, activity may only appear after longer periods of incubation (over 3 days). This was also observed for known active antimalarial drugs pyrimethamine, sulfadiazine and sulfadoxine which were tested in the same assay, the complexes showed no activity. Additionally, complexes **C1**-**C6** have a high molecular weight, thus their molar concentration at 5μg/mL is much lower than an organic molecule with a lower molecular weight. For this reason, the complexes may show no activity.

3.3. Summary

The solubility of complexes **C1**-**C12** in aqueous media was carried out with the use of a high-throughput kinetic assay. It was found that PF_6^- complexes (**C1**-**C6**) had different solubilities ranging from poor to good solubility whereas the NO_3^- complexes (**C7**-**C12**) had good solubility in both buffer solutions, generally better than the PF_6^- derivatives. Aquation studies of the complexes revealed that all but one of the chlorido complexes (**C7**) and one iodido complexes (**C12**) underwent aquation. The preliminary *in vitro* antiplasmodial activity of complexes **C1**-**C6** against the 3D7 *P. falciparum* strain showed that complex activity may be relative to the complexes' solubility in HEPES buffer. Evaluation of the complexes against NF54 *P. falciparum* strain of malaria showed to be inactive following a two- and three- day assay. Further testing up to a higher mass concentration of 20 ug/mL for complexes oh higher molecular weight may yield better IC_{50} values since their molar concentration would be higher at a higher mass concentration. Due to time constraints, the NO_3^- complexes were not screened for antiplasmodial activity. This will be pursued as part of our future work to determine if the difference in counter ion will influence bioactivity.

3.4. Experimental Section

3.4.1. Materials

Chemicals and reagents: Phosphate Buffered Saline (0.01 M in 200 mL distilled water), N-(2-Hydroxyethyl)piperazine-N'-(2-ethanesulfonic acid) (1.191 g, 5.0 mmol), reserpine, hydrocortisone, silver nitrate were obtained from Sigma Aldrich (Merck). Deuterium oxide-d2 solvent was purchased from Sigma. Deuterated methanol solvent was from purchased from Sigma.

Instrumentation:

^{1}H NMR was recorded on a 400 MHz Varian Unity Inova spectrometer.

3.4.2. Turbidimetric Assay

A 0.01 M pH 7.4 Phosphate Buffered Saline (PBS) solution was prepared by dissolving one PBS tablet, in 200 mL distilled water at 25 °C in order to yield a buffered solution containing 0.01 M phosphate buffer, 0.003 M KCl and 0.14 M NaCl. The solution was allowed to equilibrate at 25 °C for one hour upon which the pH was confirmed with a pH meter. The solution was then filtered through a 0.45 µM Nylon syringe filter in order to remove any undissolved particulates. A N-(2-Hydroxyethyl)piperazine-N'-(2-ethanesulfonic acid) (HEPES) buffer solution was prepared. This was done by dissolving 1.191 g of HEPES free acid in 180 ml of distilled H_2O. A 0.1M solution of NaOH was added in 1mL equivalents until the pH was adjusted to 7. The solution was then made up to 200 mL with distilled H_2O. A 10 mM stock solution in DMSO of each test compound was prepared and filtered through a 0.45 µM PVDF syringe filter prior to use. A preparation plate (96-well flat bottomed) was prepared by serially diluting each compound in order to achieve the desired concentrations (5.0 µM to 200 µM). The test plate was prepared by pipetting 196 µL DMSO into wells 1 – 6 and 196 µL PBS/ HEPES into wells 7 – 12. Each compound was tested in triplicate thus a single plate was used to evaluate two compounds. 4 µL of each compound (**Dpa** and **C1**-**C12**) concentration was pipetted from the preparation plate into the test plate in order to bring the total volume up to 200 µL and to ensure that a 2 % (v/v) DMSO/PBS and 2 % (v/v) DMSO/HEPES solution is achieved. Test plates were prepared in duplicate and the plates were incubated at room temperature (25 °C). The test plates were incubated for 2 hours upon which the UV-Vis absorbance readings were measured at 620 nm. The corrected absorbance readings were obtained by subtracting the blank readings from each concentration absorbance.

3.4.3. Generation of the aqua species (C1-D_2O – C12-D_2O)

Each complex with an equimolar quantity of $AgNO_3$ in deuterium oxide (750 μL) was incubated for 18 hours at 37 °C. The solution was then filtered through celite and a drop or two of TMS was added to the filtrate as an internal reference analysed with ^{1}H NMR.

3.4.4. Reaction of complexes with water

Each complex in a 75% D_2O (750 μL)/ 25% MeOD-d4 (250 μL) mixture was incubated for 18 hours at 37 °C in the absence of $AgNO_3$. The solution was filtered through celite and a drop or two of TMS was added as an internal reference analysed with ^{1}H NMR 3.4.3. was compared with that of the generated aqua species (3.4.2.).

3.4.5. Evaluation of *in vitro* activity against 3D7 *P. falciparum* strain

Compounds were solubilized in DMSO to a final concentration of 5 mM. The stock solutions of compounds were then diluted further in DMSO to generate 3 doses per log dose response dilutions within 384-well polypropylene compound storage plates. The dose response dilution plates were then diluted 1 µL into 25 µL of sterile water and 5 µL transferred into 384-well imaging plates. The confocal image analysis assay is published in detail elsewhere. In brief, the *P. falciparum* 3D7 strain was kept in continuous culture (RPMI supplemented with, 25 mM Hepes, 50 µg/mL hypoxanthine, 2.5 mg/mL Albumax II® plus 5% human serum) with sorbitol synchronization performed over two successive intra erythrocytic lifecycles to provide ring-stage parasites for use within the assays. On the day of assay, ring-stage parasite culture was adjusted to 2% parasitemia and 0.3% hematocrit and 45 µL of which was added to the compound-containing imaging plates. The assay plates were incubated for 72 h at 5% O_2, 5% CO_2 and 90% N_2. The plates were removed from incubation and allowed to equilibrate at room temperature prior to staining with 4',6-diamidino-2-phenylindole (DAPI). The imaging assay plates were then imaged on an Opera confocal imaging system. Using Accapella scripting software, the number of classified parasites was determined for each assay well. Percent inhibition of parasite proliferation was calculated and normalized to assay control data of 0.4% DMSO and 5 µM Puromycin. Percent inhibition of parasite numbers (normalized to 5 µM puromycin) was plotted against log concentration of the compounds using a 4 parameter log dose, non-linear regression analysis, with sigmoidal dose response (variable slope) curve fit using Prizm 4.0. No constraints were placed on the top, bottom or Hill slope of the curve fit in the graphing software.

3.4.6. Antiplasmodial activity against NF54 *P. falciparum* strain

Antiplasmodial testing was done against the drug sensitive strain of *P. falciparum*, NF54, obtained from the Malaria Research and Reference Reagent Resource (MR4) depository[22]. *P. falciparum* was continuously cultured at 37°C in human O-positive erythrocytes using a modified version of the method described by Trager and Jensen[23]. Culture medium was composed of 10.4 g/L RPMI 1640 (with glutamine and without $NaHC0_3$), 4 g/L glucose, 6 g/L Hepes buffer, 0.088 g/L hypoxanthine, 5 g/L albumax, and 102 ml/L (0.05 g/L) gentamicin (Sigma-Aldrich, Johannesburg, South Africa). Human blood, donated by anonymous donors, was obtained from the Western Cape Blood Service (Cape Town, South Africa) The half-maximal inhibitory concentration (IC_{50}) of each sample was determined using a modified version of the parasite lactate dehydrogenase (pLDH) assay described by [24]. The assay was performed in duplicate with a 5 point dose-response curve (1/2 serial dilutions) at a concentration range of 5.00 – 0.31 µg/mL. The data were analysed by nonlinear regression analysis using the GraphPad PRISM version 4.00 program to determine the IC_{50} of each compound. Chloroquine and artesunate (Sigma-Aldrich, Johannesburg, South Africa) were used as reference standards. Two- day assays were incubated for 48 hours at 37°C using a culture predominantly in the mature trophozoite

stage. Three- day assays were incubated for 72 hours at 37°C using a culture predominantly in the immature trophozoite (ring) stage.

3.5. References:

(1) Marcelino, P. R. F.; Moreira, M. B.; Lacerda, T. M.; da Silva, S. S. Metal-Based Drugs for Treatment of Malaria. In *Biomedical Applications of Metals*; Rai, Mahendra, Ingle, Avinash, Medici, S. (Eds. ., Ed.; Springer, Cham, **2018**; pp 167–193. https://doi.org/10.1007/978-3-319-74814-6_8.

(2) Nkoana, W.; Nyoni, D.; Chellan, P.; Stringer, T.; Taylor, D.; Smith, P. J.; Hutton, A. T.; Smith, G. S. Heterometallic Half-Sandwich Complexes Containing a Ferrocenyl Motif : Synthesis , Molecular Structure , Electrochemistry and Antiplasmodial Evaluation. *J. Organomet. Chem.* **2014**, *752*, 67–75. https://doi.org/10.1016/j.jorganchem.2013.11.025.

(3) Štarha, P.; Zdeněk, D.; Zdeněk, T. Half-Sandwich Ir(III) and Rh(III) 2,2'-Dipyridylamine Complexes: Synthesis, Characterization and in Vitro Cytotoxicity against the Ovarian Carcinoma Cells. *J. Organomet. Chem.* **2018**, *872*, 114–122. https://doi.org/10.1016/j.jorganchem.2018.07.035.

(4) Štarha, P.; Zdeněk, D.; Zdeněk, T. Half-Sandwich Ru(II) Halogenido, Valproato and 4-Phenylbutyrato Complexes Containing 2,2 -Dipyridylamine: Synthesis, Characterization, Solution Chemistry and In Vitro Cytotoxicity. *molecules* **2016**, *21* (12), 1725. https://doi.org/10.3390/molecules21121725.

(5) Almodares, Z.; Lucas, S. J.; Crossley, B. D.; Basri, A. M.; Pask, C. M.; Hebden, A. J.; Phillips, R. M.; McGowan, P. C. Rhodium, Iridium, and Ruthenium Half-Sandwich Picolinamide Complexes as Anticancer Agents. *Inorg. Chem.* **2014**, *53* (2), 727–736. https://doi.org/10.1021/ic401529u.

(6) Gupta, D.; Bhatia, D.; Dave, V.; Sutariya, V.; Gupta, S. V. Salts of Therapeutic Agents: Chemical, Physicochemical, and Biological Considerations. *Molecules* **2018**, *23* (7), 1–15. https://doi.org/10.3390/molecules23071719.

(7) Drews, J. Drug Discovery: A Historical Perspective. *Science (80-.).* **2000**, *287* (5460), 1960–1964. https://doi.org/10.1126/science.287.5460.1960.

(8) D.H. Barich, M.T. Zell, E. J. M. *Physicochemical Prop Erti Es, Formulation, and Drug Delivery*; **2016**. https://doi.org/10.1002/9781118833322.

(9) Schneider, G. Automating Drug Discovery. *Nat. Rev. Drug Discov.* **2018**, *17* (2), 97–113. https://doi.org/10.1038/nrd.2017.232.

(10) Alsenz, J.; Kansy, M. High Throughput Solubility Measurement in Drug Discovery and Development. *Adv. Drug Deliv. Rev.* **2007**, *59* (7), 546–567. https://doi.org/10.1016/j.addr.2007.05.007.

(11) Psimadas, D.; Georgoulias, P.; Valotassiou, V.; Loudos, G. Molecular Nanomedicine Towards Cancer : *J. Pharm. Sci.* **2012**, *101* (7), 2271–2280. https://doi.org/10.1002/jps.

(12) Kerns, E.; Di, L.; Carter, G. In Vitro Solubility Assays in Drug Discovery. *Curr. Drug Metab.* **2008**, *9* (9), 879–885. https://doi.org/10.2174/138920008786485100.

(13) Williams, H. D.; Trevaskis, N. L.; Charman, S. A.; Shanker, R. M.; Charman, W. N.; Pouton, C. W.; Porter, C. J. H. Strategies to Address Low Drug Solubility in DiscWILLIAMS, Hywel D.;

TREVASKIS, Natalie L.; CHARMAN, Susan A.; et Al. Strategies to Address Low Drug Solubility in Discovery and Development. Pharmacological Reviews, v. 65, n. 1, p. 315–499, 2013.Overy And. In *Pharmacological Reviews*; **2013**; Vol. 65, pp 315–499.

(14) Sugano, K.; Okazaki, A.; Sugimoto, S.; Tavornvipas, S.; Omura, A.; Mano, T. Solubility and Dissolution Profile Assessment in Drug Discovery. *Drug Metab. Pharmacokinet.* **2007**, *22* (4), 225–254. https://doi.org/10.2133/dmpk.22.225.

(15) Lin, B.; Pease, J. H. A High Throughput Solubility Assay for Drug Discovery Using Microscale Shake-Flask and Rapid UHPLC-UV-CLND Quantification. *J. Pharm. Biomed. Anal.* **2016**, *122*, 126–140. https://doi.org/10.1016/j.jpba.2016.01.022.

(16) Anthony, E. J.; Bolitho, E. M.; Bridgewater, H. E.; Carter, O. W. L.; Donnelly, J. M.; Imberti, C.; Lant, E. C.; Lermyte, F.; Needham, R. J.; Palau, M.; Sadler, P. J.; Shi, H.; Wang, F. X.; Zhang, W. Y.; Zhang, Z. Metallodrugs Are Unique: Opportunities and Challenges of Discovery and Development. *Chem. Sci.* **2020**, *11* (48), 12888–12917. https://doi.org/10.1039/d0sc04082g.

(17) Liu, Z.; Sadler, P. J. Organoiridium Complexes: Anticancer Agents and Catalysts. *Acc. Chem. Res.* **2014**, *47* (4), 1174–1185. https://doi.org/10.1021/ar400266c.

(18) Liu, Z.; Habtemariam, A.; Pizarro, A. M.; Fletcher, S. A.; Kisova, A.; Vrana, O.; Salassa, L.; Bruijnincx, P. C. A.; Clarkson, G. J.; Brabec, V.; Sadler, P. J. Organometallic Half-Sandwich Iridium Anticancer Complexes. *J. Med. Chem.* **2011**, *54* (8), 3011–3026. https://doi.org/10.1021/jm2000932.

(19) Liu, Z.; Habtemariam, A.; Pizarro, A. M.; Clarkson, G. J.; Sadler, P. J. Organometallic Iridium(III) Cyclopentadienyl Anticancer Complexes Containing C,N-Chelating Ligands. *Organometallics* **2011**, *30* (17), 4702–4710. https://doi.org/10.1021/om2005468.

(20) Soldevila-Barreda, J. J.; Fawibe, K. B.; Azmanova, M.; Rafols, L.; Pitto-Barry, A.; Eke, U. B.; Barry, N. P. E. Synthesis, Characterisation and in Vitro Anticancer Activity of Catalytically Active Indole-Based Half-Sandwich Complexes. *Molecules* **2020**, *25* (19). https://doi.org/10.3390/molecules25194540.

(21) Romero-Canelón, I.; Salassa, L.; Sadler, P. J. The Contrasting Activity of Iodido versus Chlorido Ruthenium and Osmium Arene Azo- and Imino-Pyridine Anticancer Complexes: Control of Cell Selectivity, Cross-Resistance, P53 Dependence, and Apoptosis Pathway. *J. Med. Chem.* **2013**, *56* (3), 1291–1300. https://doi.org/10.1021/jm3017442.

(22) Trager, W.; Jensen, J. B. Human Malaria Parasites in Continuous Culture. *J. Parasitol.* **2005**, *91* (3), 484–486. https://doi.org/10.1645/0022-3395(2005)091[0484:HMPICC]2.0.CO;2.

(23) Makler, M. T.; Ries, J. M.; Williams, J. A.; Bancroft, J. E.; Piper, R. C.; Gibbins, B. L.; Hinrichs, D. J. Parasite Lactate Dehydrogenase as an Assay for Plasmodium Falciparum Drug Sensitivity. *Am. J. Trop. Med. Hyg.* **1993**, *48* (6), 739–741. https://doi.org/10.4269/ajtmh.1993.48.739.

Chapter 4

Conclusions and future work

4.1. Conclusions

Six different metal chlorido- and iodido-bridged dimers, $[Ir(Cp^*)Cl_2]_2$, $[Ir(Cp^*)I_2]_2$, $[Rh(Cp^*)Cl_2]_2$, $[Rh(Cp^*)I_2]_2$, $[Ru(p\text{-cymene})Cl_2]_2$ and $[Ru(p\text{-cymene})I_2]_2$, were synthesized using reported methods.[1,2] A total of 12 cationic *N,N'*-chelated half-sandwich organometallic complexes (**C1**-**C12**) containing the **Dpa** ligand were then synthesized successfully using an adapted method from Starha *et al*.[3] where **C1**-**C6** contain the PF_6^- counterion and **C7**-**C12** contain the NO_3^- counterion. The complexes (**C1**-**C6**)[3,4] have been previously synthesized but was not studied as antiplasmodials previously. Characterisation was done successfully using the analytical techniques, FT-IR, ^1H and ^{13}C NMR, XRD, HPLC, CV and mass spectrometry. Analysis of the complexes with FTIR showed a shift in the C=N stretching frequencies as a result of the coordinated metal pulling away electron density. In addition, the characteristic P-F stretch (823-834 cm^{-1}) for complexes **C1**-**C6** and the NO_3^- symmetric (1299-1317 cm^{-1}) and asymmetric (764-771 cm^{-1}) stretching bands for **C7**-**C12** were observed. Analysis of complexes **C7**-**C12** by ^1H NMR accounted for all the protons. Due to symmetry of the dipyridylamine ligand, each peak in the aromatic region resonated for two chemically equivalent protons. A general downfield shift of three pyridyl peaks, integrated for six protons, after metalation was observed upon comparison to **Dpa** attributed to incorporation of the metal to the ligand. The presence of the *p*- cymene and Cp* moiety was also detected. Analysis of novel complexes **C7**-**C12** by ^{13}C NMR accounted for all carbon atoms. The least shielded carbons in the aromatic region were the amine carbons C_6 and C_8. Mass spectrometry results of the NO_3^- complexes displayed the $[M]^+$ in positive ESI mode. HPLC purity analysis on all complexes confirmed good purity in the range 95-99%. Single crystal structures of complexes (**C1, C2, C7,** and **C9**) were solved using single crystal X-ray diffraction, substantiating the isolation of the desired *N,N'* complexes. Complexes adopted pseudo-octahedral piano-stool geometry, a well-known geometry for half-sandwich organometallic complexes. Bond angles and bond lengths calculated were in agreement with similar complexes that have been reported. The electrochemistry of complexes **C1**-**C6** was studied by the use of the cyclic voltammetry technique. The obtained voltammogram of **Dpa** ligand showed that it was redox active but did not undergo any redox reactions. An oxidation reaction was observed for each complex. The iridium (**C1** and **C4**) and rhodium complexes (**C2** and **C5)** went from oxidation state of (III) to (IV). The ruthenium(II) complexes C3 and C6 also underwent an oxidation to Ru(III). Reductions observed could be attributed to the halogenido ligands being cleaved off.

The kinetic solubility and hydrolysis studies of the complexes were investigated. This involved determining the aqueous solubility of all complexes and ligand in two different buffers, i.e., PBS and HEPES, where one buffer mimics physiological conditions of the host (body) and the other is used in *in vitro* assays, respectively. A highly soluble compound, hydrocortisone and low soluble compound reserpine were used as positive and negative controls, respectively. A high throughput *in vitro* kinetic assay was done on all the complexes and **Dpa** ligand. Form the assay results, it was found that the PF_6 complexes, **C1**-**C6**, had a different range of solubilities from poor solubility to good solubility in both buffers. The NO_3^- complexes on the other hand had good solubility in both buffer solutions with the exception of complex **C10**, it exhibited moderate to good solubility in the HEPES buffer. A study on whether complexes will readily hydrolyse in aqueous based medium was done. This involved generation an aqua species by incubating each complex with equimolar quantity of $AgNO_3$ in D_2O for 18 hours at 37 °C. The ^1H NMR spectra of this generated aqua species was then compared to that the incubated species in 75% D_2O (750 μL)/ 25% MeOD-d4 (250 μL) without $AgNO_3$. Results obtained

showed that aquation studies of the complexes resulted in only one iodide complex **C12** undergoing aquation. The ability of the chlorido complexes **C2, C3, C8, C9** and **C12** to hydrolyse over the iodine complexes **C1, C5, C6, C10** and **C11** can be attributed to the relatively larger ionic radii of iodine which may block/ prevent hydrolysis from occurring due to an increase in the nephelauxetic effect. A greater electron cloud expansion of the metal onto the iodide ligand makes the bond between the metal and iodide ligand more covalent, whereas that of the metal and chlorine is more ionic. All but one chloride complex (**C7**) underwent aquation. Although aquation occurred, complexes that did display the ability to hydrolyse in solution, did not do so to completion, only a fraction of the complexes hydrolysed according to the peak intensities of the aqua species observed.

A study on the *in vitro* biological activity of complexes **C1**-**C6** against 3D7 and NF54 *P. falciparum* strains was conducted. The antimalarial activity of complexes **C7**-**C12** could not be obtained due to time constraints. When the complexes were tested against the CQ sensitive strain, 3D7, it was found that the ligand was inactive whereas the complexes did show some activity, however, the activity was not great. Complexes showed activity in the order **C2** > **C5** > **C6** > **C4** > **C3** > **C1**. Rhodium complexes **C2** and **C5** showed the best activity in relation to the other complexes. Iridium complexes showing the least activity with **C4** showing slightly less activity than ruthenium complex **C3**. A comparison of each chlorido derivative to its iodido analogue showed that the activity could be correlated with the complexes' solubility in HEPES buffer since the evaluation assay involves the use of it. It was established that for relatively more soluble complexes in HEPES, the better activity will be exhibited by the drug. This is by reason of concentration of complex available in solution to provide efficacy. The more soluble complexes **C4**, **C2** and **C6** showed better activity than their chlorido/ iodido derivative. Incorporation of the metals into the organic scaffold did show improved activity. Evaluation of complexes **C1**-**C6** against drug sensitive NF54 *P. falciparum* strain of malaria showed them to be inactive following a two- and three- day assay. It was concluded that this inactivity was attributed to the use of hypoxanthine in the growth media which offset the complexes' moa resulting in a lag time. Perhaps if an assay longer than a three- day assay was utilized; some activity of these complexes would have been observed. Complexes **C1**-**C6** may show activity at high mass concentration tested since they have high molecular weights, their molar concentration at 5 μg/mL is much lower than an organic molecule with a lower molecular weight.

4.2. Future work:

Crystals of complexes **C8**, **C10**, **C11** and **C12** could be grown and their crystal structures solved. With the use of single crystal X-ray diffraction, we are able to confirm that proposed the structures of the complexes were synthesized successfully, coordinating through the nitrogens of the pyridine rings and having the correct counterion. In terms of the DMSO interaction studies, the minimum number of equivalents required for the complete displacement of all chlorido or iodido ligands for DMSO needs to be investigated further for all complexes. This can be done by preparing a 1mM stock solution of each complex in dichloromethane (DCM) and a 4mM stock solution of DMSO could be added in small increments until the reaction reaches its endpoint. After each addition, the ^{1}H NMR spectrum of the sample would then be recorded. In this way, the NMR spectra could be monitored for any changes in order to determine whether any interaction does occur between each complex and DMSO. If the complex is found to interact with DMSO, the number of equivalents of DMSO required for the reaction to reach its endpoint could be determined. Other counterions could be investigated for this series of complexes in order to see what effect it will have on physicochemical properties, activity as well as cytotoxicity of the complexes. The electrochemistry of nitrate complexes **C7**-C**12** ned to be investigate using cyclic voltammetry.

The *in vitro* biological activity of **C7**-**C12** against 3D7 *P. falciparum* strains needs to be evaluated in order to assess the effect of counterion exchange on the activity. It will also be interesting to see these compounds activity as they exhibit far better solubility in aqueous based medium. Testing against the NF54 malaria strains could be repeated for complexes **C1**-**C6** (i) for an extended duration to account for the lag time, (ii) at higher concentrations (iii) hypoxanthine not to be used in the growth medium. This would have to be done for the nitrate counterion complexes (**C7**-**C12**) as well. *In vitro* cytotoxicity of known complexes **C1**-**C6** was only reported to have been performed against human ovarian carcinoma cell line, A2780, by Starha[3,4] and not against healthy cell lines. Cytotoxicity testing against healthy cell lines would have to be carried out for known complexes as well as novel complexes **C7**-**C12**.

Furthermore, more structure activity studies could be done. This could involve the synthesis of *C,N* half-sandwich organometallic complexes of ligand N-phenyl-2-pyridinamine (*Scheme 4.1* below) in an attempt to improve the therapeutic efficacy of the complexes. Modification of the ligand from *N'N* to *C'N* has been reported to improve *in vitro* anticancer activity.[5]

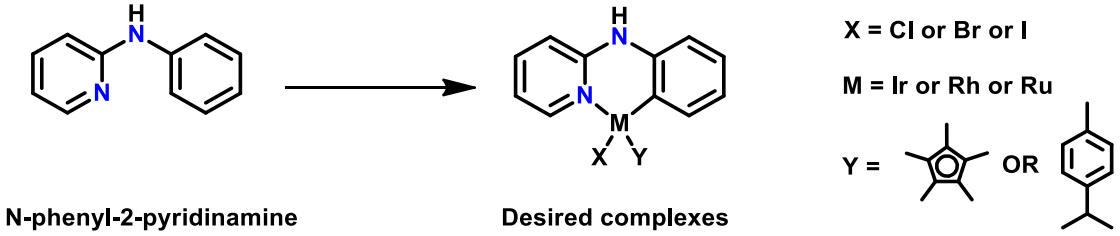

Scheme 4.3: Reaction scheme for the synthesis of N-phenyl-2-pyridinamine complexes.

4.3. References:

(1) Tönnemann, J.; Risse, J.; Grote, Z.; Scopelliti, R.; Severin, K. Efficient and Rapid Synthesis of Chlorido-Bridged Half- Sandwich Complexes of Ruthenium , Rhodium , and Iridium by Microwave Heating. *Eur. J. Inorg. Chem.* **2013**, *2013* (24), 4558–4562. https://doi.org/10.1002/ejic.201300600.

(2) Fields, A. E.; Zurwell, D.; Padgett, C. W.; Quillian, B. Bis(Pyrazolyl)Acetate and Bis(3,5-Dimethylpyrazolyl)Acetate Tris-Acetonitrile Ruthenium(II) Complexes: Synthesis, Properties, and Structure. *J. Organomet. Chem.* **2017**, *846*, 66–73. https://doi.org/10.1016/j.jorganchem.2017.05.060.

(3) Štarha, P.; Zdeněk, D.; Zdeněk, T. Half-Sandwich Ru(II) Halogenido, Valproato and 4-Phenylbutyrato Complexes Containing 2,2 -Dipyridylamine: Synthesis, Characterization, Solution Chemistry and In Vitro Cytotoxicity. *molecules* **2016**, *21* (12), 1725. https://doi.org/10.3390/molecules21121725.

(4) Štarha, P.; Zdeněk, D.; Zdeněk, T. Half-Sandwich Ir(III) and Rh(III) 2,2'-Dipyridylamine Complexes: Synthesis, Characterization and in Vitro Cytotoxicity against the Ovarian Carcinoma Cells. *J. Organomet. Chem.* **2018**, *872*, 114–122. https://doi.org/10.1016/j.jorganchem.2018.07.035.

(5) Liu, Z.; Sadler, P. J. Organoiridium Complexes: Anticancer Agents and Catalysts. *Acc. Chem. Res.* **2014**, *47* (4), 1174–1185. https://doi.org/10.1021/ar400266c.